Spring 2017

The impact of nanoparticle surface chemistry on biological systems

Angie Sue (Morris) Thorn
University of Iowa

THE IMPACT OF NANOPARTICLE SURFACE CHEMISTRY ON BIOLOGICAL SYSTEMS

by

Angie Sue (Morris) Thorn

A thesis submitted in partial fulfillment
of the requirements for the Doctor of Philosophy
degree in Chemistry in the
Graduate College of
The University of Iowa

May 2017

Thesis Supervisors: Professor Aliasger K. Salem
Professor Sarah C. Larsen

Graduate College
The University of Iowa
Iowa City, Iowa

CERTIFICATE OF APPROVAL

_____

PH.D. THESIS

_____

This is to certify that the Ph.D. thesis of

Angie Sue (Morris) Thorn

has been approved by the Examining Committee for
the thesis requirement for the Doctor of Philosophy degree
in Chemistry at the May 2017 graduation.

Thesis Committee: _____
Aliasger K. Salem, Thesis Supervisor

_____
Sarah C. Larsen, Thesis Supervisor

_____
Gary W. Small

_____
Johna Leddy

_____
Lewis L. Stevens

I dedicate this work to my parents, Val and Steve Morris, who provided endless support and encouragement during this process and throughout my life. This work is also dedicated to my grandparents, Ervin and Evelyn Morris, Russell and Mary Jo Sutton, my sister Holly VanMetre, my brother Craig Morris and my husband Luke Thorn.

Nothing in life is to be feared, it is only to be understood. Now is the time to understand more, so that we may fear less.
Marie Curie

ACKNOWLEDGEMENTS

I would like to acknowledge my family - without them this work would not have been possible. I would like to thank my parents who supported me in difficult times as well as provided guidance and advice when I needed it the most. They made me who I am today and for that I am extremely grateful. I would like to acknowledge Holly VanMetre who is one of the main reasons I made it through graduate school. Thanks for the good times studying, talking about our research and for the memories we made in Iowa City. Finally, I would like to acknowledge my husband, Luke Thorn, for believing in me even when I didn't believe in myself. I cannot thank you enough for your support and love during this chapter of my life.

I acknowledge my advisor Dr. Aliasger Salem who accepted me into his research group and provided me with countless opportunities in research and in my career. Thank you for all you have done for me and being an outstanding mentor. I would not be where I am today without your help.

There are many other individuals who I would like to thank for helping me during my graduate career. First, I thank Dr. Sarah Larsen for supporting me and for being a great role model. I acknowledge all of the current and previous members of the Salem research group who were willing to help me with my many questions and for providing useful feedback for my projects. Specifically, Sean Geary for all of his help with writing and valuable guidance in research. Kae Wongrakpanich for training me when I joined the Salem research group. Sean Lehman whom I collaborated with many times in research and teaching. Finally, I would like to thank Behnoush Khorsand for not only helping me with research but for always being a great friend.

ABSTRACT

The unique properties of nanomaterials, such as their small size and large surface area-to-volume ratios, have attracted tremendous interest in the scientific community over the last few decades. Thus, the synthesis and characterization of many different types of nanoparticles have been well defined and reported on in the literature. Current research efforts have redirected from the basic study of nanomaterial synthesis and their properties to more application-based studies where the development of functionally active materials is necessary. Today such nanoparticle-based systems exist for a range of biomedical applications including imaging, drug delivery and sensors. The inherent properties of the nanomaterial, although important, are not always ideal for specific applications. In order to optimize nanoparticles for biomedical applications it is often desirable to tune their surface properties. Researchers have shown that these surface properties (such as charge, hydrophobicity, or reactivity) play a direct role in the interactions between nanoparticles and biological systems can be altered by attaching molecules to the surface of nanoparticles.

In this work, the effects of physicochemical properties of a wide variety of nanoparticles were investigated using in vitro and in vivo models. For example, copper oxide (CuO) nanoparticles were of interest due to their instability in biological media. These nanoparticles undergo dissolution when in an aqueous environment and tend to aggregate. Therefore, the cytotoxicity of two sizes of CuO NPs was evaluated in cultured cells to develop a better understanding of how these properties effect toxicity outcomes in biological systems. From these studies, it was determined that CuO NPs are cytotoxic to lung cells in a size-dependent manner and that dissolved copper ions contribute to the cytotoxicity however it is not solely responsible for cell death. Moreover, silica nanoparticles are one of the most commonly used nanomaterials because they are easy to synthesize and their properties (such as size, porosity and surface chemistry) can be fine-tuned. Silica nanoparticles can be found in thousands of commercially

available products such as toothpastes, cosmetics and detergents and are currently being developed for biomedical applications such as drug delivery and biomedical imaging. Our findings herein indicate that the surface chemistry of silica nanoparticles can have an effect on lung inflammation after exposure. Specifically, amine-modified silica NPs are considered to be less toxic compared to bare silica nanoparticles. Together, these studies provide insight into the role that material properties have on toxicity and allow for a better understanding of their impact on human and environmental health.

The final aim of this thesis was to develop surface-modified nanoparticles for drug delivery applications. For this, biodegradable, polymeric NPs were used due to their inert nature and biocompatibility. Furthermore, polymeric NPs are excellent for loading drugs and using them as drug delivery vehicles. In this work, poly (lactic-co-glycolic acid) (PLGA) NPs were loaded with a therapeutic peptide. These NPs were then coated with chitosan (a mucoadhesive polymer) for the treatment of allergic asthma or coated with a small cationic mitochondrial targeting agent for the treatment of ischemia/reperfusion injury.

Taken as a whole, this thesis sheds light on the impact of NPs on human health. First by providing useful toxicological data for CuO and silica NPs as well as highlighting the potential of surface-modified polymeric NPs to be used in drug delivery-based applications.

PUBLIC ABSTRACT

The unique properties of nanoparticles, such as their small size and large surface area-to-volume ratios, have attracted tremendous interest in the scientific community over the last few decades. A nanomaterial is defined as having one or more dimension in the nanometer (or 10^{-9} meters) size range. Although nanoparticles are already present in many consumer products such as toothpastes, cosmetics and sunscreens, it is not clear how exposure to nanoparticles will impact human and environmental health. Furthermore, there are conflicting and inconsistent toxicity profiles in the scientific literature for any given nanomaterial. Therefore, it is difficult to accurately assess the safety of nanoparticles upon human exposure. The first section of this thesis provides useful information concerning nanoparticle toxicity to the lungs. This work is important because inhalation is a major route of exposure for humans and it is necessary to understand the harm that nanoparticles can have on lung cells and tissue.

The second aim of this work was to use polymeric nanoparticles in a drug delivery-based application. Here, polymeric nanoparticles were used to encapsulate a drug. This is advantageous to protect the drug from degrading in the body and to target it to a specific tissue or organ. This nanoparticle-based system was found to be effective for preventing the onset of allergic asthma as well as for treating heart cells during injury.

Taken as a whole, this thesis addresses the impact of nanoparticles on human health by providing useful toxological data as well as highlighting the potential polymeric nanoparticles to be used in drug delivery-based applications.

TABLE OF CONTENTS

LIST OF TABLES

LIST OF FIGURES

1. INTRODUCTION

Nanomaterials, having long been used throughout history, are recognized for possessing unique material characteristics and have inspired scientists to gain a better understanding of their properties and potential applications. One of the most well-known nanomaterials, colloidal gold, has been used in stained glass windows that date back to the 4th century. During the 1850s, Michael Faraday sparked the scientific community's interest in nanometer-sized particles after delivering a lecture entitled "Experimental Relations of Gold (and Other Metals) to Light" where he discussed his findings about the absorption/transmission properties of colloidal gold suspensions in relation to the size of suspended particles.[1] Although Faraday did not call them "nanoparticles" he was one of the first experimentalists to explore the field we now refer to as "nanotechnology". However, interest in nanomaterials did not really take off until Richard Feynman's lecture in 1959 to the American Physical Society at the California Institute of Technology "There's Plenty of Room at the Bottom".[2] Feynman discussed the advantages of manipulating material (even single atoms) on a smaller scale than what was currently achievable at the time and challenged scientists to advance the field of what is now known as nanotechnology. From the 1980's onward, nanotechnology has progressed at an extremely fast pace and nanomaterials have been developed for many industrial and clinical applications.

Nanomaterials are defined as materials in which one or more dimension is in the nanometer-size range. Some classify a nanomaterial as having a size less than 1000 nm although it is common for nanomaterials to be categorized as 1-100 nm. The International Union of Pure and Applied Chemistry (IUPAC) defines a nanoparticle as a "particle of any shape with dimensions in the 1×10^{-9} and 1×10^{-7} m range".[3] Sometimes the word "nanoparticle" refers to a material that displays properties different than the bulk material and for most materials, this phenomenon occurs at sizes less than 100 nm. Other times "nano" is used as a prefix for structures with dimensions smaller than 500 nm. The latter definition will apply to this writing.

Nanotoxicology is the study of the toxic effects caused by or associated with nanomaterials on human health and the environment. Because of the rapid growth of nanoscience, both commercially and industrially, over the past few decades, there has been a large focus on the safety issues accompanying nano-sized materials. This is reflected in the drastic increase in the number of nanotoxicity-related articles published over the past 15 years (Figure 1-1). Besides the use of nanomaterials in science, they are increasingly being used in many commercially available consumer products such as toothpastes, shampoos, paints, sunscreens, cosmetics, food products, electronics, paper and fabrics.[4-10] Clearly, there is a large amount of human exposure to nanomaterials from consumer products alone, not to mention the rapidly developing nanomaterial-based biomedical applications and as a result concerns have been raised about the short and long-term implications of nanomaterial exposure on both human health and the environment. While these materials are appealing for many novel applications because of their unique physicochemical properties that are drastically different than the bulk material (such as high surface area-to-volume ratio and surface reactivity), it is unclear how these properties impact human health and the environment.

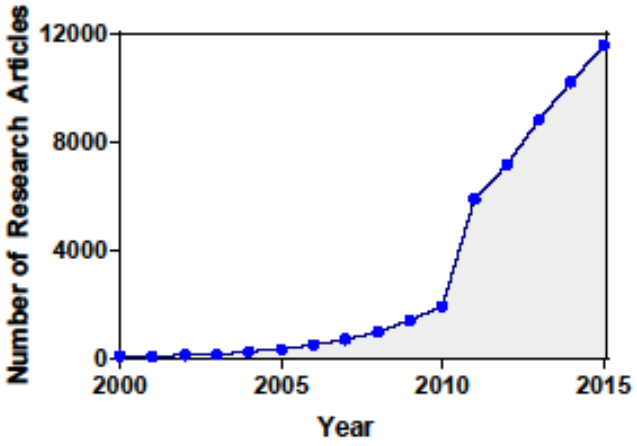

Figure 1-1. Number of nanotoxicity research articles published from 2000-2015. The data were collected from Thompson Reuters Web of Science™ by searching "Nanotoxicity" and refining the publications to only include research articles.

Over the last few decades, research and development of nanomaterial-based medicines (termed "nanomedicine") has led to the formation of hundreds of start-up companies aimed at commercializing novel therapies or drug delivery systems.[11-12] Although nanomaterials are being implemented in diagnostic and imaging devices among several other medical applications, drug delivery dominates the nanomedicine market. The incorporation of nanomaterials into drug delivery systems has the potential to improve medicine by allowing one to control the release of a drug in a sustained manner and target the drug to a specific organ or tissue. Many researchers are designing pH-sensitive materials in which the release profile of the drug from the nanocarrier is directly dependent upon environmental pH.[13-14] These types of materials are commonly applied to cancer therapy because of the slightly acidic (pH 6.4-6.9) microenvironment of solid tumors compared to the neutral microenvironment of heathy cells.[15-17] Nanomaterials also help overcome limitations in many pharmaceutical applications, one being the loading and delivery of poorly soluble drugs in an efficient manner.[18] Site-specific therapies can also be achieved by altering the physicochemical properties of nanomaterials in order to target drugs to certain cells (e. g tumor cells) or tissues and to minimize the side-effects of drugs to healthy tissues.[19-21]

There are clear advantages to employing nanomaterials in biomedical applications, however, with the surge of nanotechnology in the past few decades, it is critical to evaluate the health effects of direct and indirect exposure to engineered nanomaterials. The study of nanotoxicity is vital to address these concerns and to aid in the development of safe, biocompatible nanomaterials.

1.1. Physicochemical Properties of Nanoparticles and Their Effects on Biological Systems

Since the early 2000's researchers have recognized the need for extensive nanotoxicity studies of various commonly used nanomaterials. Not only are these studies important for developing new biomedical applications that could be implemented in a clinical setting but also for evaluating the safety of nano-sized materials in the workplace where large scale synthesis of nanomaterials takes place and knowledge of safe working doses is necessary to keep workers free of harmful side effects.[22] There are

many factors that can contribute to the nanotoxicity of a particular material including chemical composition, size, shape, dissolution and surface chemistry (Figure 1-2).

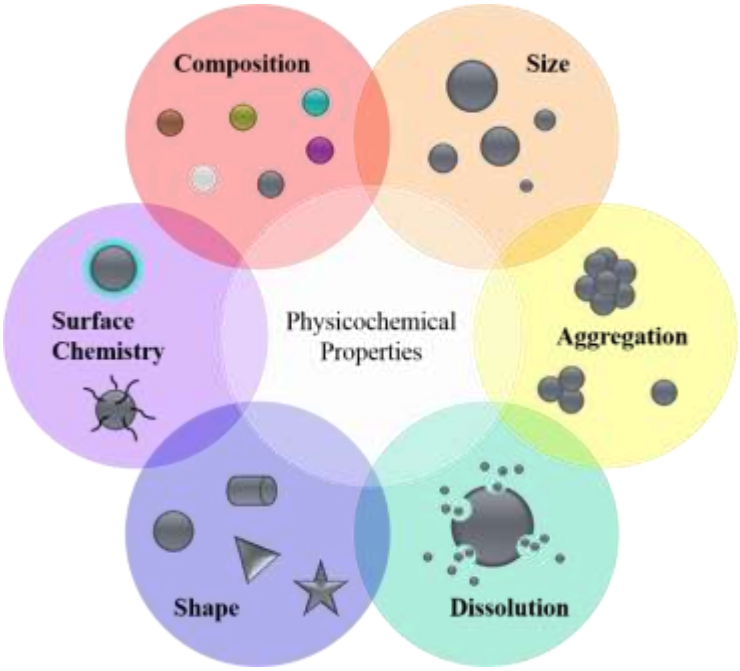

Figure 1-2. Physicochemical properties of nanomaterials that influence toxicity.

1.1.1. Composition

The chemical composition of nanomaterials used in medicine varies widely depending on the application. For example, magnetic nanoparticles (i.e. iron oxide), gold nanoparticles and quantum dots are commonly used in biomedical imaging techniques as contrast agents[23-24] whereas silver nanoparticles are often used in medical devices because of their antimicrobial properties.[25-26] In terms of biochemistry, nanomaterials of various compositions can have very different effects on physiological systems and resultantly very different toxicities. Therefore, when designing systems where there is the potential for human exposure, it is important to consider the inherent toxicity of the material. Metal and metal oxide nanoparticles are present in a wide variety of consumer products such as sunscreens and cosmetics as well as actively being developed for biomedical applications, however, there is a large amount of scientific evidence that demonstrates their toxic effects on biological systems.[27] An article published in 2008

compared the toxicity of several types of metal oxide (CuO, TiO_2, ZnO, Fe_2O_4, Fe_3O_4 and Fe_2O_3) nanoparticles, carbon nanoparticles and carbon nanotubes on human lung epithelial cells (A549). [28] Of all of the materials tested, copper oxide nanoparticles were the most cytotoxic, causing significant amounts of DNA damage and reactive oxygen species (ROS) production. Zinc oxide nanoparticles also decreased the cell viability of A549 cells due in part to DNA damage, however, there was no increase in intracellular ROS production. In contrast, both types of iron oxide nanoparticles displayed only small amounts of cytotoxicity and were considered the least harmful to A549 cells. Although many metal nanomaterials promote nanotoxicity, gold nanomaterials are generally considered safe although their long term toxic effects are yet to be sufficiently characterized.[29] Biodegradable nanomaterials such as poly (lactic-co-glycolic acid) PLGA and chitosan tend to be less toxic than inorganic nanomaterials.[30-31]

1.1.2. Size

Size is a major factor that influences the interactions of nanomaterials with cells. Many researchers have reported size-dependent nanotoxicity of materials of the same composition.[32-34] A number of factors can be responsible for such size-related differences in toxicity including the well described example where cellular uptake rate is a primary influence.[35] In general, nanoparticles with sizes greater than 500 nm enter cells via phagocytosis, primarily mediated by specialized phagocytes, whereas smaller particles are internalized by receptor-mediated endocytosis.[36] Chithrani et al. investigated the cellular uptake of gold nanoparticles of various sizes (14 – 100 nm) in human epithelial (HeLa) cells and observed maximum uptake was observed for 50 nm nanoparticles.[37]

Gold nanoparticles are considered relatively nontoxic, however, there are numerous published results suggesting that the size of gold nanoparticles has an impact on the nanotoxicity. For example, Coradeghini et al. reported significant differences in the biological response of mouse fibroblast cells when treated with differently sized gold nanoparticles.[38] Specifically, 5 nm gold nanoparticles inhibited colony formation in mouse fibroblast cells to a greater extent than 15 nm gold particles at concentrations above 50 μM. The same researchers also concluded that 5 nm gold nanoparticles had a greater effect on

cell morphology compared to the larger 15 nm nanoparticles. One study published by Zhang et al. showed that the trend of smaller nanoparticles being more toxic in vitro does not always translate to in vivo models but reinforces the fact that size is an important factor when trying to minimize toxicity.[39] This group evaluated several different sizes (5, 10, 30 and 60 nm) of polyethylene glycol (PEG)-coated gold nanoparticles on toxicity in mice. The results indicated that 10 nm and 60 nm PEG-coated gold nanoparticles caused a greater amount of liver damage in mice compared to 5 nm or 30 nm PEG-coated gold nanoparticles and therefore were considered more toxic.

Several studies have reported that silica nanoparticles exhibit size-dependent nanotoxicity. Based on these size-dependent studies, the trend was that the smaller the silica nanoparticles, the more toxic they become. In one investigation, amorphous silica nanoparticles ranging from 16-335 nm in diameter were evaluated for their cytotoxicity in human endothelial cells.[40] The 16 nm particles were the most cytotoxic based several different assays and the cytotoxicity decreased as particle sized increased. In another publication, a similar trend was seen with silica nanoparticles of 20 nm and 100 nm in size where the smaller nanoparticles were more cytotoxic to two separate kidney cell lines (LLC-PK1 and HK-2).[34]

1.1.3. Shape

As nanotechnology advances, the types of nanomaterials being developed is growing rapidly and diversifying. One physical parameter that is being manipulated is shape. Spherical particles are the most common geometry of nanomaterials used today, however, there are a variety of unconventional shapes emerging such as rods, tubes and stars. As an example, mesoporous silica can be synthesized into spheres or rod-like shapes which can alter the nanotoxicity of the material. Rod-like shapes have higher aspect ratios compared to spheres. In one study, three types of mesoporous silica nanomaterials with varying aspect ratios were investigated for their effect on nanotoxicity.[41] It was found that mesoporous nanostructures with larger aspect ratios (nanorods) had a greater impact on the proliferation and overall function of human melanoma cells compared to spherical nanoparticles.

1.1.4. Dissolution

Depending on the composition of the material, dissolution can play a large role in the nanotoxicity. Nanoparticles made of metals or metal oxides, such as copper oxide, zinc oxide and silver, release toxic ions from the surface of the material and these ions can disrupt normal cellular functions.[22] A study by Wongrakpanich et al. reported that both 4 nm and 24 nm copper oxide nanoparticles release Cu^{2+} ions into the cell culture medium and after 48 hours, almost 60% of the copper was in the form of Cu^{2+} ions.[32] Studer et al. investigated the effects of intracellular solubility on cytotoxicity in Chinese hamster oocytes and HeLa cells.[42] To do this, two types of nanoparticles were used: degradable copper oxide nanoparticles and copper oxide nanoparticles that were stabilized with a carbon layer on the surface. In doing so, the direct effect of dissolved metal ions on cytotoxicity could be established. The results indicated that applying a carbon coating to the surface of copper oxide nanoparticles significantly reduced the amount soluble Cu^{2+} released from the nanoparticles and the cytotoxicity was reduced in both cells lines for the stabilized carbon-coated nanoparticles compared to bare copper oxide nanoparticles. Cytotoxicity caused by Cu^{2+} has been linked to an increase in intracellular and mitochondrial ROS as well as DNA damage.[32, 43]

1.1.5. Surface Functionalization

Surface chemistry play a large role in the interaction of nanomaterials with biological systems and subsequently, the toxicity of nanomaterials. This has been demonstrated through numerous in vitro and in vivo experiments. For example, surface silanols on silica nanoparticles are consider to be very reactive and thus contribute in large to the toxicity of the material. Several studies have shown that functionalization of silica nanoparticles with amine-functional organic molecules, such as aminopropyltriethoxysilane (APTES), significantly increased the cell viability of RAW267.4 macrophage cells by reducing the amount of nanoparticle-mediated ROS.[44] The same APTES-functionalized nanoparticles caused less lung inflammation in mice compared to bare silica nanoparticles as indicated by a lower number of immune cells present in BAL fluid and a lower amount of ROS in lung cells.[45] In the

same experiment, bare silica nanoparticles caused a significant weight drop in mice (a sign of toxicity) whereas the APTES-functionalized silica nanoparticles caused no significant change in mouse weight compared to untreated controls. As previously mentioned, coating metal oxide nanoparticles with a more inert material such as carbon, can act to prevent toxic metal ions from dissociating from the surface and as a result, reduce nanotoxicity.[42] Other commonly used coatings to alter the surface properties of nanomaterials include polymers such as chitosan, dextran and PEG, and biologically relevant molecules like proteins and peptides.[46-47]

1.2. Mechanisms of Nanoparticle Toxicity in Biological Systems

1.2.1. Oxidative Stress

There are many different mechanisms by which nanomaterials can cause toxicity in physiological systems (Figure 1-3). One of the major routes is through the generation of reactive oxygen species (ROS). ROS are chemically reactive compounds produced during biological processes such as mitochondrial respiration and inflammation.[48] These compounds (such as hydrogen peroxide, superoxide and hydroxyl radicals) are byproducts of the metabolism of oxygen. ROS occur naturally in biological systems and are involved in cell signaling as well as maintaining homeostasis. When molecular oxygen is reduced by the enzyme nicotinamide adenine dinucleotide phosphate (NADPH) oxidase, superoxide anions are formed. Although cells are equipped to be able to function with small amounts of ROS, too much can lead to a state of oxidative stress.[49] Nanomaterials are known to cause oxidative stress as a mechanism of toxicity. This increase in ROS can be irreversibly harmful to cells causing membrane damage, protein oxidation, DNA damage, mitochondria dysfunction, apoptosis, and genotoxicity.

There are many in vitro studies confirming that cells exposed to nanomaterials generate a higher level of ROS compared to healthy cells. Nonporous silica nanoparticles (50 nm in diameter) have been shown to induce a significantly higher levels of ROS in RAW264.7 macrophages compared to untreated cells.[44, 50] Copper oxide nanoparticles increase the amount of both intracellular and mitochondrial ROS in A549 lung cells.[32] Multi-walled (MW) carbon nanotubes, both short (0.1-5 nm in length) and long (0.1-20

nm in length), titanium dioxide nanoparticles and aluminum oxide nanoparticles caused higher levels of ROS in rat kidney cells (NRK-52E) compared to control cells.[51] In vivo studies also support the theory that nanomaterial-induced ROS are damaging to physiological systems. The same silica nanoparticles used in the study by Lehman et al. were evaluated in a murine model of inhalation.[44-45] A significant amount of ROS was observed in the lung cells of mice that were administered of 0.5 mg of nanoparticles intratracheally. In this case, higher levels of ROS directly correlated to other markers of toxicity such as reduced body weight in mice, membrane damage and immune cell recruitment to the lungs although the specific role of ROS on the inflammatory response is not clear. There is evidence suggesting that increased ROS can lead to membrane damage via lipid peroxidation and promote proinflammatory signaling.[52-54]

1.2.2. DNA Damage and Genotoxicity

DNA damage is another important parameter which can be used to assess nanotoxicity. As mentioned earlier DNA damage can occur indirectly through the action of ROS, however, nanomaterials can also physically damage DNA upon entering the nucleus. Nanomaterials can enter the nucleus via nuclear pores or by being entrapped in the nucleus during mitosis both of which can lead to DNA damage.[55] Determining the potential of a nanomaterial to promote DNA damage is a key aspect of nanotoxicity as this damage can lead to genotoxicity (generation of mutations) which may ultimately result in cancer. Multiple studies have demonstrated that silver nanoparticles can cause damage to DNA both in vitro and in vivo.[56-57] Copper oxide nanoparticles were also shown to have genotoxic effects in A549 lung cells as indicated by elevated concentrations of DNA repair proteins, RAD51 and MSH2.[58] Other nanomaterials that have been linked to genotoxicity include cobalt nanoparticles, fullerenes and zinc oxide nanoparticles although for these and several other types of materials, there are conflicting results published in the literature about their genotoxic potential.[59-62]

1.2.3. Mitochondrial Dysfunction

Loss of mitochondrial function is another cause of nanotoxicity since mitochondria are involved in the production of ATP and provide cells with the energy they need to survive and maintain biological functions. Excess ROS generated during oxidative stress is thought to damage mitochondria by altering the mitochondrial membrane potential and permeability.[63] Yu et al. reported that zinc oxide nanorods (15 nm in width and 82 nm in length) were cytotoxic to normal mouse skin epidermal cells (JB6 Cl 41-5a) and induced autophagy by means of excess ROS and mitochondrial damage.[64] Other examples of materials that disrupt mitochondrial function in vitro and/or in vivo include silica nanoparticles[65], silver nanoparticles[66] and titanium dioxide nanoparticles.[67]

1.2.4. Inflammation

Inflammation is a natural biological defense mechanism that is triggered by a range of factors including toxins, the introduction of foreign matter or pathogens, or damaged tissue. Inflammation is a complex process that involves the recruitment of immune cells to the site of injury/infection by pro-inflammatory cytokines.[68] Numerous studies have shown that nanomaterials can cause inflammation when introduced to a physiological system. For example, when nonporous silica nanoparticles were instilled into the lungs of mice, there was an increase in the number of immune cells, such as neutrophils and macrophages, present in the bronchoalveolar lavage (BAL) fluid compared to the control group.[45] Another study demonstrated that pulmonary exposure of single-walled carbon nanotubes in mice caused an increase in the number of macrophages, lymphocytes and neutrophils in the BAL fluid as well as elevated levels of pro-inflammatory cytokines (TNF-α, IL-1β and TGF-β1).[69]

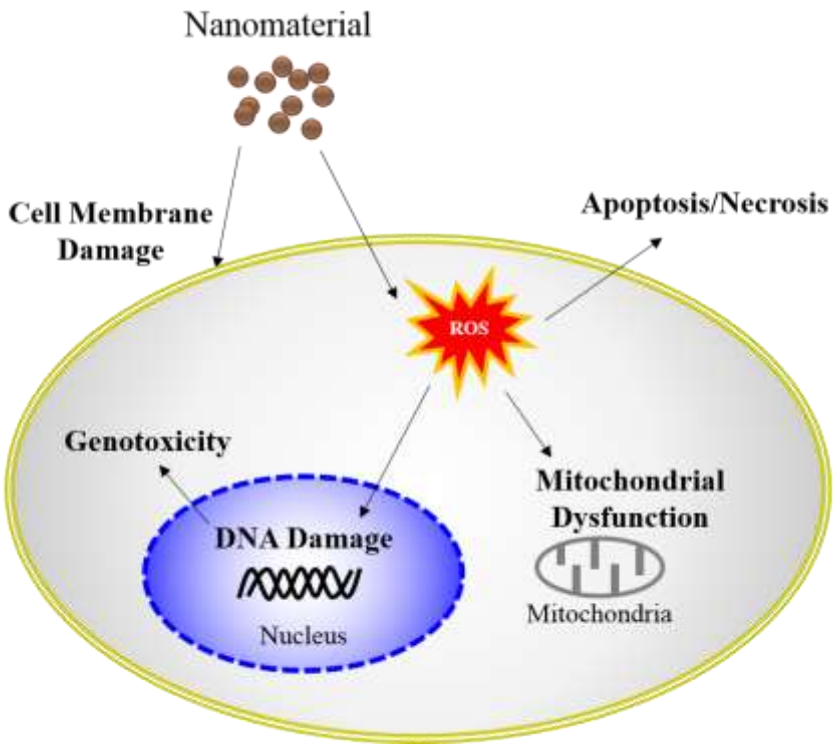

Figure 1-3. Summary of nanomaterial-related mechanisms of cell death.

1.3. Experimental Methods for Nanoparticle Risk Assessment

As the potential for human exposure to nanomaterials rises, there is a need to establish reliable methods, both in vitro and in vivo, for evaluating nanotoxicity. In vitro assays are generally used for toxicity screening of chemicals. They are less time consuming and labor intensive compared to in vivo models and can provide mechanistic details of nanotoxicity.[70] However, in vitro analyses do not always correlate with in vivo studies and are often too simplistic to accurately predict the toxicological outcomes in animal models. Moreover, in vitro methods are limited in the depth of information they can provide. For example, they cannot predict the biodistribution or fate of nanomaterials once they are administered to animals. Many researchers employ a combination of in vitro and in vivo methods in order to get a more comprehensive toxicity profile of the nanomaterial.

1.3.1. In Vitro Assays

In vitro cell viability assays are among the most commonly used techniques for evaluating nanotoxicity. MTT (3-(4,5-Dimethylthiazol-2-yl)-2,5-diphenyltetrazolium bromide) and MTS ((3-(4,5-dimethylthiazol-2-yl)-5-(3-carboxymethoxyphenyl)-2-(4-sulfophenyl)-2H-tetrazolium)) are two widely used reagents to assess the mitochondrial metabolic activity of cells. Both assays are based upon the reduction of tetrazolium salts by the enzymes present in metabolically active cells. Upon reduction of the tetrazolium salts, a formazan product is produced accompanied by a measurable color change. The relative amount of purple formazan product formed can be determined using spectrophotometry. During necrosis or apoptosis, the metabolic activity of cells decreases resulting in a decrease in formazan production and subsequently a lower absorbance compared to viable cells. Once the linear relationship of formazan production versus number of cells is determined for a specific cell type, then this reaction can be used to evaluate nanotoxicity.

Measurement of ROS is frequently used as an indicator of nanotoxicity. Most ROS assays are based upon the oxidation of cell-permeable probes such as 2',7'-dichlorofluorescein diacetate (DCFH-DA) and dihydroethidium (DHE). For example, DCFH-DA is a nonionic compound that can diffuse into cells .[71] After entering cells, DCFH-DA can be enzymatically hydrolyzed by esterases into the DCFH form. Then, DCFH can be oxidized by intracellular ROS into a highly fluorescent compound (DCF). The amount of DCF present in cells can be quantified using analytical techniques such as flow cytometry and is directly proportional to the concentration of intracellular ROS. Although DCFH-DA is the most widely used probe for ROS, there can be several factors that can lead to inaccurate results.[72-73] For example, many researchers claim that DCFH-DA can be used to detect hydrogen peroxide (H_2O_2) however, there are numerous other species that can be involved in the conversion of DCFH-DA to its fluorescent form including hydroxyl radicals ($^{\bullet}OH$) and redox-active metal ions such as Fe^{2+}. Because these dye-based assays are sensitive to numerous intracellular species, precautions should be taken to avoid interference and misinterpretation of data.

1.3.2. In Vivo Assays

A large amount of nanotoxicity data published in scientific journals is comprised of cell culture systems, but it is common for these simplistic assays to be inaccurate at predicting toxicity outcomes in animal models. There are a variety of techniques that can be used to determine nanomaterial toxicity in vivo.

Because inhalation is a major route of human exposure, many studies have aimed to evaluate nanoparticle-induced lung inflammation. In an inhalation study where the animals are exposed to nanomaterials, the lungs can be washed (termed "bronchoalveolar lavage") and the fluid collected for analysis. The number of total cells and immune cells (such as macrophages, neutrophils and eosinophils) in BAL fluid are counted and compared to control animals that were not exposed to nanomaterials. Increased concentration of immune cells in the lungs is a sign of inflammation and often related to nanotoxicity. Another assessment for lung inflammation is the quantification of inflammatory cytokines in BAL fluid (such as interleukin (IL)-6, tumor necrosis factor (TNF)-α and interferon (INF)-γ).[74]

When nanomaterials enter the blood stream, they accumulate in the major organs of the animal depending on their size, shape and surface chemistry.[75] After administration, nanomaterials can localize in the liver. Therefore, a technique for assessing nanotoxicity is to determine if there are any abnormalities in liver function. There are several markers for liver damage. Bilirubin, for example, is a liver enzyme that occurs naturally in the body and is involved in heme metabolism. Elevated levels of bilirubin in the blood plasma or serum is an indication that the liver is not functioning normally[76] and can be a result of nanotoxicity.[77] Other markers for liver damage are alanine aminotransferase (ALT) and aspartate aminotransferase (AST) enzymes. All of the liver enzymes mentioned here can be detected by well-established analytical methods, the most common being colorimetric analysis using spectrophotometric detection.[78-81]

Histology can be used as a visual method to determine damage and/or inflammation in organs or tissues as a result of nanomaterial-dependent toxicity. After tissues or organs are extracted from the

animal, they must be preserved with a chemical fixative (formaldehyde, for example), embedded in a medium such as paraffin and then cut into very thin sections. Afterwards, the sections are stained and imaged with light microscopy. Hematoxylin and Eosin (H&E) stains are of the most widely used stains for histological analysis. In H&E staining, the nucleus of cells are stained blue by hematoxylin while eosin stains the cytoplasm and extracellular matrix pink. This dye is often used to examine the infiltration of immune cells (e.g. macrophages) into a tissue after nanomaterial exposure.[82] Immunohistochemistry is another histology method in which anitbodies are used to tag cytokines (or other proteins) located within tissue sections.[83]

2. SIZE DEPENDENT TOXICITY OF COPPER OXIDE NANOPARTICLES IN LUNG CELLS

2.1. Abstract

The increasing use of copper oxide (CuO) nanoparticles (NPs) in medicine and industry demands an understanding of their potential toxicities. In this study, we compared the in vitro cytotoxicity of CuO NPs of two distinct sizes (4 and 24 nm) using the A549 human lung cell line. Despite possessing similar surface and core oxide compositions, 24 nm CuO NPs were significantly more cytotoxic than 4 nm CuO NPs. The difference in size may have affected the rate of entry of NPs into the cell, potentially influencing the amount of intracellular dissolution of Cu^{2+} and causing a differential impact on cytotoxicity.

2.2. Introduction

In recent years, engineered NPs have been utilized in many fields, including biomedical sciences, engineering and industry.[84] Aside from the negative impact that these NPs may have on a range of valuable "off-target" non-human life forms[85-87], the increased use of engineered NPs also raises the risk of human exposure, often via the respiratory and gastrointestinal tracts, due to the increased release of these particles into the environment.[74, 88] This raises a concern regarding the possible cytotoxicity and side effects of NPs upon human exposure.[89] Nanoscale particles have very high surface-to-volume ratios when compared to the bulk phase, exhibiting unique physicochemical properties that may render them cytotoxic under certain circumstances.[87, 90-92]

CuO NPs contain a single phase, tenorite.[93] CuO NPs are used for numerous applications in the electronic and optoelectronic industries such as in gas sensors, semiconductors and thin films for solar cells[94-96] CuO NPs also have desirable traits for many medical applications. Recent work has shown that CuO NPs have microbicidal activity against both fungi and bacteria[97-101] and have been shown to reduce

bacterial biofilm formation.[102-103] CuO NPs also have a high potential to be used as a MRI-ultrasound dual imaging contrast agent.[104]

In order to employ these metal-based engineered NPs in biomedical applications, their behavior in physiological systems needs to be addressed and fully understood. For example, particle dissolution can occur under biological conditions, specifically in the presence of natural coordinating organic acids, resulting in the release of dissolved metal ions to the surrounding solution. Dissolution can also lead to decreased particle size and in turn increased particle mobility.[105-107] These are important considerations for the use of NPs in biomedical research because these are factors that could be directly related to cytotoxicity.

In this study, two sizes of CuO NPs were compared; 4 nm CuO NPs and 24 nm CuO NPs. The goals of the current study were to compare the cytotoxicity of differently sized CuO NPs and investigate the specific causes of cytotoxicity induced in vitro using a human lung cell line as a representative cell type of the respiratory tract.[108] This study attempts to provide insight into the factors that affect the cytotoxicity of CuO NPs.

2.3. Methods and Materials

2.3.1. Nanoparticle Characterization

The CuO NPs used in this study were extensively characterized for the size, surface area, core and surface composition. The average particle sizes of CuO NPs were determined using transmission electron microscopy (JEOL JEM-1230 TEM). Surface areas were measured using a multipoint Brunauer-Emmett-Teller (BET) surface analyzer (Quantachrome Nova 4200e) using nitrogen as the adsorbent. The bulk and surface compositions were determined using X-ray diffraction (XRD) and X-ray photoelectron spectroscopy (XPS), respectively. Data generated from these characterizations are summarized in Table 2-1. Large (24 nm) CuO NPs were purchased from Sigma-Aldrich while small (4 nm) CuO NPs were synthesized in the lab according to the following protocol. A copper-containing precursor, $Cu(OAc)_2$

(1.74 g), was added to 100 mL methanol. The solution was then refluxed for several minutes to dissolve the precursor. Afterwards 3 mL of water was added to this solution. Upon completely dissolving $Cu(OAc)_2$, a solution of methanol (50 mL) containing 0.7 g of NaOH was added dropwise and further refluxed for 50 hours. The resultant black precipitate was collected by evaporating the methanol on a rotary evaporator followed by multiple washings using acetone (20 mL), water (20 mL) and ethanol (20 mL) respectively. At each washing step, the nanoparticles were collected via centrifugation at 22,000 rpm. Finally, the collected precipitate was dried in the oven overnight at 106 °C and finely ground using a mortar and pestle.

2.3.2. Cell Culture

The human alveolar lung adenocarcinoma cell line, A549, was kindly provided by Peter S. Thorne, Department of Occupational and Environmental Health, College of Public Health, University of Iowa. A549 cells were maintained in RPMI-1640 media (Gibco, Life technologies) supplemented with 10% fetal bovine serum (FBS, Atlanta Biologicals), 1 mM sodium pyruvate (Gibco), 10 mM HEPES (Gibco), 1 mM Glutamax (Gibco) and 50 µg/mL gentamycin sulfate (IBI Scientific). Cells were incubated at 37°C in a 5% CO_2 humidified atmosphere and were shown to be free of mycoplasma.

2.3.3. Cytotoxicity Assay

A549 cells were plated 1 day prior to NP treatment in 96-well plates at a concentration of 1×10^4 cells/well. In all cell-based experiments, all treatments (4 nm CuO NPs, 24 nm CuO NPs, $Cu(NO_3)_2$ and $NaNO_3$) were dispersed in media using a sonic dismembrator (Fisher Scientific) at 40% amplitude for 1 minute at 1 mg/mL (12.6 mM CuO) before dilution. $Cu(NO_3)_2 \cdot 3H_2O$ and $NaNO_3$ were purchased from Sigma-Aldrich. $Cu(NO_3)_2$ was included in the study to evaluate the effect on cell viability of dissolved Cu^{2+} in solution. These two types of CuO NPs and $Cu(NO_3)_2$ were added by normalizing against Cu^{2+} concentration. $NaNO_3$ was used as a negative control to confirm no cytotoxicity was contributed from NO_3^{2-} in $Cu(NO_3)_2$. Cells were exposed to different concentrations of Cu^{2+} ranging from 0.06 – 1.57 mM (or 5 – 125 µg/ml CuO) for 1, 4, 24 and 48 hours. At the end of the indicated incubation period, the

treatment in each well was replaced with 100 µL of fresh media and 20 µL of MTS tetrazolium compound (CellTiter 96® AQ_{ueous} One Solution, Promega). After 1 - 4 hours, the absorbance was recorded at 490 nm using a Spectra Max plus 384 microplate spectrophotometer (Molecular Devices). Cell viability was expressed as a percentage of the absorbance value obtained for the untreated cells. All absorbance values were corrected with a blank solution (100 µL of fresh media and 20 µL of MTS tetrazolium compound).

2.3.4. Dissolution of Cu^{2+} from CuO NPs

In separate experiments, nanoparticles (4 nm and 24 nm CuO NPs) were dispersed in complete RPMI-1640 media using a sonic dismembrator at 40% amplitude for 1 minute before dilution. The NP suspensions at different concentrations of Cu^{2+} ranging from 0.06 – 1.57 mM (or 5 – 125 µg/mL CuO) were incubated at 37 °C and 5% CO_2 to mimic the same conditions as in cytotoxicity assays. After 4 different time points (1, 4, 24 and 48 hours), the NP suspensions were centrifuged at 10,016 × g for 25 minutes to pellet the CuO NPs. Supernatants were collected, diluted in 5 mM HNO_3 and was analyzed via inductively coupled plasma–optical emission spectroscopy (ICP-OES, Varian, Agilent Technologies) to determine the dissolved Cu^{2+} concentration. In addition, a droplet of the supernatant was placed on a TEM grid and imaged to test the presence of any smaller nanoparticles that could not be removed from the centrifugation process.[107]

2.3.5. Determination of Intracellular Reactive Oxygen Species (ROS)

A549 cells were plated in 60 mm^2 dishes at a concentration of 2×10^5 cells/dish. Twenty four hours following plating, the cells were treated with 4 mL of 4 nm CuO NPs, 24 nm CuO NPs, $Cu(NO_3)_2$ or $NaNO_3$. The two types of CuO NPs and $Cu(NO_3)_2$ were added such that equal amounts of Cu^{2+} (0.12 µM Cu^{2+} concentration) were added for each treatment. $NaNO_3$ was used as a negative control for NO_3^{2-} in $Cu(NO_3)_2$. Following the 1, 4, 24 or 48 hour treatment, the cells were trypsinized with 0.25% trypsin-EDTA and centrifuged at 230 × g for 5 minutes. The cells were washed with PBS containing 5 mM pyruvate and incubated for 40 minutes at 37 °C with 10 µM of the commercially available dye,

dihydroethidium (DHE), in PBS containing pyruvate. Following incubation with the dye, the cells were analyzed using flow cytometry (FACScan: Becton Dickinson Immunocytometry Systems). The mean fluorescence intensity (MFI) of 20,000 cells was recorded. All groups were normalized to the untreated control group. Antimycin A (an electron transport chain blocker) which was used as a positive control increased the DHE oxidation levels by 3- to 5-fold (data not shown).

2.3.6. Determination of Mitochondrial Reactive Oxygen Species (ROS)

A549 cells were seeded at a concentration of 2×10^5 cells/well in 60 mm^2 dishes one day prior to adding the treatments. Two different sizes of CuO NPs (4 and 24 nm) and $Cu(NO_3)_2$ were added such that cells were exposed to equal amounts of Cu^{2+} (0.12 µM Cu^{2+}) for each treatment. $NaNO_3$ was added as a control. At two different time points (1 and 24 hours), cells were removed from dishes by trypsinization, stained with MitoSOX (final concentration of 2 µM for 15 minutes) and the fluorescence was measured via flow cytometry. The mean fluorescence intensity (MFI) of 10,000 cells per sample was calculated. All groups were normalized to the control (untreated) group. Antimycin A was used as a positive control and showed a MFI approximately 28-fold greater than the control.

2.3.7. Intracellular Cu^{2+} Uptake

A549 cells were seeded at a concentration of 4×10^5 cells/well in 60 mm^2 dishes one day prior to the addition of treatments. Two different sizes of CuO NPs (4 and 24 nm) and $Cu(NO_3)_2$ were added such that cells were exposed to equal amounts of Cu^{2+} for each treatment. At 4 different time points (1, 4, 24 and 48 hours), cells were gently washed twice with warm PBS and removed from dishes by trypsinization. Cells were collected and centrifuged at 230 × g for 5 minutes, gently washed once with warm PBS and resuspended in 1 mL complete medium. These repeat washing cycles were introduced to the experiment to ensure the complete removal of extracellular CuO NPs and Cu^{2+}. A small aliquot (20 µL) of the cell suspension was used to determine cell concentration using a hemocytometer. The rest of cell suspension was digested with concentrated HNO_3 (3 mL) using microwave digestion (MARS 6, CEM Corporation) and the Cu^{2+} concentration in the digestate was quantified via ICP-OES. The limit of

detection for Cu^{2+} using ICP-OES is 5 µg/L. The Cu^{2+} in the digestate was used to calculate the amount of CuO in the cells (assumption: Cu^{2+} in the digestate is due to internalized CuO NPs or Cu^{2+}). The intracellular Cu^{2+} from each sample was normalized against cell number.

2.3.8. Statistical Analysis

Data are expressed as mean ± SD. For the cytotoxicity assay, a non-linear regression with second order polynomial (quadratic), least squares fit was used. For all other experiments, One-way ANOVA with Bonferroni's post-test (comparing all groups to the control group and comparing 4 nm with 24 nm CuO NPs) was performed. All statistical analyses were conducted using GraphPad Prism version 6.05 for Windows (GraphPad Software). The p-values of less than 0.05 were considered significant.

2.4. Results and Discussion

2.4.1. CuO NP Characterization

The average sizes of the CuO NPs used in these studies were 4 ± 1 nm ("small") and 24 ± 9 nm ("large") (Figure 2-1). The Brunauer-Emmett-Teller (BET) surface areas of the small and large CuO NPs were 118 ± 4 m^2/g and 22 ± 0.4 m^2/g, respectively.[107] Bulk phase analysis with X-ray diffraction indicated that both the small and large CuO NPs consisted of a single phase; tenorite and surface analysis using X-ray photoelectron spectroscopy (XPS) revealed that in both particle types the copper atoms are in the same oxidation state (Cu(II)) in the near surface region (Figure 2-2). These characterization data are summarized in Table 2-1.

Table 2-1. Physicochemical characterization of CuO nanoparticles.

Physicochemical property	Technique	Small CuO NPs	Large CuO NPs
Particle size (nm)	TEM	4 ± 1	24 ± 9
Surface area (m^2/g)	BET	118 ± 4	22 ± 0.4
Bulk composition	XRD	CuO	CuO
Surface composition	XPS	CuO	CuO

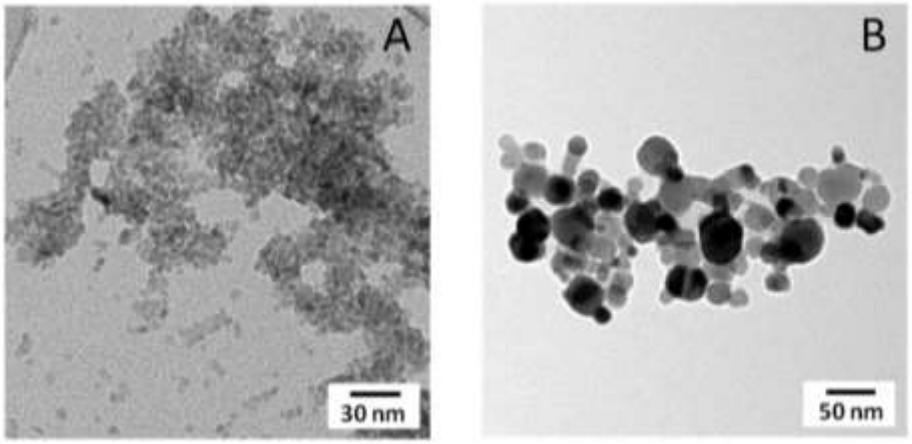

Figure 2-1. Transmission Electron Microscopy (TEM) images representing small (A) and large (B) CuO NPs which were used in this study. The average particle sizes of small and large CuO NPs, as determined using TEM, were 4 ± 1 nm and 24 ± 9 nm, respectively.

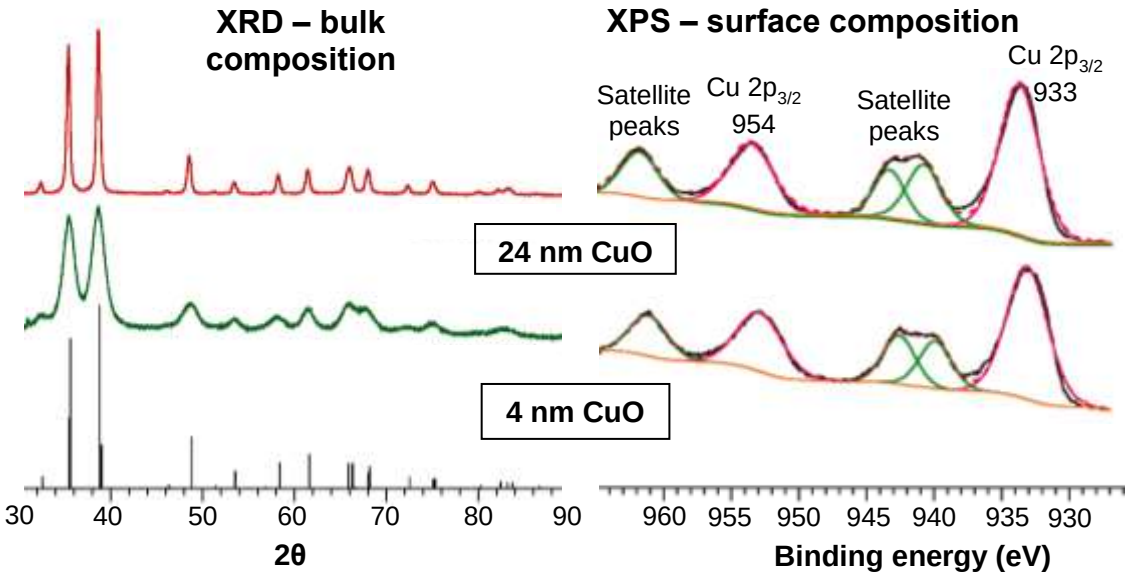

Figure 2-2. Bulk (left) and surface (right) characterization of small (4 nm) and large (24 nm) CuO NPs using X-ray diffraction (XRD) and X-ray photoelectron spectroscopy (XPS).

2.4.2. Cytotoxicity of 4 nm and 24 nm CuO NPs in A549 Cells

After the particles were dispersed by sonication in RPMI-1640 media, the two differently sized CuO NPs were added to A549 cells at concentrations ranging from 0.06 – 1.57 mM (of Cu^{2+}) for 1, 4, 24 or 48

hours and the percent cell viability (relative to untreated control cells) was determined immediately after each incubation period using an MTS assay. The results (Figure 2-3) suggest that cytotoxicity yielded from A549 cells were dependent on both time of exposure to, and concentration of, either 4 nm CuO NPs or 24 nm CuO NPs. In addition, it was also noted that, at 1, 4, 24 and 48 hour time points, there were significant differences (p-value < 0.05 for 1 hour, p-value < 0.001 for 4, 24 and 48 hours) in percent cell viability of A549 cells after treatment with 4 nm CuO NPs versus 24 nm CuO NPs. In short, it was apparent that 24 nm CuO NPs exhibited higher cytotoxicity compared to 4 nm CuO NPs. The higher cytotoxicity was particularly evident at 4 hours, 24 hours and 48 hours and when concentrations of loaded Cu were 0.94 – 1.57 mM, 0.31 – 1.57 mM and 0.31 – 0.94 mM, respectively.

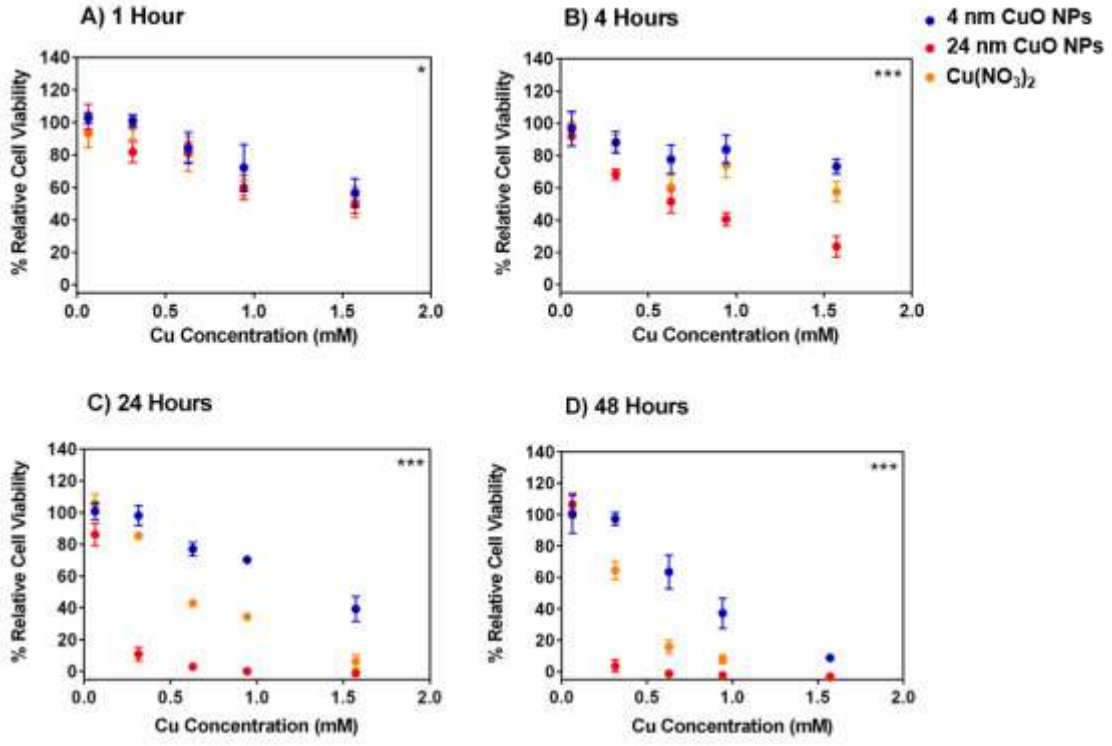

Figure 2-3. Cytotoxicity of 4 nm versus 24 nm CuO NPs: relative cell viability (%) of A549 cells after treatment with various concentrations of small and large CuO nanoparticles, $Cu(NO_3)_2$ solution and $NaNO_3$ solution for A) 1 hours, B) 4 hours, C) 24 hours and D) 48 hours. The data were plotted according to concentration (mM) and expressed as mean ± SD (n = 3-4). $NaNO_3$ was used as a control for nitrate effects and showed minimal cytotoxicity at all concentrations and all time points tested with relative cell viability > 95% (data no shown). Nonlinear regression, second order polynomial (quadratic), least squares fit were conducted to determine significant differences between 4 nm and 24 nm CuO NP treatments. *** $p < 0.001$, * $p < 0.05$

2.4.3. Effect of dissolved Cu^{2+} ions on A549 cytotoxicity

$Cu(NO_3)_2$ was used as a treatment alongside solid CuO NPs in order to determine the effect of dissolved Cu^{2+} on cell viability. $NaNO_3$ was used as a negative control to confirm that nitrate ions had no cytotoxic effects and that any decrease in cell viability can instead be attributed to Cu^{2+} in solution. There was no impact on cell viability due to treatment with NaNO3 relative to untreated cells at any time point or at any concentration (data not shown). However, the introduction of free Cu^{2+} from $Cu(NO_3)_2$ demonstrated both time- and concentration-dependent cytotoxicity in A549 cells. When compared to the cytotoxicity from NPs, it was found that cells that were treated with free Cu_{2+} showed lower cell viability

than cells that were treated with 4 nm CuO NPs but showed higher cell viability than cells that were treated with 24 nm CuO NPs (Figure 2-3). This was apparent especially at 4, 24 and 48 hour incubation periods.

In an attempt to investigate the underlying cause of CuO NP cytotoxicity, the dissolution of Cu^{2+} from the two differently sized CuO NPs was measured using ICP-OES after the particles were sonicated with RPMI-1640 media and incubated at 37 °C, 5% CO_2 for 1, 4, 24 and 48 hours (Figure 2-4). Three concentrations of CuO NPs (0.06, 0.63 and 1.57 mM) were chosen to represent the range of concentrations tested in the cytotoxicity assay. Because the TEM analysis of the supernatant did not show any particle presence, the concentrations obtained using ICP-OES can be attributed entirely to dissolved Cu^{2+}. In another study where CuO NP dissolution was tested in the presence of citric and oxalic acid the concentrations reported by ICP-OES consisted of both dissolved and smaller CuO nanoparticles.[107] The concentration of free Cu^{2+} in the media increased as the initial concentration of 4 nm and 24 nm CuO NPs in the media increased. For all concentrations tested the complete dissolution of Cu^{2+} from either type of NPs was not observed after 48 hours. Both types of CuO NPs released Cu^{2+} at similar levels at 24 and 48 hours which is approximately 50% of the original concentrations. However, the rates of free Cu^{2+} dissolution were different. Smaller 4 nm CuO NPs achieved ~50% dissolution into the surrounding medium over a 1 hour incubation period. Larger 24 nm CuO NPs took longer to reach ~50% Cu^{2+} dissolution (over 24 hours). Thus, 4 nm CuO NPs had a faster extracellular Cu^{2+} dissolution rate when compared to 24 nm CuO NPs.

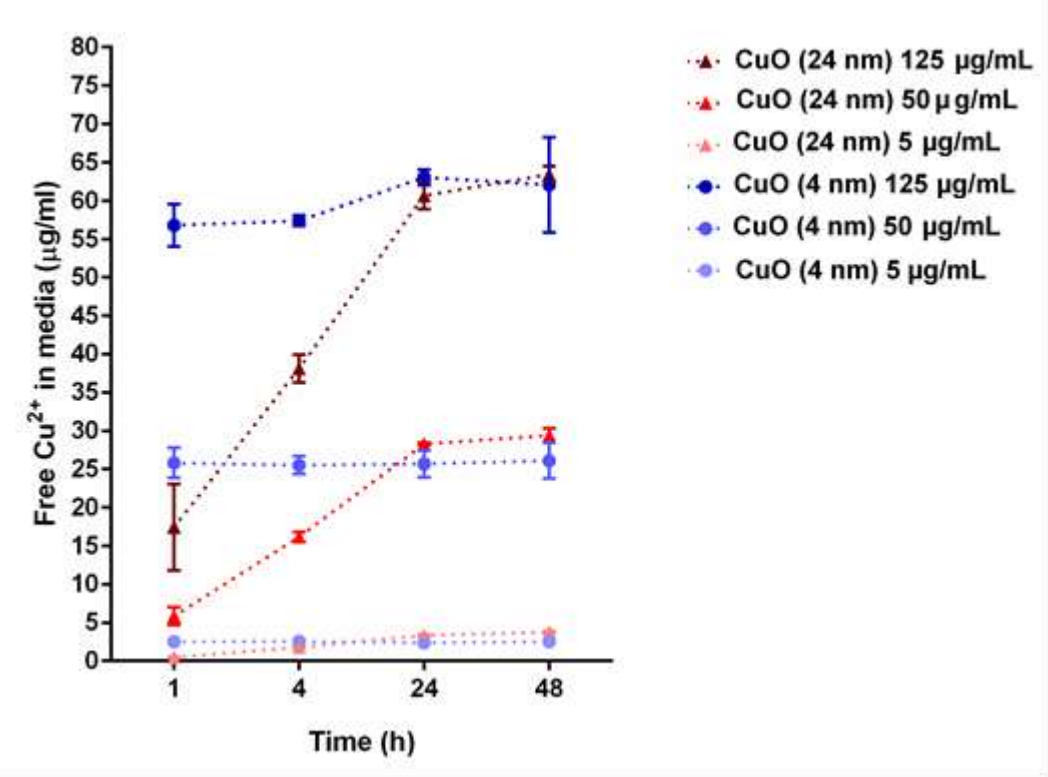

Figure 2-4. Dissolution of Cu^{2+} from small and large CuO NPs: varying concentrations of particles (5, 50 and 125 µg/ml which are equal to 0.06, 0.63 and 1.57 mM, respectively) were sonicated at 40% amplitude for 1 minute and then incubated in RPMI-1640 complete media for 1, 4, 24 and 48 hours. The data were plotted using free Cu^{2+} in media against time and expressed as mean ± SD (n = 3).

That there is a direct relationship between the degree of cytotoxicity and the concentration of soluble extracellular Cu^{2+} after 24 and 48 hours of exposure (Figure 2-3) suggests that free Cu^{2+} in solution may be one of the major causes of cytotoxicity seen with the small NPs used in these studies. In fact, free Cu^{2+} ions may have contributed to most of the cytotoxicity caused by the 4 nm Cu NPs. This preliminary assessment is based on the finding that the 4 nm CuO NPs released approximately 50% of their total loaded Cu as Cu^{2+} at 1 hour (Figure 2-4) and were less cytotoxic than the soluble $Cu(NO_3)_2$ exposed to the A549 cells at twice the concentration (for the 24 and 48 hour treatments), tentatively indicating at this stage that other factors were negligible in causing cytotoxicity. However, it appears to be a different situation for the 24 nm CuO NPs where it is likely that other or, more likely, additional factors may have contributed to the cellular cytotoxicity caused by these NPs aside from the extracellular release

of Cu^{2+} ions. This is because 24 nm CuO NPs caused greater cytotoxicity than 4 nm CuO NPs despite the finding that 4 nm NPs had a faster Cu^{2+} dissolution profile than 24 nm CuO NPs. Also, the 24 nm CuO NPs were significantly more toxic than soluble Cu^{2+} from $Cu(NO_3)_2$ which was exposed to cells at more than twice the concentration of soluble Cu^{2+} released by the CuO NPs.

2.4.4. Evaluation of intracellular and mitochondrial pro-oxidants induced by CuO NPs

Intracellular prooxidant levels (intracellular $O_2^{\bullet-}$) in A549 cells after treatment with 4 nm or 24 nm CuO NPs for 1, 4, 24 or 48 hours were assessed through the detection of DHE oxidation, which is indicative of superoxide anions ($O_2^{\bullet-}$) as well as other prooxidants. The results demonstrated that, at 1 hour and 4 hours (Figure 2-5A and 2-5B), there was a significant drop in prooxidant levels in cells treated with 24 nm CuO NPs which was not observed for the other treatments, including the 4 nm CuO NPs treatment. This finding for the 24 nm CuO NPs is possibly due to antioxidant defense mechanisms induced in the A549 cells in response to a metal-based NP challenge and has been shown to occur at 4 – 8 hours post-treatment in a previously published study where A549 cells were characterized for prooxidant levels after treatment with CuO NPs.[109-110] When prooxidants were measured at 24 and 48 hours (Figure 2-5C and 2-5D) there were significant increases (2-fold and 4-fold, respectively) in the cells that were treated with 24 nm CuO NPs compared to controls ($p < 0.001$), possibly due to exhaustion of the antioxidant defense system. In comparison, cells treated with 4 nm CuO NPs over 24 and 48 hours did not exhibit a significant increase in prooxidant levels compared to untreated cells. When 4 nm and 24 nm CuO NPs were compared, cells that were treated with 24 nm CuO NPs over 24 and 48 hours exhibited significantly higher levels of prooxidants when compared with cells that were treated with 4 nm CuO NPs ($p < 0.001$). Cells treated with free Cu^{2+} produced 2-fold higher levels of prooxidants at 24 and 48 hours than untreated cells. Overall, these results are consistent with the cytotoxicity assays (Figure 2-3) and confirm that 24 nm CuO NPs were more toxic when compared to free Cu^{2+} and 4 nm CuO NPs. It is possible that differences in prooxidant levels account for differences in cytotoxicity (Figure 2-3) observed when comparing 24 nm CuO NPs with $Cu(NO_3)_2$.

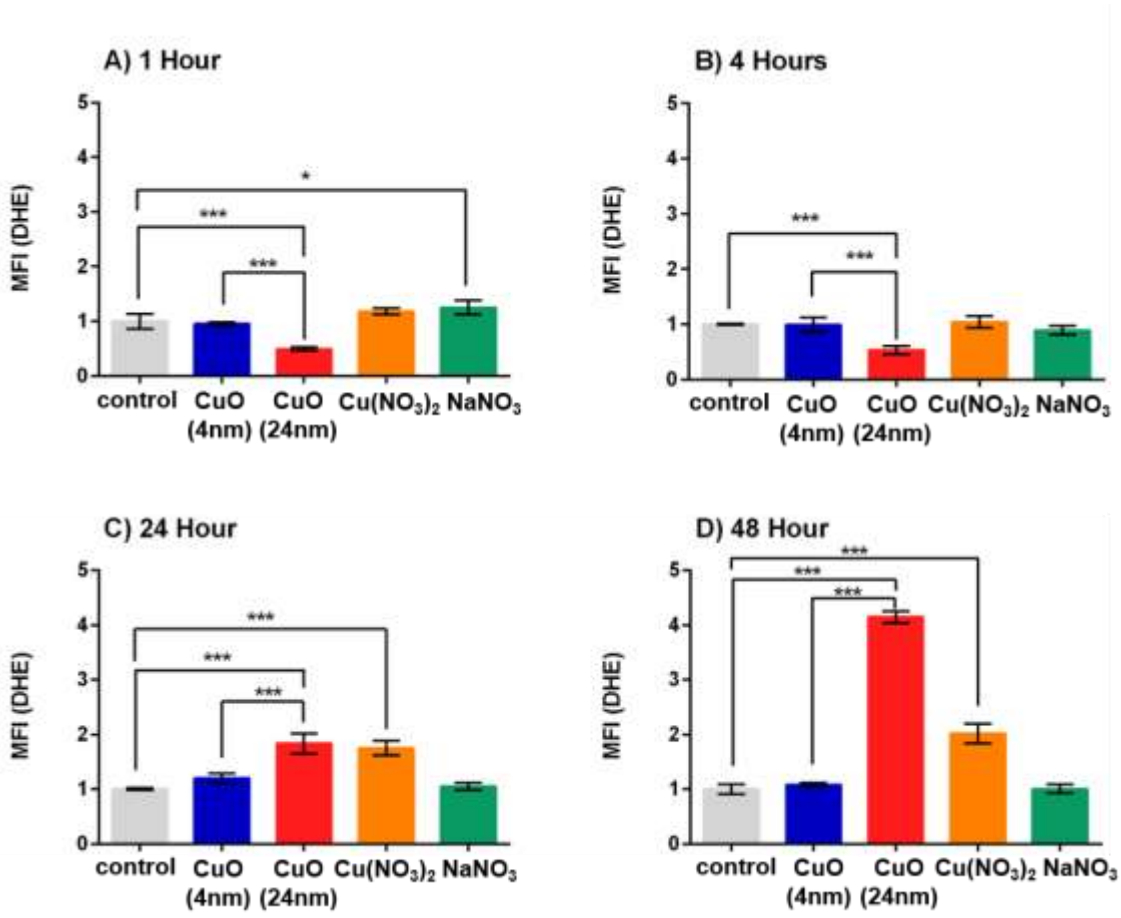

Figure 2-5. Intracellular pro-oxidants as detected by dihydroethidium oxidation (DHE): cells were incubated with small and large CuO NPs, $Cu(NO_3)_2$ and $NaNO_3$ at a dose of 0.12 µM Cu^{2+} concentration (10 µg/ml CuO NPs) for 1 hour (A), 4 hours (B), 24 hours (C) and 48 hours (B). Antimycin A increased the MFI by 3- to 5-fold when compared to the control group (data not shown). MFI represents mean fluorescence intensity which was normalized to the control group. Data are expressed as mean ± SD (n = 3). One-way analysis of variance with Bonferroni's multiple comparisons post-test was performed. *** $p < 0.001$, * $p < 0.05$.

In addition to quantitating intracellular $O_2^{\bullet-}$ and other prooxidants, mitochondrial superoxide production was measured in variously treated A549 cells using MitoSOX red 30. Two incubation periods (1 and 24 hours) were tested. It was found that at 1 hour, there were no substantive differences when comparing 24 nm CuO NPs with either the untreated control or the group treated with 4 nm CuO NPs (Figure 2-6A). At 24 hours, cells that were treated with 24 nm CuO NPs had significantly more mitochondrial superoxide (12-fold higher than the control group) ($p < 0.001$ when compared to control

and 4 nm CuO NPs). Cells that were treated with $Cu(NO_3)_2$ had 1.6-fold higher levels of mitochondrial ROS than the untreated cells. Mitochondrial ROS level in cells that were treated with 4 nm CuO NPs was comparable to untreated cells (MFI equal to 1) (Figure 2-6B). Treatment of cells with $NaNO_3$ showed no significant change when compared to the untreated cells at both incubation periods. The results obtained here and with the intracellular superoxide measurements performed above demonstrate that 24 nm CuO NPs induced higher mitochondrial and intracellular ROS than 4 nm CuO NPs and this difference in ROS production was likely to be another major cause of cytotoxicity for cells treated with the 24 nm CuO NPs.

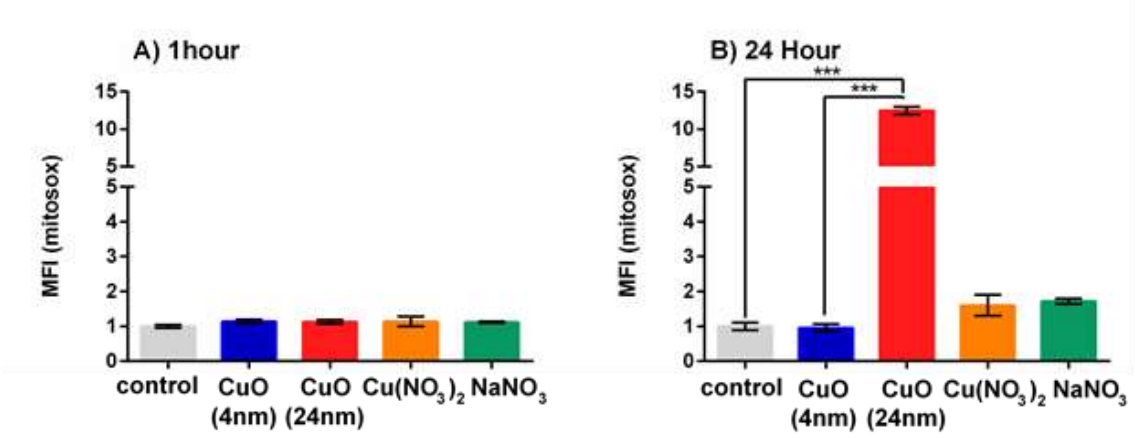

Figure 2-6. Mitochondrial pro-oxidants as detected by MitoSOX oxidation: cells were incubated with 4 nm and 24 nm CuO NPs, $Cu(NO_3)_2$ and $NaNO_3$ at a dose of 0.12 µM Cu^{2+} concentration (10 µg/mL CuO NPs) for 1 hour (A) and 24 hours (B). Antimycin A increased the MFI by 10- to 16-fold when compared to the control group at 1 hour and 24 hours, respectively (data not shown). MFI represents mean fluorescence intensity which was normalized to the control group. Data are expressed as mean ± SD (n = 3-5). One-way analysis of variance with Bonferroni's multiple comparisons post-test (the comparison between all groups to the control and between small - large CuO NPs) was performed. *** $p < 0.001$, * $p < 0.05$.

2.4.5. Quantification of the intracellular Cu^{2+} from cells that were treated with 4 nm and 24 nm CuO NPs

Both types of NPs studied here possessed similar surface and core oxide compositions (Figure 2-2) and the smaller 4 nm CuO NPs exhibited faster extracellular Cu^{2+} dissolution rates than the larger 24 nm CuO NPs (Figure 2-4), leading us to suspect that 4 nm CuO NPs may have been more cytotoxic than 24 nm CuO NPs. However, results from the MTS assays (Figure 2-3) showed that 24 nm CuO NPs were significantly more cytotoxic than 4 nm CuO NPs. This was particularly evident at 24 and 48 hours for the

lower Cu concentrations (Figure 2-3). Therefore, there are likely to be other factors, aside from Cu^{2+} dissolution rates, that contribute to the increased cytotoxicity of 24 nm CuO NPs. It is possible that these two types of NPs have different modes of entry or rates of uptake because of their difference in size, which consequently may affect the levels of Cu^{2+} accumulating within the cells. Although the presence of surface acetate groups (coming from the precursor used in the NP synthesis) in 4 nm CuO NPs can contribute ~2% to the mass if a monolayer coverage is assumed that can lower the actual exposure in the case of 4 nm Cu, it does not account for the significant differences in cell viability.

To study the possibility of different modes of entry or rates of uptake depending on the particle size, cells were incubated with 4 nm, 24 nm CuO NPs and $Cu(NO_3)_2$ for a range of times (1, 4, 24 and 48 hours), and then intracellular Cu^{2+} was measured using ICP-OES (Figure 2-7). In this experiment, cell suspensions were subjected to microwave digestion with concentrated HNO_3 thus; this intracellular Cu^{2+} that was detected via ICP-OES could come from either free Cu^{2+} or CuO in particulate form. At all incubation periods, the only group demonstrating relatively high intracellular Cu^{2+} was the one where the cells were treated with 24 nm CuO NPs ($p < 0.001$). Cells that were treated with 4 nm CuO NPs or $Cu(NO_3)_2$ showed low intracellular Cu^{2+} concentrations compared to the cells treated with 24 nm CuO NPs. These results suggest that 24 nm CuO NPs are more rapidly and more efficiently taken up by A549 cells that 4 nm CuO NPs.

There have been numerous reports on the cytotoxicity of CuO NPs both in vivo and in vitro.[111-116] There is still, however, a large degree of conjecture as to the mechanism(s) by which these NPs mediate their cytotoxicity. These differences are likely to stem from multiple variables between studies including the cell type studied and the properties of the particles used. This is further confounded by the possibility that multiple mechanisms may be responsible for nanotoxicity of CuO NPs as opposed to one major causative factor.

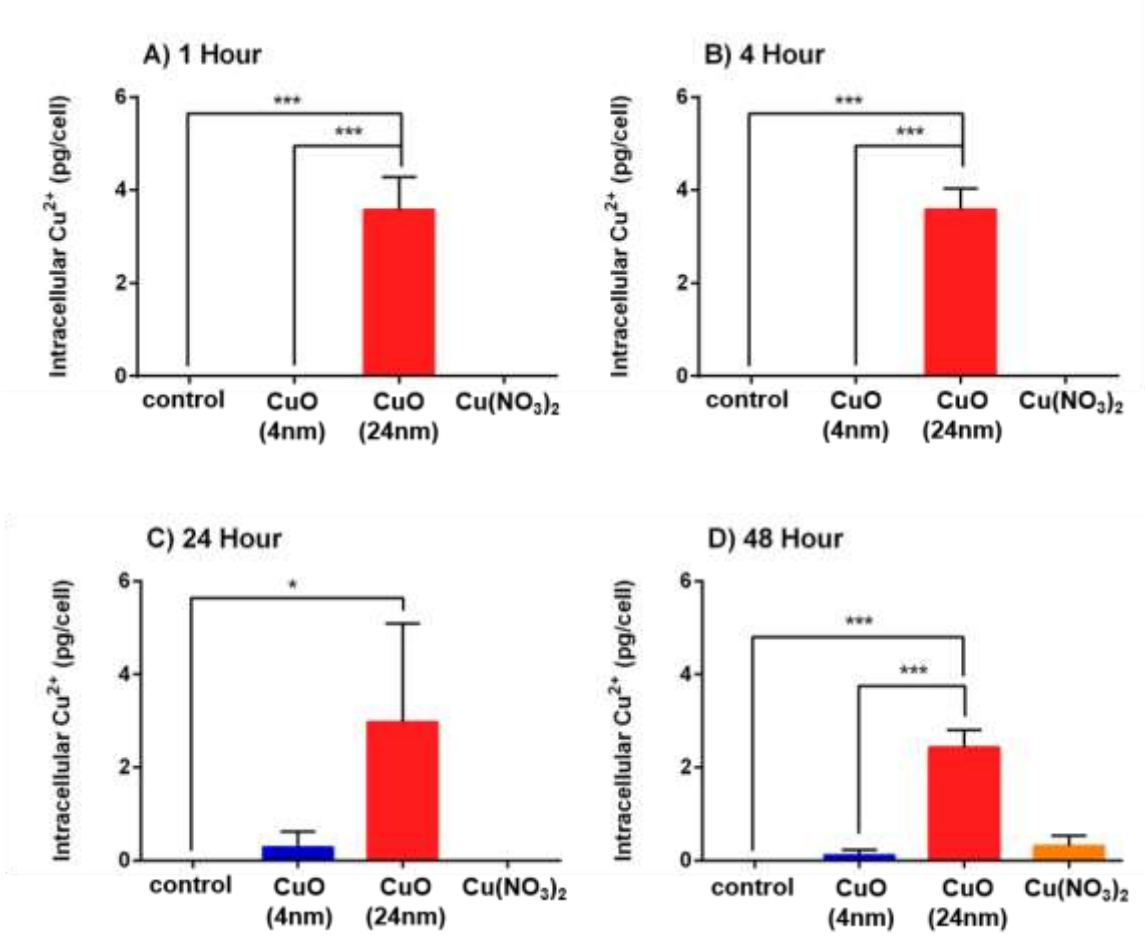

Figure 2-7. Intracellular Cu^{2+} uptake: cells were incubated with 4 nm and 24 nm CuO NPs, $Cu(NO_3)_2$ and $NaNO_3$ at a dose of 0.12 µM Cu^{2+} concentration (10 µg/mL CuO NPs) for 1 hour (A), 4 hours (B), 24 hours (C) and 48 hours (D). Data are expressed as mean ± SD (n = 3). One-way analysis of variance with Bonferroni's multiple comparisons post-test (the comparison between all groups to the control and between 4 nm and 24 nm CuO NPs) was performed. *** $p < 0.001$, * $p < 0.05$.

Previous studies addressing CuO NPs toxicity showed that among various metal oxide NPs, CuO NPs were among the most cytotoxic.[28, 116] Also, CuO NPs have higher cytotoxicity when compared with CuO microparticles.[43, 117-118] However, to the best of our knowledge, comparisons in toxicity of CuO NPs at the very small sizes used here have not been previously reported in the literature. Here, we measured and observed the differences in cytotoxicity of two groups of differently sized CuO NPs (4 nm and 24 nm). Surprisingly, the larger CuO NPs (24 nm) demonstrated higher cytotoxicity as well as inducing higher intracellular and mitochondrial ROS production than the smaller CuO NPs (4 nm), despite both

groups of NPs having identical chemical compositions and the 4 nm CuO NPs showing faster extracellular Cu^{2+} dissolution rates. Interestingly, cells treated with 24 nm CuO NPs showed comparatively high intracellular Cu^{2+} (Figure 2-7). This disparity in intracellular Cu^{2+} levels was likely due to the larger volumes (> 200-fold) of 24 nm NPs over 4 nm NPs. To a less significant degree, it is also possible that the rates of NP uptake were different, with uptake being slower for the 4 nm CuO NPs. The rate of entry and amount uptake of CuO NPs into the cell may have ultimately affected the level of intracellular accumulation of Cu^{2+} and consequently impacted on cytotoxicity in A549 cells. CuO NPs have been previously shown to rely on endocytosis to enter A549 cells.[110] Entry into acidic compartments (e.g. endolysosomes) usually ensues endocytosis and it has been demonstrated that CuO NPs release Cu^{2+} more rapidly at lower pH 6.[105] It may be that smaller 4 nm CuO NPs used here were not taken up by endocytosis as readily as 24 nm CuO NPs, perhaps due to their smaller diameter, which is substantially below the optimal size to trigger endocytosis[119], and may have relied upon an inefficient route of entry such as diffusion across the cell membrane. Such a situation, combined with the large volume differences, could have resulted in significant differences in intracellular Cu^{2+} levels and impacted on cytotoxicity through mechanisms dependent on ROS generation, although additional contributions to cytotoxicity through ROS–independent pathways cannot be ruled out, such as the inactivation of vital proteins through chelation or the inactivation of metalloproteins.[88] Based on our findings it is likely that the two differently sized CuO NPs investigated here imparted their cytotoxic effects through mostly disparate mechanisms. The smaller (4 nm) and less toxic CuO NPs are likely to have impacted on cytotoxicity through an undefined pathway caused by the extracellular release of Cu^{2+} which occurred at a faster rate compared to the larger (24 nm) CuO NPs, whilst the larger CuO NPs appeared to have mediated their higher cytotoxic impact through the promotion of greater intracellular and mitochondria ROS levels as a result of increased intracellular access.

2.5. Conclusions

Exposure of A549 cells to 4 nm versus 24 nm CuO NPs was performed to assess their cytotoxicity and multiple techniques were performed in an attempt to verify the potential causes of cell death. As a general conclusion, we found that NP-induced cell death may be a result of multiple contributing and cofounding factors, however, the predominant causal factor appeared to be dependent upon the size of the CuO NPs. We conclude that the extracellular dissolution of Cu^{2+} ions from CuO NPs can be cytotoxic to A549 cells and this seemed to be the primary reason for the cytotoxicity generated by the 4 nm CuO NPs. Despite having similar physicochemical properties (aside from size), the larger 24 nm CuO NPs proved to be significantly more cytotoxic than smaller 4 nm CuO NPs and we can surmise that this was due to post-internalization events resulting in significantly enhanced levels of prooxidants. Evaluating the cytotoxicity of CuO NPs is essential in order to address the safety of using such materials in biomedical applications where there is the potential for environmental and human exposure. Further evaluation of subtle differences in CuO NP physicochemical properties and the effect of those subtle differences on intracellular behavior and how they impact on cytotoxicity of off-target organisms is warranted and would be of benefit to further understand the potential and limitations of translational and human health applications of copper oxide NPs.

This chapter was adapted from Wongrakpanich, A.; Mudunkotuwa, I. A.; Geary, S. M.; Morris, A. S.; Mapuskar, K. A.; Spitz, D. R.; Grassian, V. H.; Salem, A. K., Size-dependent cytotoxicity of copper oxide nanoparticles in lung epithelial cells. Environ Sci-Nano 2016, 3 (2), 365-374.

3. IMPACT OF SERUM ON COPPER OXIDE NANOPARTICLE TOXICITY IN LUNG CELLS

3.1. Introduction

The rapid growth of nanotechnology in the 21st century has brought forth an immense variety of nanomaterials which are the platform for the development of numerous consumer products and applications. Currently, there are countless nanomaterials commercially available in a wide array of compositions, sizes and shapes and novel materials being developed on a regular basis. It is not surprising that with such high demand of nano-sized materials comes industrial-scale mass production. As large-scale production increases, so does the likelihood of human and environmental exposure. Like any new technology, there are safety concerns that need to be addressed and at this point it is not clear how long-term exposure of nanomaterials will effect human and environmental health. While efforts are being made to assess nanomaterial toxicity and implement safety regulations, there is a lack of standardization in the field which has led to inconsistent results from one study to the next. The basis for these conflicting data is a result of varying methods used across studies. In addition, it is often difficult to directly compare in vitro outcomes to those determined in vivo. Although the evaluation of nanomaterial toxicity in vivo is more relevant to biological systems compared to in vitro testing, it is costly, time consuming and there are ethical concerns that need to be considered. Therefore, the development of reliable and consistent in vitro assays are highly-desirable and can be used as a tool to screen nanomaterial toxicity before moving into animal models.

One of the most common routes of exposure of nanoparticles is through inhalation. As a result, there are many published studies evaluating the lung toxicity of nanoparticles using cultured lung cells as a model. A popular choice for assessing nanoparticle toxicity in vitro is the human-derived bronchial epithelial cell line known as BEAS-2B.[120-122] This cell line was established in the 1980s to study aging, differentiation and carcinogenesis of normal human bronchial epithelial cells.[123-126] Lechner and colleagues recognized that in the event of bronchogenic carcinoma, epithelial cells undergo terminal

squamous differentiation and they used this transformation to study the carcinogenic effects of substances.[126] A problem with using cultured bronchial epithelial cells, however, was that they underwent squamous differentiation when the calcium concentration of the cell culture medium was above 150 µM[126] and also in the presence of as little as 2% FBS.[125] Therefore, a serum-free cell culture medium was developed (known as LCH-9) to control squamous differentiation, maintain the original properties of the epithelial cells and to allow them to grow in replicative cultures.[123]

Although BEAS-2B cells are frequently used in the study of nanoparticle toxicity, the culture method varies greatly across these studies. Figure 1 shows a summary of the types of media used to culture BEAS-2B cells from research reports published in 2016 where nanotoxicity was the key focus. The most common medium used to culture the cells in these studies was Dulbecco's Modified Eagle Medium (DMEM) supplemented with 10% FBS. The majority of cell culture medium used was supplemented with 10% FBS rather than serum-free. As stated previously, BEAS-2B cells undergo terminal squamous differentiation when exposed to as little as 2% FBS.

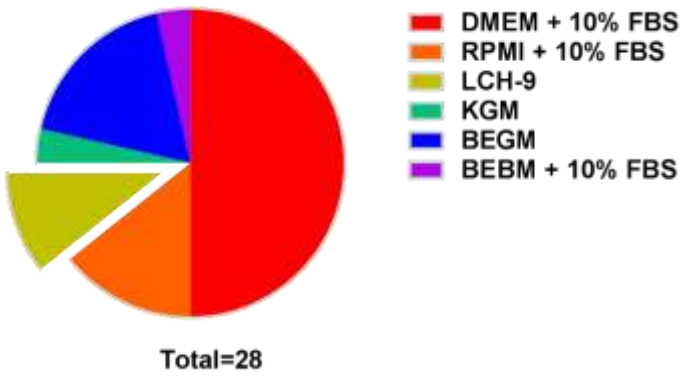

Figure 3-1. Summary of medium used to culture BEAS-2B cells in nanotoxicity articles published in 2016.

Because of the inconsistencies in culture methods of BEAS-2B cells published in the scientific literature, the goal of our study was to determine whether the presence of FBS in cell culture medium impacts the toxicity outcomes of copper oxide (CuO) nanoparticles (NPs). Previously, we established that

there is a size-dependent effect on the cytotoxicity of A549 cells from CuO NPs.[32] In the present study, we investigated NP-induced cell death from the same CuO NPs in BEAS-2B cells cultured in medium supplemented with varying amounts of FBS. To provide some insight into the cytotoxicity, aggregation and cell uptake of the NPs was also evaluated. The broader implications of this study are to highlight the dramatic effect that cell-culture method has on BEAS-2B cytotoxicity to demonstrate the importance of consistency in nanotoxicological evaluations.

3.2. Methods and Materials

3.2.1. CuO NP Characterization and Aggregation

CuO NPs (see Chapter 2.3.1 for source) were suspended in water and a small drop was placed on a carbon-coated copper grid. After about 1 minute, the water was removed and the samples were analyzed using a transmission electron microscope (TEM) (JEOL JEM-1230). Particle size distributions were determined using ImageJ software. To study aggregation, CuO NPs were suspended in LCH-9 medium containing various concentrations of fetal bovine serum (FBS) (0-10%). Hydrodynamic diameter and polydispersity index (PDI) was measured using a ZetaSizer NanoZS (Malvern)

3.2.2. Cell Culture

BEAS-2b cells were purchased from ATCC and maintained in LCH-9 medium (Thermo Fisher Scientific). BEAS-2B cells were grown in 75 cm^2 tissue culture flasks that were coated with 0.01 mg/mL fibronectin (Sigma), 0.03 mg/mL collagen (Sigma) and 0.01 mg/mL bovine serum albumin (Sigma).

3.2.3. Cytotoxicity Studies in BEAS-2B Cells

To study the dose effects of CuO nanoparticles, BEAS-2B cells were removed from the culture dishes using trypsin with 0.5% polyvinylpyrrolidone (PVP). Next, the cells were resuspended in LCH-9 medium with or without 10% FBS. The cells were seeded into a pre-coated (as mentioned above) 96-well plate at a density of 1×10^4 cells per well. The cells were incubated with the medium at 37 °C and 5% CO_2 for 24 hours. Then, 200 µL of copper oxide nanoparticle suspension or copper nitrate (Provider) (4-

100 µg/mL of copper) dissolved in LCH-9 medium with and without 10% FBS was added to the 96-well plate. Cells treated with LCH-9 medium or LCH-9 medium plus 10% FBS served as control groups and were used to normalized copper-treated groups. The treatments were incubated with the cells for 24 hours after which, they were removed and replaced with 100 µL of fresh medium. Then, 20 µL of MTS reagent (provider) was added to each well and incubated at 37 °C for up to 4 hours. The 96-well plates were centrifuged at 500 × g for 20 minutes to sediment any remaining copper oxide nanoparticles and 70 µL of supernatant was carefully removed from the original plate added to a new 96-well plate for analysis. A SpectraMax plate reader was used to determine the absorbance of each sample at 490 nm.

To determine the effect of serum on CuO nanoparticle toxicity, cells were removed from the culture dishes as mentioned above and resuspended in LCH-9 medium containing varying concentrations of FBS (0-10%). Then, cells were plated in a pre-coated 96-well plate at a concentration of 1×10^4 cells per well. The cells were left to incubate for 24 hours at 37 °C and 5% CO_2. Next, CuO NPs were suspended in LCH-9 medium containing various concentrations of FBS at 40 µg/mL of copper. Copper nitrate was dissolved in medium containing various concentrations of FBS at the same copper concentration. Then, the previous medium was removed from the cells and replaced with 200 µL of nanoparticle suspension or copper nitrate solution. After 24 hours, the treatment was removed and the MTS assay was performed exactly as mentioned above. Controls (containing cells only) were prepared for each concentration of FBS in which the data were normalized to as well as method blanks for each concentration of FBS used during spectrophotometric analysis.

3.2.4. Cell Uptake of CuO NPs in BEAS-2B

BEAS-2B cells were seeded into pre-coated 60 mm cell culture plates at a density of 2×10^5 cells per dish using LCH-9 medium alone, LCH-9 medium containing 3% FBS or LCH-9 medium containing 10% FBS. After 24 hours of incubation at 37 °C and 5% CO_2, the cells were treated with 4 mL of nanoparticle suspensions (10 µg/mL) in medium alone or medium containing 3% or 10% FBS. After 24 hours, the treatments were removed and the cells were gently washed three times with PBS to remove any residual

CuO nanoparticles or free Cu ions. Then, the cells were removed from the dishes using trypsin/PVP and centrifuged at 230 × g for 5 minutes. The supernatent was removed and the cells were resuspended in 1 mL of PBS. A small amount (30 µL) of each sample was collected to count the number of cells using trypan blue. After counting the cells, they were centrifuged at 230 × g for 5 minutes. The PBS was removed from the cell pellet and replaced with 100 µL of concentrated nitric acid for digestion overnight. After digestion, each sample was then diluted with 5 mL of 1% nitric acid for analysis with ICP-MS. A standard curve was prepared using copper nitrate dissolved in 1% nitric acid (0-500 ppb) and analyzed alongside the cell samples. Indium was used as an internal standard for all samples and calibration solutions.

3.2.5. Statistical Analysis

Data are expressed as mean ± standard deviation. All statistical analysis was performed using GraphPad Prism software. One-way ANOVA was used in combination with Tukey's post-test. P-values are as follows: * $p < 0.05$, ** $p \leq 0.01$, *** $p \leq 0.001$, **** $p \leq 0.0001$

3.3. Results and Discussion

3.3.1. CuO NP Characterization

The CuO NPs used in the study were previously characterized another study.[32] Two sizes of NPs were used in this study, 5 nm and 35 nm as determined with TEM (Figure 3-1). The 5 nm parties were spherical and highly aggregated during TEM analysis (Figure 3-1A). The larger, 35 nm NPs were not as uniform in shape as the smaller particles and were not as aggregated (Figure 3-1B). The 35 nm NPs had a broad size distribution of 35 ± 19 nm whereas the smaller particles were more monodispersed and had a size distribution of 5 ± 1 nm (Figure 3-1C). Previous X-ray diffraction (XRD) analysis of the particle surfaces confirmed that both sizes of NPs consisted of a single tenorite phase and X-ray photoelectron spectroscopy (XPS) analysis showed that the oxidation state of copper was the same in both types of NPs

(Cu(II)) (see Figure 2-2). Furthermore, both types of NPs released similar amount of Cu^{2+} into the cell culture medium after 24 hours.[32] These characterization steps were performed to verify that the only physicochemical differences between the two types of CuO NPs was their size.

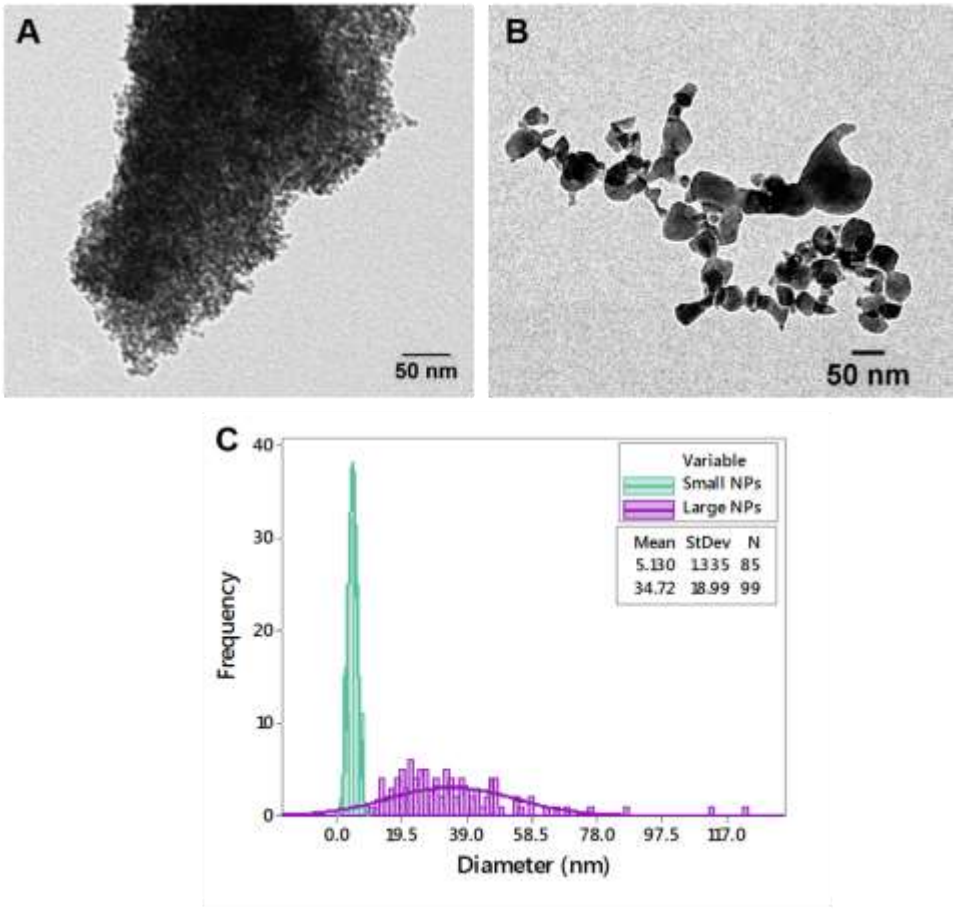

Figure 3-2. TEM image of (A) 5 nm CuO NPs and (B) 35 nm CuO NPs. (C) Particle size distributions of CuO NPs determined from TEM images.

3.3.2. Serum Effects on CuO NP Cytotoxicity in BEAS-2B Cells

As mentioned previously, BEAS-2B cells are a commonly used cell line to study lung toxicity of nanoparticles. The majority of the published studies using this cell line used media that has been supplemented with 10% FBS. Therefore, to elucidate the role of serum on CuO NP cytotoxicity, cells were cultured in a 96-well plate in either LCH-9 medium or LCH-9 containing 10% FBS. The only difference between these groups was the presence or absence of serum in the media. The cells were then

treated for 24 hours with varying concentrations of 5 nm and 35 nm CuO NPs after which, the MTS assay was performed to quantify percent relative cell viability. We formerly established that the CuO NPs used in this study can dissolve into Cu^{2+} ions (as much as 50% after 24 hours, Figure 2-4).[32] Therefore, copper nitrate was used as a control to test the toxicity of soluble copper ions on BEAS-2B cells.

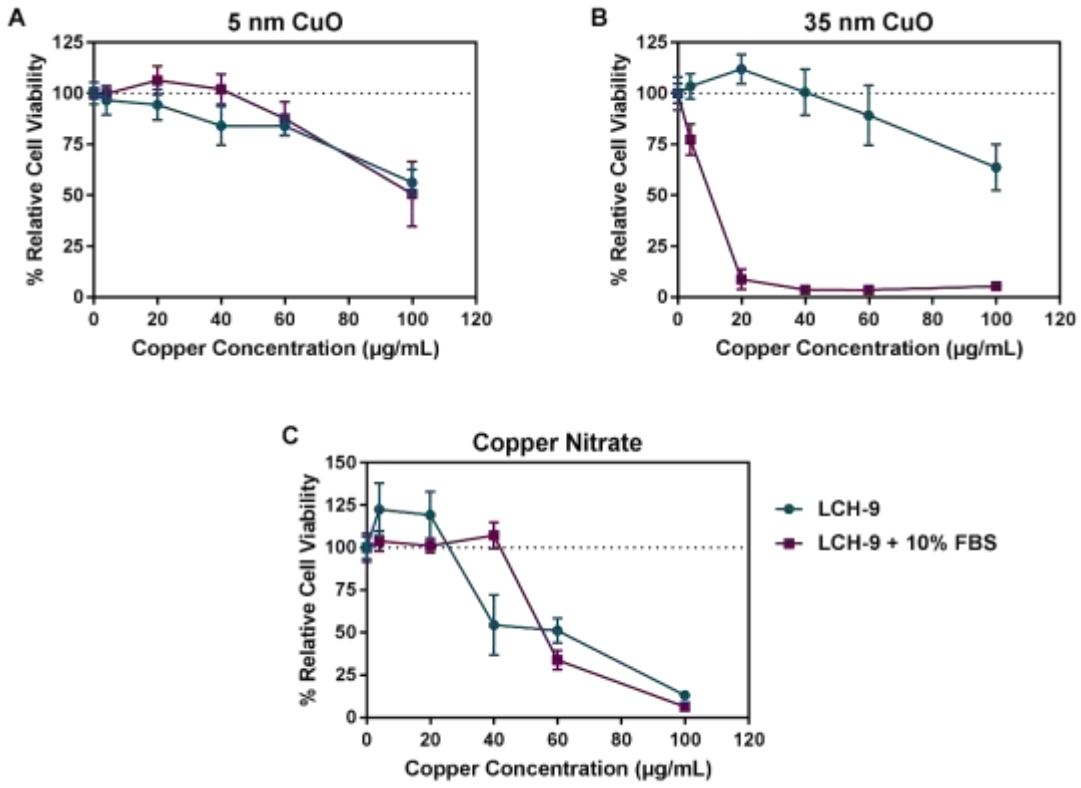

Figure 3-3. Effect of FBS on the cytotoxicity of BEAS-2B cells treated with various concentrations of (A) 5 nm CuO NPs, (B) 35 nm CuO NPs and (C) copper nitrate in either LCH-9 medium or LCH-9 medium containing 10% FBS. Cells were treated for 24 hours.

The cells were treated with the same range of copper concentrations either in particulate form or soluble copper in the case of copper nitrate. Figure 3-3A shows the cytotoxicity results from the 5 nm CuO NPs. At all concentrations tested, there was no significant differences in the relative viability of cells cultured with or without FBS. Remarkably, the presence of serum had a dramatic effect on relative viability of the cells treated with 35 nm CuO NPs (Figure 3-3B). When the cells were cultured in LCH-9

medium alone, there was notable cytotoxicity only at the highest concentration tested (100 µg/mL copper). In contrast, when the medium was supplemented with 10% FBS, there is a decrease in cell viability at every dose. In fact, complete cell death was observed at concentrations above 5 µg/mL of copper.

The cells that were treated with copper nitrate responded similarly with or without FBS for the 5 µg/mL and 20 µg/mL doses (Figure 3-3C). However, there was discrepancy between the two culture methods at the 40 µg/mL dose. At this dose, the relative viability of cells cultured with LCH-9 decreased to around 50% while the cells cultured with serum-supplemented LCH-9 medium remained viable. This phenomenon is not readily apparent at the higher doses.

Because DMEM with 10% FBS is the most common medium used to culture BEAS-2B cells, we tested the cytotoxicity of both sizes of CuO nanoparticles in cells cultured in this medium and found that the outcomes were similar to cells cultured in LCH-9 with 10% FBS. The 4 nm CuO NPs caused little cytotoxicity whereas the 35 nm CuO NPs were extremely cytotoxic to BEAS-2B cells at all concentrations tested. These data demonstrate the large effect that cell culture method has on BEAS-2B cells and the importance of standardization in in vitro cytotoxicity assays. Because of the inconsistency in experimental methods used from study to study, it is difficult to draw concrete conclusions for CuO NPs in BEAS-2B cells.

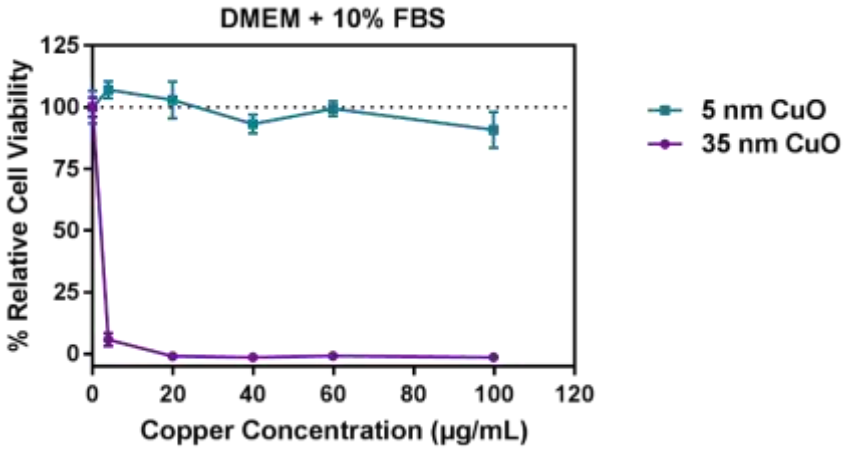

Figure 3-4. Effect of CuO NPs on the cytotoxicity of BEAS-2B cells cultured in DMEM medium supplemented with 10% FBS. Cells were treated for 24 hours.

Clearly, these data show that culturing BEAS-2B cells with and without serum has an effect on cytotoxicity outcomes depending on the size of CuO NPs being used and at soluble copper concentrations around 40 µg/mL. To gain further insight, we next investigated the effect of varying serum concentration on BEAS-2B cytotoxicity. In this study, cells were cultured in 96-well plates in LCH-9 medium supplemented with 0-10% FBS. The cells were then treated with CuO NPs or copper nitrate at a copper concentration of 40 µg/mL for 24 hours before using the MTS assay to determine the relative percent cell viability. Interestingly, BEAS-2B cells treated with 5 nm CuO NPs had a relative cell viability of around 75% at 0% FBS, however, at 1% FBS, the cell viability rose to 100% and remained near 100% for all higher concentrations of FBS used. The same trend was observed for the copper nitrate treatment only with the rise in cell viability occurring at 2% FBS rather than 1% as seen in the 5 nm CuO treatment. It is possible that the cytotoxicity observed for the 5 nm CuO NPs is due to dissolved Cu^{2+} ions. Our previous work revealed that smaller CuO NPs undergo dissolution much faster than larger NPs and can release significant amounts of Cu^{2+} after just 1 hour in solution. In fact, at the dose tested here (50 µg/mL of CuO NPs or 40 µg/mL equivalent copper concentration) the soluble Cu^{2+} concentration after 1 hour is around 25 µg/mL. Moreover, the release of Cu^{2+} from smaller CuO NPs remains constant at this concentration

over the course of 24 hours. However, it takes the larger NPs 24 hours to release the same amount of Cu^{2+} that the smaller NPs release in just the first hour. These release kinetics and the resulting early exposure of cells to significant concentrations of soluble Cu^{2+} could play a role in the decreased viability of cells treated with 5 nm CuO NPs and cultured in LCH-9 medium with no FBS. As mentioned previously, 10% FBS appears to prevent cells from Cu^{2+}-induced death at 40 μg/mL copper as seen in Figure 3-3 and the same trend is apparent in Figure 3-5 for copper nitrate and 5 nm CuO treatments.

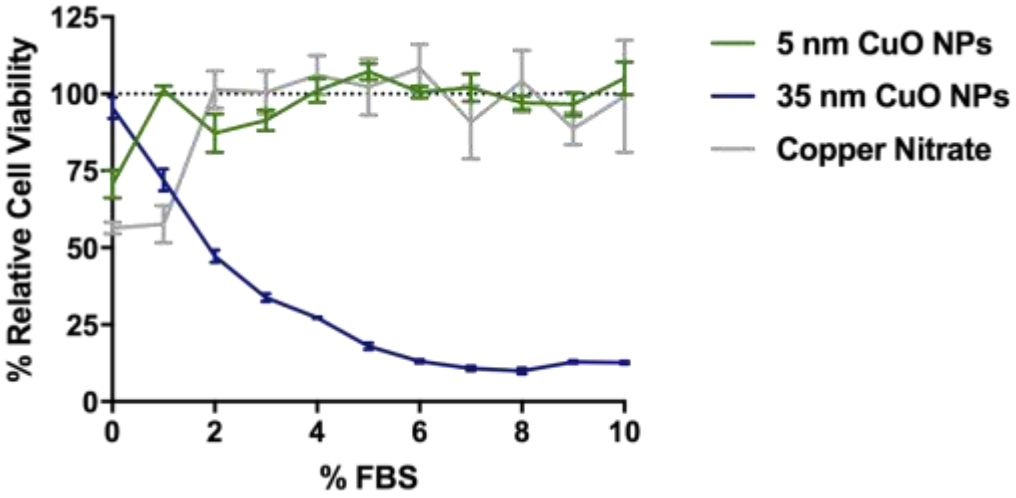

Figure 3-5. Cytotoxicity results of BEAS-2B cells treated with 5 nm CuO NPs, 35 nm CuO NPs and copper nitrate (copper concentration of 40 μg/mL for all treatments) in LCH-9 medium supplemented with varying concentrations of FBS. Cells were treated for 24 hours.

BEAS-2B cells treated with 35 nm CuO NPs exhibited the opposite trend in cell viability compared to the 5 nm CuO NP and copper nitrate-treated cells (Figure 3-5). There is a systematic, dose-dependent decrease in the relative cell viability for increasing concentrations of FBS used to culture the cells. These results imply that serum plays a direct role in the susceptibility of BEAS-2B cells to undergo 35 nm CuO NP-related cell death. A similar trend was observed when BEAS-2B cells were cultured in DMEM

medium containing 10% FBS (Figure 3-4) demonstrating that serum is a key player in BEAS-2B toxicity outcomes to CuO NPs and needs to be carefully considered when comparing results across multiple studies.

3.3.3. Effect of Serum on NP Aggregation

Nanoparticles are commonly employed for their small size and unique material properties that are exclusive to the nanometer size-range. However, many types of readily aggregate in aqueous solutions especially when introduced to complex matrices such as biological media.[127] Aggregation of nanoparticles can have a significant impact on many biological interactions such as cell uptake which is known to be a size-dependent process.[128] Furthermore, serum in biological fluids is known to strongly adsorb to the surface of solid particles and this can play a major role in the degree of aggregation of NPs as well as influence the interactions of NPs with cells.[129-130] Here, the aggregation of CuO nanoparticles was investigated in LCH-9 culture medium with and without FBS (Figure 3-2). Table 3-1 summarizes the hydrodynamic diameters of each type of NP measured after suspending them in LCH-9 medium containing increasing amounts of FBS. When the nanoparticles were suspended in LCH-9 medium only (0% FBS), the average hydrodynamic diameters of the two size of NPs were 326 ± 27 nm for the smaller NPs and 648 ± 56 nm for the larger NPs. Clearly, both types of NPs undergo aggregation in the presence of LCH-9 medium. Through TEM analysis described previously, it was determined that the average diameter of the smaller nanoparticles was 5 nm with a narrow size distribution. However, when suspended in LCH-9 medium, they form agglomerates of more than 65-times their original size and these agglomerates can vary in size. Similarly, the larger NPs utilized in this study measured around 35 nm in diameter from TEM analysis but formed aggregates of more than 18-times the size of a single a particle in LCH-9 medium. Because of the broad innate size distribution of the 35 nm NPs (Figure 3-1C) there is a resulting large size distribution of aggregates formed after suspension in LCH-9 medium.

Table 3-1. Summary of hydrodynamic diameters and PDI of CuO NPs in LCH-9 medium containing 0-10% FBS.

		5 nm CuO NPs		35 nm CuO NPs	
		Avg Diameter ± SD (nm)	PDI ± SD	Avg Diameter ± SD (nm)	PDI ± SD
% FBS	0	326 ± 27	0.7 ± 0.2	648 ± 56	0.3 ± .01
	1	232 ± 96	0.6 ± 0.2	284 ± 50 *	0.23 ± 0.03
	5	210 ± 117	0.4 ± 0.1	297 ± 44 *	0.27 ± 0.05
	10	174 ± 28	0.4 ± 0.1	300 ± 138 *	0.23 ± 0.05

As seen in table 3-1, there was a trend toward smaller aggregate size when higher concentrations of FBS were present in the medium for both sizes of NPs. Despite the trend, there were no significant differences between the average hydrodynamic diameters of the 5 nm CuO NPs in any of the solutions tested most likely due to the high degree of variability in size of the aggregates formed. However, average hydrodynamic diameters of the larger, 35 nm NPs, were statistically smaller in all the solutions containing FBS compared to LCH-9 alone (0% FBS). It is intriguing that both sizes of NPs form similarly sized aggregates in the presence of FBS even though they clearly have unique size distributions determined through the physicochemical characterization which was mentioned above.

PDI can be used as an indication of monodispersity where highly monodispersed samples have low PDI values (<0.1) and samples with broad size distributions have PDI values closer to 1. As indicated in Table 3-1, the larger CuO NPs were more monodispersed compared to the smaller CuO NPs indicated by PDI values of 0.3 and 0.7, respectively, when no FBS was present. The addition of FBS had different effects on monodispersity between the two type of NPs. Specifically, there was a decrease in PDI for the 5 nm CuO NPs with increasing amounts of FBS present in the LCH-9 medium. This implies FBS had an influence on the uniformity of aggregates formed by 5 nm CuO NPs in cell culture medium. Interestingly, FBS did not have a notable effect on the PDI of the 35 nm CuO NPs at any of the concentrations tested.

3.3.4. NP Uptake in BEAS-2B Cells

Cell uptake is a major player in NP-induced cytotoxicity. From our previous work, we determined, by ICP-OES, that larger CuO NPs were taken up by A549 cells more readily compared to the smaller NPs.[32] The cells incubated with larger CuO NPs had significantly more intracellular copper after 24 hours compared to cells exposed to smaller CuO NPs. The same trend was observed in the current study (Figure 3-6). BEAS-2B cells treated with 35 nm CuO NPs had over 200-times more intracellular Cu^{2+} compared to BEAS-2B cells treated with 5 nm CuO NPs. The 5 nm CuO NPs were able to enter BEAS-2B cells to some extent indicated by the 3-fold average increase in intracellular Cu^{2+} of 5 nm CuO NP-treated cells compared to the control cells that were only exposed to LCH-9 medium without any NPs, however, these data were not significantly different from each other or from the control.

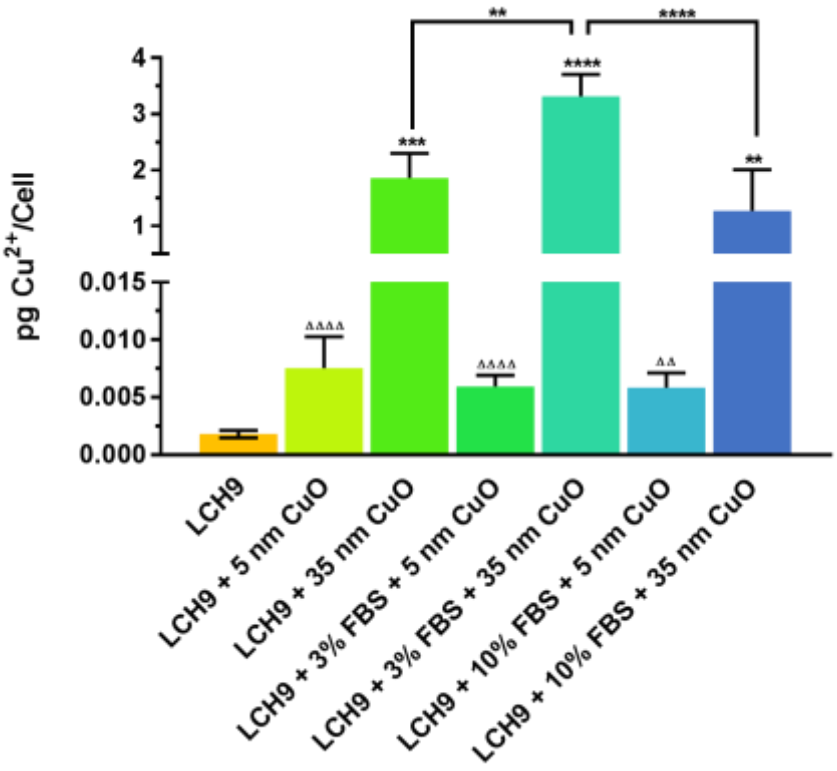

Figure 3-6. Uptake of CuO NPs in BEAS-2B cells after 24 hours. A control group exposed to only LCH-9 medium without any NPs was used to determine the baseline signal (labeled "LCH9"). All NP treatments were 10 µg CuO NPs/mL medium. The "*" symbol without brackets represents the significant difference of the experimental group versus the control (LCH9). ** $p \leq 0.01$, *** $p \leq 0.001$, **** $p \leq 0.0001$; The "Δ" symbol represents the significant differences of 5 nm CuO NPs compared to 35 nm CuO NPs at the same concentration of FBS. The number of symbols corresponds to the p-values mentioned above.

Although it has been previously established that larger CuO NPs are taken up more readily by lung cells compared to smaller CuO NPs, we wanted to investigate the effect of serum on NP uptake in BEAS-2B cells and determine whether it contributes to cell death. As seen in Figure 3-6, there was no difference in CuO NP uptake for BEAS-2B cells cultured in various concentrations of FBS (0, 3 and 10% FBS) and treated with 5 nm CuO NPs. We can conclude that for the smaller size of CuO NPs, serum does not enhance nor inhibit cell uptake. Because there was little cytotoxicity observed at this concentration of NPs (10 µg CuO NPs/mL or 8 µg copper/mL) the increase in intracellular copper does not appear to be detrimental to cells for any of the culture methods used.

For the larger 35 nm CuO NPs, there were significant differences in BEAS-2B cell death at the lower NP concentrations when varying concentrations of FBS were used to culture the cells. For example, the percent relative cell viability of BEAS-2B cells treated with 5 µg/mL of 35 nm CuO NPs (or 4 µg copper/mL) decreased from around 100% to about 77% when the concentration of FBS in LCH-9 medium was increased from 0% to 10%, respectively. Since there was a significant decrease in cell viability from 35 nm CuO NPs with increasing FBS concentration, it was hypothesized that higher concentrations of FBS might lead to enhanced NP uptake which could account for differential cytotoxicity when varying amounts of serum are present in LCH-9 medium. The results shown in Figure 3-6 suggest that serum did enhance uptake of 35 nm CuO NPs in BEAS-2B cells when the concentration of FBS in the LCH-9 medium increased from 0% to 3%. However, when the FBS content was increased even further to 10%, the uptake of 35 nm CuO NPs returned to levels similar to 0% FBS suggesting that the uptake of 35 nm CuO NPs is influenced by FBS to some extent but is not directly FBS-dependent. Because of this conclusion, the systematic decrease in the cytotoxicity of BEAS-2B cells cultured in increasing concentrations of serum (shown in Figure 3-5) is not caused by CuO NP uptake since it appears as though there is no direct correlation between uptake and FBS concentration used to culture the cells.

3.4. Conclusions

In this study, it is apparent that the culture method of BEAS-2B cells plays a direct role in the toxicity outcomes of CuO NPs. Of the two sizes of NPs that were investigated, 35 nm CuO NPs were drastically more cytotoxic to BEAS-2B cells when LCH-9 medium was supplemented with 1% or more FBS while 5 nm CuO NPs seemed to be less cytotoxic to BEAS-2B cells cultured in serum containing medium. At this point, the mechanism of FBS-related NP cytotoxicity is not clear. We do not believe it is due to particle aggregation since both sizes of NPs aggregate to a similar degree in the presence of serum. In addition, soluble Cu^{2+} is not the major contributor to BEAS-2B cell cytotoxicity due to the distinct differences seen in the cell viability results between the copper nitrate treatment and 35 nm CuO NP treatment when

varying concentrations of FBS were used to culture the cells. Uptake of CuO NPs by BEAS-2B cells is a size-dependent process that does not appear to be largely affected by serum. Based on our findings herein, it can be concluded that when using BEAS-2B cells for nanotoxicity studies, it is critical to consider the cell culture method especially when comparing separate studies as the results may vary according to the medium used. Further work is needed to determine the exact mechanism of CuO NP toxicity. Future efforts will be focused more towards the cellular phenotypic differences that may arise in BEAS-2B cells from exposure to serum[131] and how these changes impact nanotoxicity.

4. PULMONARY TOXICITY OF BARE SILICA NANOPARTICLES VERSUS AMINE-MODIFIED SILICA NANOPARTICLES

4.1. Abstract

Amorphous silica nanoparticles (NPs) possess unique material properties that make them ideal for many different applications. However, the impact of these materials on human and environmental health needs to be established. We investigated nonporous silica NPs both bare and modified with amine functional groups (3-aminopropyltriethoxysilane (APTES)) to evaluate the effect of surface chemistry on biocompatibility. In vitro data showed there to be little to no cytotoxicity in a human lung cancer epithelial cell line (A549) for bare silica NPs and amine-functionalized NPs using doses based on both mass concentration (below 200 μg/mL) and exposed total surface area (below 14 m^2/L). To assess lung inflammation, C57BL/6 mice were administered bare or amine-functionalized silica NPs via intra-tracheal instillation. Two doses (0.1 and 0.5 mg NPs/mouse) were tested using the in vivo model. At the higher dose used, bare silica NPs elicited a significantly higher inflammatory response, as evidence by increased neutrophils and total protein in bronchoalveolar lavage (BAL) fluid compared to amine-functionalized NPs. From this study, we conclude that functionalization of nonporous silica NPs with APTES molecules reduces murine lung inflammation and improves the overall biocompatibility of the nanomaterial.

4.2. Introduction

Inorganic nanomaterials (<100 nm in size), including silica NPs, have been increasingly utilized in a wide variety of applications due to their unique material properties such as tunable size and ease of surface functionalization.[132-134] There are well-established methods for the synthesis of silica NPs in addition to commercial availability that make them prime candidates for applications such as drug delivery[135-137] and biomedical imaging.[138-139] Silica NPs are also commonly used as additives in many products including cosmetics, varnishes and printer toners.[52, 140]

Silica materials are composed of silicon dioxide (SiO_2) and are present in crystalline and amorphous forms. Quartz is the most common form of crystalline silica. Amorphous and crystalline silica NPs can enter the body through different routes, one of the most common being inhalation of free silica into the lungs which can potentially lead to pulmonary disorders.[141] The toxicity of crystalline silica has been studied for many years, especially in connection with chronic bronchitis, emphysema and silicosis.[142-144] While toxicity related to inhalation of larger, crystalline silica has been well-documented[145-147] more studies are needed to evaluate amorphous particles in the nanometer size range. Although silica NPs are used in many applications because of their small size and large surface area, these same properties could lead to increased toxicity in biological systems compared to larger silica particles.[52, 92] For example, the small size of NPs allows for increased interactions with biological tissues and enhanced cellular uptake.[52, 148-149] It is recognized that particles less than 1 μm in aerodynamic diameter penetrate more distally into lung tissue whereas larger particles (> 5 μm) deposit primarily in the upper airways.[150-151] Previously, amorphous silica NPs were considered to be less toxic than crystalline silica; however recent studies found that amorphous silica particles induce substantial lung inflammation.[50] In addition to size, surface charge of the NPs could influence NP-cell interactions.[152-153] As the potential for human exposure increases, it is critical to evaluate the safety of nano-sized materials especially in occupational settings where engineered nanomaterials are manufactured or handled in bulk quantity.[154] Furthermore, development of methodologies for production of safe silica particles that would produce less toxicity/inflammation are very important. In the last several years, many efforts have been made in particle surface modification with the aim to decrease their potential toxicity.[155-156]

Numerous in vitro studies have been published in the literature investigating the cytotoxicity of amorphous silica NPs on cultured cell lines.[140, 157-159] While in vitro experiments are commonly used to predict the toxicity of engineered silica NPs in vivo, the results often are not informative because of the over-simplified environment of cell culture experiments versus animal models where there is a more complex, physiological environment.[160-162] Although the evaluation of the side effects of silica NPs have

been investigated previously, there is a lack of data in the literature where both in vitro and in vivo studies have been performed using the same batch of silica NPs and reported together in a single study.

Many applications such as gene delivery,[134, 163] DNA binding/transport,[164] and biomedical imaging[165] have been developed utilizing amorphous silica NPs where the surface is functionalized with amine groups in order to change the chemical properties of the material. It is important to investigate how the surface chemistry of silica NPs affects the interaction with biological systems and if there is an influence on toxicity as a result of amine functionalization. Here we present in vitro and in vivo data in lung models evaluating the toxicity of 50 nm amorphous silica NPs with and without amine-functionalization. Cell toxicity of bare silica NPs and amine-modified silica NPs was measured in human bronchoalveolar cells at three time points. Mice were treated with two different doses of particles via intra-tracheal instillation and markers of pulmonary inflammation in the lungs were evaluated 24 hours after exposure. Silica NP treatments were compared to a crystalline form of silica (Min-U-Sil®5) which is known to be hazardous to human health.[166-167] Our studies provide evidence that surface chemistry plays an important role in silica NP-induced inflammation in murine lungs that cannot be fully detected by in vitro studies alone.

4.3. Methods and Materials

4.3.1. Synthesis of Silica NPs

Nonporous silica (or Stober silica) was prepared following a modified procedure from the literature.[132] In this synthesis no surfactant was used, and ammonia was used as the basic catalyst. In a glass vessel 120 mL anhydrous ethanol (Decon Labs) was combined with 6.0 mL aqueous ammonia (Sigma-Aldrich) and stirred for 5 minutes. Tetraethyl orthosilicate (TEOS, 4 mL, Sigma) was used as the silicon source and added to the ammonia/ethanol mixture. The reaction mixture was stirred at room temperature for 24 hours and then centrifuged at 11,000 × g for 30 minutes to obtain the products, which were washed in triplicate with water and dried at 60 °C overnight.

4.3.2. Surface Functionalization

Functional groups were covalently attached to the NP surface using a post-synthesis grafting method.[168] Functionalization with amine groups was carried out by refluxing a mixture of 4 grams of aminopropyltriethoxysilane (APTES, Sigma) with 1.00 gram of silica nanoparticles in 60 mL of toluene for 48 hours. The reaction mixture was then centrifuged at 11,000 × g for 20 minutes, washed three times with 20 mL of dichloromethane and dried overnight at 80° C.

4.3.3. Material Characterization

NPs were characterized by powder X-ray diffraction, nitrogen adsorption isotherms and thermogravimetric analysis. Diffraction patterns were obtained using a Siemens D5000 X-ray diffractometer using a Cu Kα radiation source ($\lambda = 0.154$ nm). A powder pattern was obtained from 2θ = 1 - 10 with a 0.04 step size, 1 s/step. Nitrogen adsorption experiments were conducted using a Nova 1200 Nitrogen Adsorption Instrument (Quantachrome). Approximately 100 mg of powder was dried at 120 °C under vacuum overnight. A seven-point BET isotherm and a 50-point adsorption/desorption isotherm in a liquid nitrogen bath were obtained, using pure nitrogen gas as the adsorbate. Surface area was calculated using the BET (Brunauer-Emmett-Teller) method. Functionalized NPs were evaluated by thermogravimetric analysis using a TA Q5000 TGA instrument with a heating rate of 5 °C/minute. The sample was heated from room temperature to ~800 °C under a flow of nitrogen. Mass loss during the run was used to approximate the loading of the organic functional group. Scanning electron microscopy (SEM) was used to image the particles and determine average particle diameter. Particles were dispersed on to silicon wafers on aluminum stubs and then sputter coated (Emitech K550x) with gold and palladium for 3 minutes at 10 mA. Zeta potential of particles were measured in water using a Zeta Sizer nano ZS (Malvern Instrument Ltd.). Fine ground silica (Min-U-Sil®5 quartz, Berkeley Springs, West Virginia) was used as a positive control for in vivo experiments.

4.3.4. In Vitro Cytotoxicity Studies

Adenocarcinoma human alveolar basal epithelial (A549) cells were cultured in RPMI-1640 (Gibco®, Life Technologies Corporations) medium containing 10% fetal bovine serum (Atlanta Biologics), 10 mM HEPES (Gibco®), 50 µg/mL gentamycin sulfate (IBI Scientific), 1 mM sodium pyruvate (Gibco®) and 1 mM Glutamax (Gibco®). Cells were incubated at 37 °C and 5% CO_2. Cells were passaged prior to confluence.

A549 cells were plated into 96-well plates at a density of 1×10^4 cells per well. After 24 hours of incubation, the media was removed and replaced with 200 µL of media containing various silica particles types and concentrations. Cells incubated with medium alone served as a control and was used to calculate percent relative cell viability. The cells were exposed to each treatment for 4, 24 or 48 hours after which, the treatment was removed and the cell viability was assessed using the MTS assay (CellTiter 96 AQueous One Solution Cell Proliferation Assay, Promega Corporation). Once the treatment was removed, 100 µL of media was added to the wells along with 20 µL of MTS reagent. The cells were incubated with MTS reagent for 1-4 hours. In order to avoid unwanted scattering of light by the silica nanoparticles during analysis, the 96-well plates were centrifuged at 500 × g for 20 minutes and 70 µL of media was carefully removed for absorbance measurements at 490 nm using a SpectraMax Plus 384 microplate reader (Molecular Devices). A background absorbance value was established using media and MTS reagent in the absence of cells and all sample data was corrected accordingly.

4.3.5. In Vivo Toxicology Studies

For in vivo studies, mice (C57Bl/6, males, 12 – 16 wks old, The Jackson Laboratory) were used. After arrival, animals were acclimatized for 10-14 days before exposure while housed in our vivarium in polypropylene, fiber-covered cages in HEPA-filtered Thoren caging units. Food (sterile Teklad 5% stock diet, Harlan) and water (via an automated watering system) were provided ad libitum. Light-dark cycle (12 hours) was maintained in the animal room. All protocols were approved by the Institutional Animal Care and Use Committee at the University of Iowa. Mice were weighed twice per week (PR 5002 Delta

Range balance, Mettler Toledo Inc.) and monitored throughout the study for any signs of distress. Mice were weighed before intratracheal instillation and 24 hours after exposure to treatments.

Silica NPs were suspended in PBS by sonication for 30 minutes immediately before use. The mice were dosed with 50 μL of NP suspension via intratracheal instillation one time. Two doses were tested, low 0.1 mg/mouse (4 mg/kg) and high 0.5 mg/mouse (20 mg/kg). Mice were anesthetized by inhalation of 3% isoflurane (Fortec vaporizer, Cyprane). Mice were euthanized 24 hours after exposure and bronchoalveolar lavage fluid and lungs were collected.

Lungs were lavaged in situ three times with 1 mL of sterile isotonic saline using a cannula inserted into the trachea as described previously.[169] The BAL fluid was centrifuged at 800 x g for 5 minutes at 4 °C to collect all cells after which the cells were resuspended in Hank's balanced salt solution. The total numbers of white cells were quantified using a hemocytometer. The supernatant from each sample was frozen at -80 °C until analysis for total protein and lactate dehydrogenase (LDH) activity. The cells were cytospun (Thermo Shandon, Thermo Scientific) at 800 x g for 3 minutes, then stained with HEMA 3 staining kit (Fisher Scientific Company LLC). The numbers of neutrophils, macrophages, lymphocytes and eosinophils in each BAL sample were determined. BAL fluid was assayed for total protein (Bradford Assay, Bio-Rad Laboratories, Inc.) and LDH enzyme activity (LDH) (Roche Diagnostics) in order to quantify the membrane integrity of cells.

Generation of free radical species was assessed using Oxiselect in vitro reactive oxygen species (ROS)/reactive nitrogen species (RNS) assay kit (Cell Biolabs, Inc.). Half of the left lobe of lung tissue was resuspended at 25-30 mg/mL in PBS and homogenized on ice. Samples were spun at 10,000 × g for 5 minutes. The supernatant was collected and stored at -80°C until analysis. Then, the samples were incubated for 45 minutes with dichlorodihydrofluorescein (DCFH), which reacts with free radicals to form a fluorescent product. The fluorescence intensity of each sample was measured using 480 nm excitation and 530 nm emission. Levels of total free radicals in each sample were determined by

comparison with the predetermined DCF standard curve. The levels were normalized for total protein content in homogenates.

4.3.6. Statistical Analysis

The data are expressed as the mean ± standard error. The differences between data sets were determined using GraphPad Prism version 6 (Graphpad Software, Inc.) with Tukey's test for multiple comparisons along with two-way analysis of variance (ANOVA). A p-value < 0.05 was the threshold considered for statistical significance.

4.4. Results and Discussion

4.4.1. Particle Characterization

The average diameter of amorphous silica NPs used in this study was 50 nm (Figure 4-1). The diameter of NPs plays an important role in particle-cell interactions. Multiple studies have shown that when comparing variously sized particles of the same composition, the optimal diameter in terms of being taken up by cells is 50 nm or less.[37, 148, 170-171] Using a seven-point nitrogen adsorption isotherm, the surface area of the bare silica NPs and APTES functionalized silica NPs was found to be 66 (±3) m^2/g and 42 (±2) m^2/g, respectively. Using thermogravimetric analysis, the organic loading was approximated to be 0.582 mmol of APTES per gram of material (Table 4-1). The APTES-functionalization was also confirmed by the increase in zeta potential before and after the covalent attachment of amine molecules to the particle surface (-25 mV and 19 mV, respectively). Min-U-Sil® quartz had an average diameter of ~700 nm although there was a large size distribution (Figure 4-1) and had a higher negative surface potential (-36 mV) compared to the silica NPs.

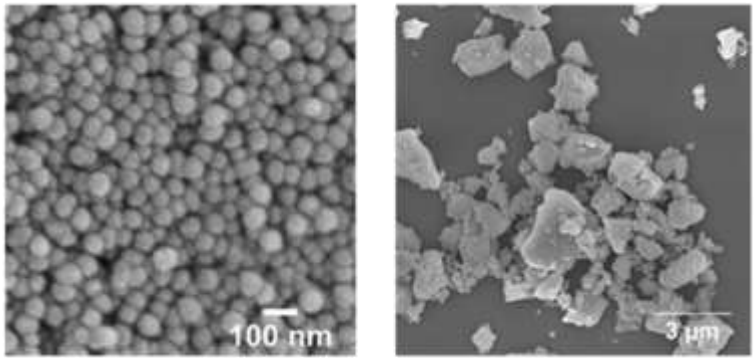

Figure 4-1. SEM image of nonporous silica nanoparticles (left) and Min-U-Sil (right).

Table 4-1. Physicochemical characterization of silica materials.

Particle Type	Diameter (nm)[a]	Surface Area (m^2/g)	APTES Loading (mmol/g)	Z-Potential (mV)
Bare Silica NPs	54 ± 9	66 ± 3	-	-25 ± 12
APTES-NPs	50 ± 8	42 ± 2	0.582 ± 0.009	19 ± 4
Min-U-Sil® Quartz	700	7.6 ± 0.3	-	-36 ± 6

[a]Determined using SEM image analysis with ImageJ software

4.4.2. In Vitro Cytotoxicity

A549 human lung epithelial cells are commonly used as a model system for evaluating lung damage after NP exposures.[172] In order to assess the cytotoxicity of nonporous silica NPs on alveolar lun g cells we employed the colorimetric MTS cell viability assay. The NPs were suspended in culture medium and incubated with A549 cells for 4, 24 or 48 hours. Figure 4-2 (A, B and C) shows the cell viability of A549 cells when using various concentrations of bare and APTES-functionalized silica NP treatments. There was a slight reduction in cell viability for the APTES-modified silica NPs after 4 hours of treatment with 10 and 50 µg/mL (74% and 72% relative cell viability, respectively), while only the highest concentration (200 µg/mL) of bare silica NPs displayed a significant reduction in cell viability to 70%. At longer time points, 24 and 48 hours, there was some apparent cytotoxicity to A549 cells from the bare silica NPs at the highest dose (72% and 75% relative cell viability, respectively); however it was not significant from the control. The APTES-modified silica NPs also induced significant toxicity after 48 hours of treatment but the trend was not dose-dependent.

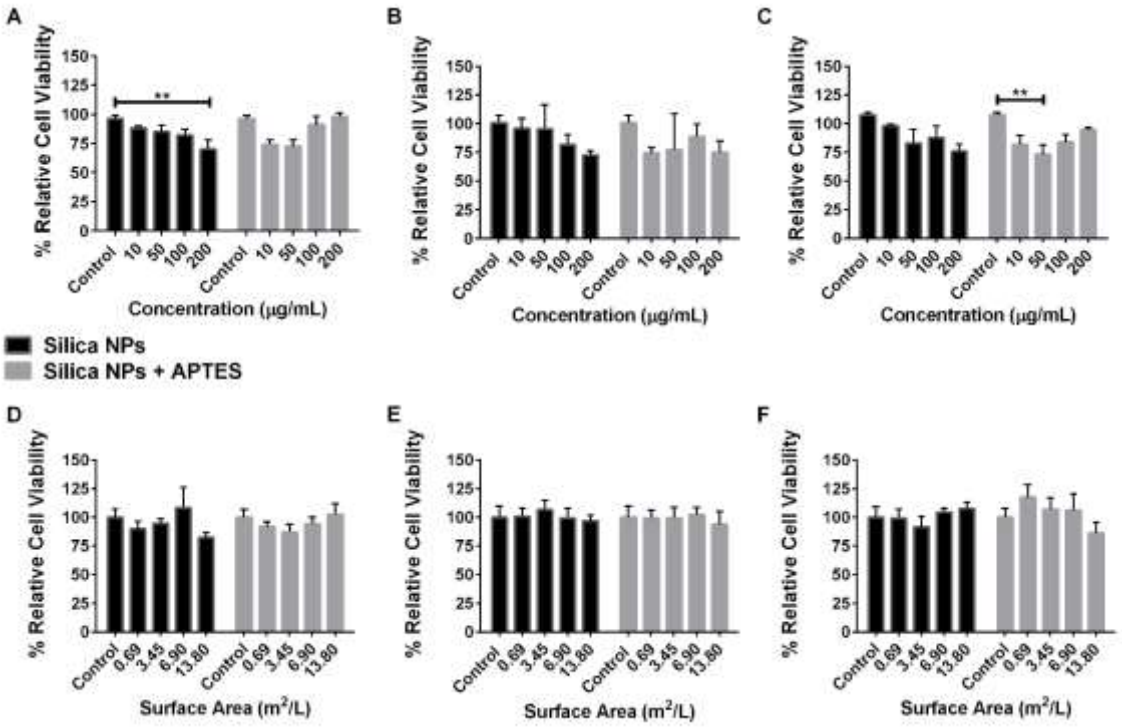

Figure 4-2. Percent relative cell viability of A549 cells treated with bare silica NPs (black) and APTES-functionalized NPs (grey). The first row shows percent relative cell viability from doses prepared using mass concentration of NPs ranging from 10-200 μg/mL at 4(A), 24(B) and 48(C) hours. The second row shows percent relative cell viability from doses prepared using exposed surface area of NPs ranging from 0.96-13.80 m2/L at 4(D), 24(E) and 48(F) hours. Data are expressed at mean ± standard error. ** $p < 0.01$

Using mass concentration when comparing different particle types may not be completely accurate since the number of available surface molecules that could potentially interact with cells increases as the surface area increases.[52, 173] Previous studies have demonstrated that toxicity outcomes can vary differently with mass concentration than with exposed surface area of NPs.[174] Because APTES-functionalized NPs have a lower surface area, there would be less exposed surface area per treatment compared to bare silica NPs when the samples are prepared via mass concentration. Therefore, the MTS assay was repeated with the same time points, however, the particle treatments were normalized to exposed particle surface area per volume of medium (Figure 4-2 D, E and F). Subsequent analysis by the MTS assay indicated that there was no significant cytotoxicity caused by either type of NPs.

Nowak et al. reported that when A549 cells were treated with 20 nm silica NPs (bare and APTES functionalized) at concentrations below 250 µg/mL, there was no significant decrease in cell viability after 72 hours of exposure.[157] The same group also saw a greater amount of uptake of amine functionalized silica NPs compared to bare silica NPs over the course of 10 hours. The larger 50 nm silica NPs investigated in our studies perhaps affected the cells in a similar manner explaining the low cytotoxicity at the concentrations tested (10-200 µg/mL). Another group, Lin et al., used nonporous silica NPs of a similar size to those used in our study (46 nm) to determine the cytotoxic effect on A549 cells after 24, 48 and 72 hours of silica NP exposure.[140] The NPs were administered using mass concentration doses in the range of 10-100 µg/mL. Their study is in agreement with our cell viability data at 48 hours where at the lowest concentration of 10 µg/mL there was negligible cytotoxicity from bare silica NPs. At 100 µg/mL, there was an increase in the cytotoxicity after 48 hours of bare silica NP exposure reported by Lin et al.; however, we saw no significant difference at the same concentration compared to the control cells. Although in vitro experiments are commonly used to screen drugs or treatments for cytotoxic effects, it is difficult to use the results to predict inflammatory responses in animal models.[175] In addition, there are many limitations when using cultured cells in a cytotoxicity assay as it cannot represent the complexity of a biological environment such as the lungs where there are numerous cell types or airway surface molecules present and the nature and impact of the inflammatory response cannot be easily predicted. Furthermore, most in vitro studies are performed in submerged culture conditions that may influence the overall cellular response to tested material. Amorphous silica NPs were found to be less toxic to human lung cells when cells were exposed at an air-liquid interface (ALI).[176] However, when pulmonary surfactant was added to cell cultures at an ALI, amine-modified silica NPs augmented cytotoxicity but not the release of IL-8.[177]

4.4.3. Effects of NP Treatments on Mouse Body Weight

Mice exposed to 0.1 mg of NPs for 24 hours demonstrated, no significant change in body weight associated with any of the particle types compared to the control (Figure 4-3). When the dose was

increased to 0.5 mg silica per mouse, a decrease in the body weight in treated mice was evident for each different silica type tested after 24 hours although only the bare silica NP treatment was significantly different from the control (5% decrease). These results indicate that at a dose of 0.5 mg NPs per mouse, unmodified silica NPs have greater adverse side effects compared to APTES-functionalized NPs and quartz.

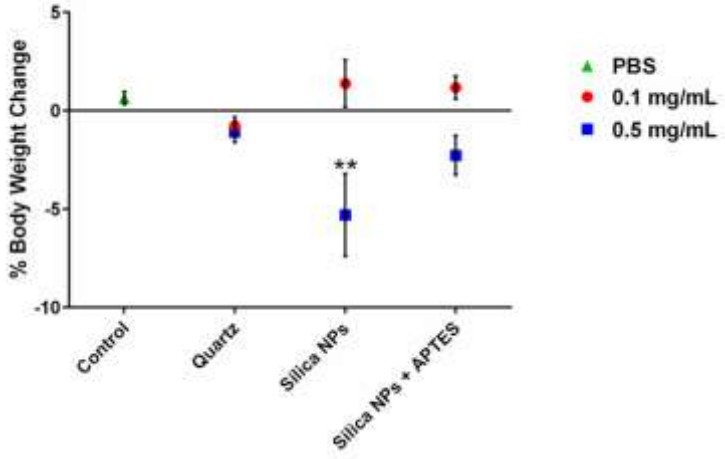

Figure 4-3. Percent change in body weight of mice after 24 hours of treatment of 0.1 mg/mouse and 0.5 mg/mouse. Control mice were treated with PBS instead of particles. ** $p < 0.01$

4.4.4. Total and Differential Cells, Total Protein and LDH Activity in Brochoalveolar Lavage (BAL) Fluid

To investigate silica NP-induced inflammation of the lungs, the total numbers of cells present in BAL fluid of silica NP treated mice were counted 24 hours after bronchial instillation. At the dose of 0.1 mg NPs per mouse there was a significantly higher number of total cells in the BAL fluid of mice exposed to unfunctionalized silica NPs (Figure 4-4A) and quartz compared to the control group. When the higher dose (0.5 mg/mouse) was used, all treatments had higher numbers of total cells, compared to control mice. However, the only significant difference observed was the 10-fold increase in total cells in BAL fluid when mice treated with bare silica NPs and control mice were compared (Figure 4-4B). Our results suggest that, when a higher dose was implemented, that 50 nm unmodified silica NPs trended

toward being more toxic than the larger crystalline quartz and the APTES-functionalized silica NPs. Thus, surface functionalization of silica NPs with APTES was beneficial in terms of reducing lung inflammation.

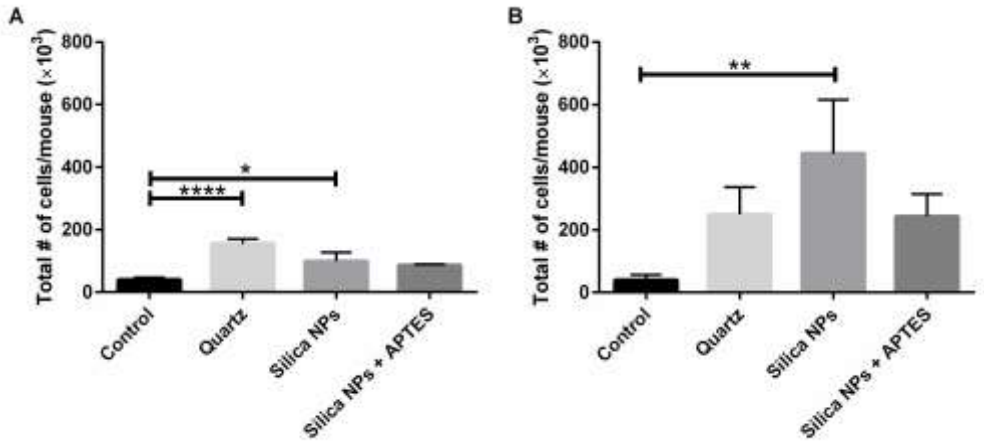

Figure 4-4. Total number of cells in BAL fluid after administration of 0.1 mg silica/mouse (A) or 0.5 mg silica/mouse (B). * $p < 0.05$, ** $p < 0.01$, **** $p < 0.0001$

Neutrophils, macrophages, lymphocytes and eosinophils were quantified in BAL fluid to provide insight into lung inflammation caused by silica NPs (Figure 4-5). There was no eosinophils recruitment into BAL fluid in any of the experimental groups; thus no eosinophils are listed in the plots. For both doses tested, there was no noticeable difference in the number of lymphocytes between all of the groups, with numbers being very low (also not shown in plot). At a dose of 0.1 mg particles per mouse (Figure 4-5A), both types of silica NPs and quartz induced a greater influx of macrophages into the lungs compared to the control sample but only the quartz treatment yielded values that were significantly different.

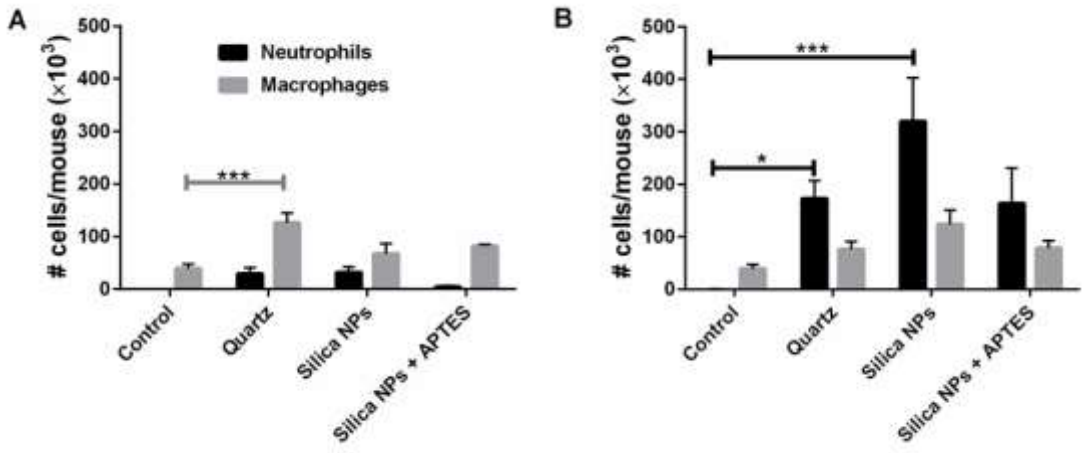

Figure 4-5. Neutrophils and macrophages in BAL fluid after administration of 0.1 mg silica/mouse (A) or 0.5 mg silica/mouse (B). * $p < 0.05$, *** $p < 0.001$

Once tissue damage has occurred, neutrophils are recruited to the site of injury by cytokine/chemokines and serve as a marker of lung inflammation.[178] None of the treatments (at 0.1 mg/mouse) resulted in significant increases in neutrophils compared to control mice. However, it was noted that the APTES-functionalized silica NPs induced very low levels of neutrophil infiltration in the lungs compared to other treatments (Figure 4-5A). At the higher dose of 0.5 mg silica NPs per mouse (Figure 4-5B), there was a 1000-fold increase in neutrophil numbers in the BAL fluid of mice exposed to bare silica NPs and approximately a 500-fold increase in neutrophils resulting from APTES-functionalized silica NP treatment compared to control mice. A 500-fold increase in neutrophils infiltrating into the lungs was also noted for mice treated with quartz. Although all types of silica materials tested induced neutrophil recruitment at 0.5 mg per mouse, there were significantly more neutrophils (about twice as many) in the mice exposed to bare silica NPs compared to the other two treatment groups (Figure 4-5B). It is also likely that the increase in total cell infiltration into the lungs noted in Figure 4-4B for mice treated with bare silica NPs was probably mostly due to the increase in the numbers of neutrophils. A study by Brown et al. indicated that 50 nm bare silica NPs and amine-functionalized NPs both induced neutrophil recruitment in rats to a similar degree (24 hours after

instillation) compared to the control.[179] However, they used a dose of 30 μg silica per animal, whereas in our study the doses were higher and could potentially be the reason we saw a larger difference between the bare silica NP and amine-silica NP treatments. Our results show that the modification of 50 nm silica NPs with amine groups reduces the amount of acute inflammation, particularly neutrophil infiltration, in the lungs of mice.

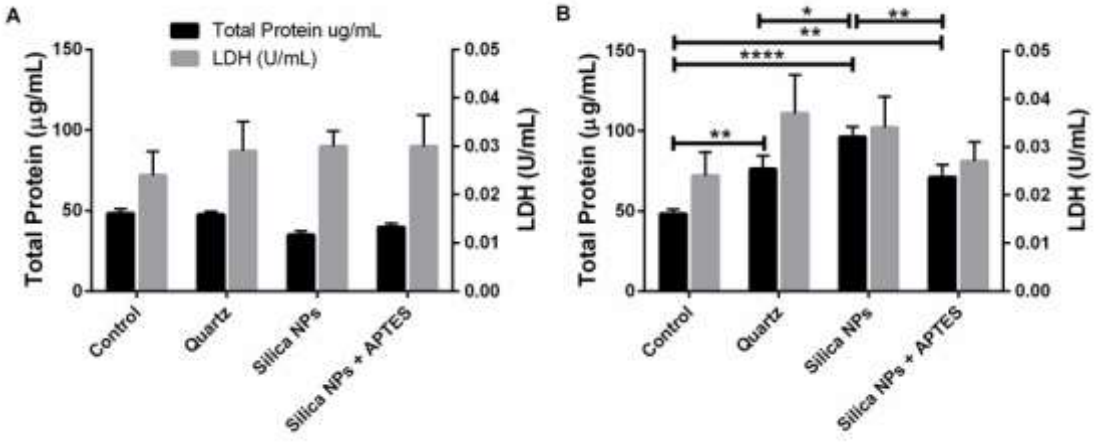

Figure 4-6. Total protein and LDH activity after administration of 0.1 mg silica/mouse (A) or 0.5 mg silica/mouse (B). * $p < 0.05$, ** $p < 0.01$, **** $p < 0.0001$

An increase in the total protein concentration in BAL fluid is a sign of lung injury due to increased alveolar-capillary permeability. Another marker of cytotoxicity is a spike in LDH concentration of BAL fluid indicating that the membrane integrity is compromised. Therefore, the total amount of protein in BAL fluid of mice was determined in order to investigate in vivo pulmonary toxicity as well as LDH enzyme activity (Figure 4-6). There was no significant increase in either total protein or LDH activity for the lower dose (0.1 mg/mouse) treatments for any of the sample groups (Figure 4-6B). However, at the higher dose (0.5 mg/mouse), there was a significant difference in the total protein for all of the treatments compared to the control (Figure 4-6B). Again, while there was some indication of inflammation from both types of NPs, there was a significantly larger amount of total protein in the mice treated with bare

silica NPs compared to APTES-functionalized silica NPs and quartz treatments. Although the levels of LDH were not significantly different they tended to mirror the results for total protein (Figure 4-6B).

4.4.5. Generation of Intracellular Reactive Oxygen Species (ROS)/Reactive Nitrogen Species (RNS)

It is well known that elevated concentrations of intracellular reactive oxygen species (ROS) and reactive nitrogen species (RNS) are indicative of oxidative stress. The results reported herein (Figure 4-7) showed that all experimental treatments induced significantly increased levels of oxidative stress at a dose of 0.5 mg/mouse compared to the controls (Figure 4-7B). Importantly, there was a 60% increase and a 35% increase in the amount of ROS/RNS in mice treated with bare silica NPs and amine-modified silica NPs, respectively. The difference in ROS/RNS production between the two particle types was significant (p-value < 0.01) and we conclude that bare silica NPs induced increased oxidative stress in murine lungs compared to amine-modified silica NPs.

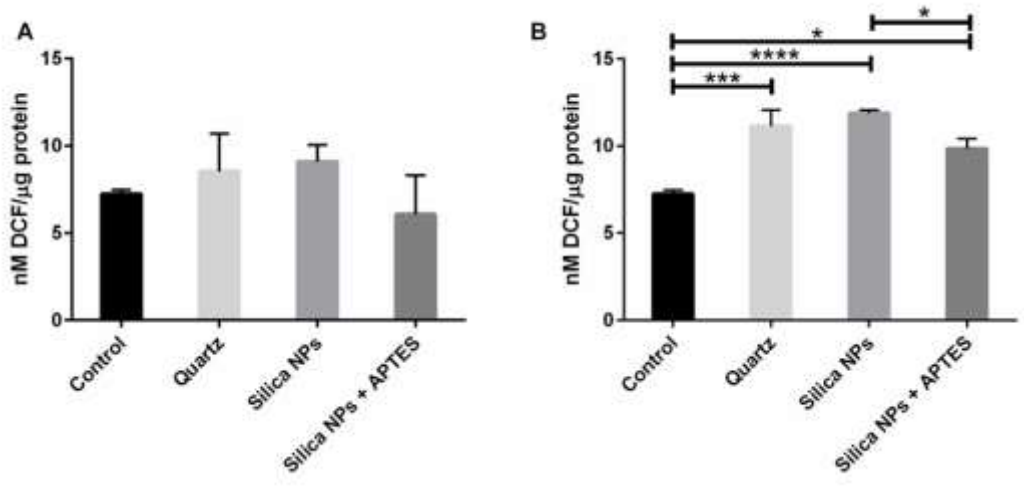

Figure 4-7. Production of intracellular ROS/RNS after administration of 0.1 mg silica/mouse (A) or 0.5 mg silica/mouse (B). * $p < 0.05$, *** $p < 0.001$, **** $p < 0.0001$

There is a large amount of evidence in the literature indicating that silanol groups on the surface of silica materials play a major role in particle-cell interactions and can cause degradation of membrane

proteins as well as free radical production.[180-183] The increase in intracellular ROS/RNS after treatment with bare silica NPs could be related to a higher concentration of exposed surface silanol groups compared to amine-functionalized silica NPs where the silanol moieties are replaced with aminopropyl functional groups. Our work demonstrates that silica NP-induced ROS/RNS can be reduced by functionalizing the surface with amine groups.

4.5. Conclusions

Modification of amorphous silica NPs with APTES resulted in significantly reduced inflammatory responses in the lungs of mice treated with these particles versus unmodified amorphous silica NPs. This was indicated by decreased accumulation of total cells, especially neutrophils, as well as a marked decrease of total protein in the BAL fluid from lungs of mice. Furthermore, surface modification of silica NPs also significantly reduced ROS production in the alveolar tissue. These findings strongly support the process of surface modification of silica NPs to reduce their potential inflammatory effects. In addition, the difference in the inflammation response observed for the two different NP formulations in vivo was not correlative with in vitro studies involving lung cell cultures.

This chapter was adapted from Morris, A. S.; Adamcakova-Dodd, A.; Lehman, S. E.; Wongrakpanich, A.; Thorne, P. S.; Larsen, S. C.; Salem, A. K., Amine modification of nonporous silica nanoparticles reduces inflammatory response following intratracheal instillation in murine lungs. Toxicology Letters 2016, 241, 207-215.

5. CHITOSAN-COATED PLGA NANOPARTICLES FOR ASTHMA THERAPY

5.1. Abstract

Asthma is a common lung disease affecting over 300 million people worldwide and is associated with increased reactive oxygen species (ROS), eosinophilic airway inflammation, bronchoconstriction and mucus production. Targeting of novel therapeutic agents to the lungs of patients with asthma may improve efficacy of treatments and minimize side effects. We previously demonstrated that Ca^{2+}/calmodulin-dependent protein kinase (CaMKII) is expressed and activated in the bronchial epithelium of asthmatic patients. CaMKII inhibition in murine models of allergic asthma reduces key disease phenotypes, providing the rationale for targeted CaMKII inhibition as a potential therapeutic approach for asthma. Herein we developed a novel cationic nanoparticle (NP)-based system for delivery of the potent and specific CaMKII inhibitor peptide, CaMKIIN, to airways. CaMKIIN-loaded NPs abrogated the severity of allergic asthma in a murine model. These findings provide the basis for development of innovative, site-specific drug delivery therapies, particularly for treatment of pulmonary diseases such as asthma.

5.2. Introduction

Asthma is a chronic, wide-spread disease that occurs in people of all ages. Exposure of the respiratory epithelium to allergens is the initiating event in allergic asthma which is characterized by excessive pulmonary inflammation, airway hyperreactivity and mucus production. New studies have shown enhanced oxidative stress in patients with asthma.[184-185] Specifically, our group has shown that Ca^{2+}/calmodulin-dependent protein kinase II (CaMKII) plays a pivotal role in ROS generation[186-188] and contributes to asthma phenotypes in asthmatic patients and in vivo models of allergic asthma.[189-190] Despite contemporary stepwise treatment approaches, 5-10% of the estimated 26 million Americans with asthma do not achieve adequate symptom control[191], in part because molecular disease mediators are not specifically targeted.[192-193]

Delivery of therapeutic agents, specifically to the respiratory epithelium, is likely to quell core asthmatic phenotypes and has the potential to improve drug efficacy.[194] Nanoparticle delivery systems allow for local delivery of drugs while offering additional advantages such as sustained release of therapeutic molecules over a desired amount of time, ability to deliver both water soluble and lipophilic drugs, the need for fewer administered doses and decreased enzymatic degradation of drug.[195-196] Poly(lactic-co-glycolic acid) (PLGA) is a well-established biodegradable polymer that is FDA approved for use in a wide variety of biomedical applications and can be utilized to fabricate NPs in which therapeutically active molecules are entrapped.[194, 197]

In the case of pulmonary drug delivery, it has been shown that drug-loaded PLGA NPs offer superior therapeutic effects over delivery of soluble drug alone.[21] The increase in therapeutic effects for PLGA NP systems can be attributed to sustained release of the drug over time and a longer residence time of NPs in the lungs compared to drug alone.[198] Furthermore, the surface chemistry of PLGA NPs can easily be manipulated to increase the bioavailability of the system.

In this study we tested the hypothesis that, in response to allergen challenge, CaMKII contributes to the induction of hallmark features of allergic asthma. Utilizing a novel drug delivery system, we exposed mice to a CaMKII inhibitor peptide encapsulated in PLGA NPs. These NPs were directly delivered to the lung via oropharyngeal instillation (OP).[199] Furthermore, we found chitosan coating of the CaMKIIN-loaded PLGA-NPs increased uptake in lung cells compared to uncoated NPs and led to reduced core features of allergic asthma including inflammation, mucus production and airway hyperreactivity.

5.3. Methods and Materials

5.3.1. PLGA NP Fabrication

PLGA NPs were prepared using the well-established double emulsion solvent evaporation method. PLGA (50 mg, Resomer® RG503, viscosity 0.32-.044 dL/g, MW 24,000-38,000, Boehringer Ingelheim KG) and amine-end capped PLGA (50 mg, MW 10,000-20,000, PolyScitech) were dissolved in a mixture

of 2.35 mL ethyl acetate (EA) and 0.250 mL of dimethyl sulfoxide (DMSO). Sixty milliliters of 2.5% (w/v) poly (vinyl alcohol) (PVA, Mowiol® 8-88, 87-89% hydrolyzed, MW 67,000, Sigma-Aldrich) in 10 mM phosphate buffered saline (PBS) was prepared and 9 mL was added to a 20 mL scintillation vial along with 1 mL EA. Fluorescently-labeled CaMKIIN peptide (sequence: H - KRP PKL GQI GRA KRV VIE DDR K (HF488) - NH2; HF488: HiLyte™ Fluor 488 acid) (AnaSpec Inc) was dissolved in a solution of water containing 1% PVA (w/v) at a concentration of 5 mg/mL. To prepare the nanoparticles, the organic and aqueous phases were emulsified using a probe sonicator (Fisher Scientific). First, 125 µL of the CaMKIIN solution was sonicated into the polymer/EA/DMSO solution at 40% amplitude for 60 seconds. Next, this emulsion was sonicated into 9 mL 2.5% PVA solution containing 1 mL EA. Finally, the emulsion was poured into the remaining 51 mL 2.5% PVA solution. The particle suspension was stirred using a magnetic stir bar for 30 minutes, followed by centrifugation at 4,500 × g for 5 minutes to pellet larger unwanted particles. The supernatant was removed and centrifuged at 10,000 × g for 30 minutes to form a pellet of NPs. NPs were then washed by discarding the supernatant and replacing it with water, followed by centrifugation at 10,000 × g. The particles were washed twice to remove residual surfactant. After washing, the particles were frozen at -80°C overnight and lyophilized (LABCONCO).

Nanoparticles were loaded with a near infrared fluorescent dye (XenoLightTM DiR, Perkin Elmer) to evaluate biodistribution. Particles were prepared according to the method described above except only a single emulsion was used. Due to the poor aqueous solubility of the dye, it was added directly to 100 mg PLGA dissolved in 2.5 mL EA. This solution was sonicated into 9 mL 2.5% PVA solution containing 1 mL EA. Then the emulsion was poured into 51 mL 2.5% PVA and the particle suspension was stirred using a magnetic stir bar for 30 minutes. The same collection, washing, and storage procedures as described above were used.

5.3.2. Chitosan Purification

Chitosan (low molecular weight, deacetylation degree 96.1%, Sigma-Aldrich) was purified according to a previously established method.[74] Chitosan (2 g) was dissolved in 200 mL 1% (v/v) acetic

acid then filtered (Whatman 541 filter paper). The filtrate was titrated with 1 N NaOH until the pH was approximately 8.5 to precipitate the chitosan. The precipitate was removed via filtration and resuspended in 500 mL buffer (0.1 M sodium bicarbonate, pH 8.3). Next, 2.5 g sodium dodecyl sulfate (SDS) and 3.72 g ethylenediaminetetraacetic acid (EDTA) were added to the solution and stirred using a magnetic stir bar for 30 minutes. The insoluble chitosan was filtered, rinsed and dialyzed (Snakeskin) in nanopure water for 24 hours. During dialysis, the water was changed after 10 hours and every hour afterwards. The chitosan was collected from the dialysis tubing, frozen at -80°C overnight and lyophilized.

5.3.3. Chitosan Coating of NPs

Dry NPs were suspended in 0.5 mL of chitosan (3 mg/mL) dissolved in 1% (v/v) acetic acid. After complete resuspension, NPs were centrifuged at 10,000 x g for 20 minutes. The supernatant was removed and replaced with 1 mL water.

5.3.4. Physicochemical Characterization of PLGA NPs

Physical characterization of the NPs was performed using a scanning electron microscope (SEM, Hitachi S4800). Dry NPs were dispersed in water. A small drop of NP suspension was placed on a silicon wafer fixed to an aluminum stub. After all water had evaporated, the sample was sputter-coated (Emitech Sputter Coater K550, Quorum Technologies) with a mixture of gold and palladium before imaging. Hydrodynamic diameter, zeta potential and polydispersity index (PDI) of the NPs were determined in water using dynamic light scattering (DLS, Zeta Sizer NanoZS, Malvern Instruments).

5.3.5. CaMKIIN Loading and Release

To assess CaMKIIN loading, PLGA NPs were dissolved in 0.3 N NaOH (1 mg/100 µL). Once all NPs were degraded, the solution was neutralized to pH 7 using 1 N HCl. The concentration of fluorescently-labeled CaMKIIN in the sample was determined by linear regression using standard CaMKIIN solutions ranging from 0.4-50 µg/mL (diluted in PBS). The standards and samples were analyzed simultaneously in a 96-well plate using a SpectraMax Plus 384 microplate reader (Molecular

Devices) with an excitation wavelength of 500 nm and emission collected at 530 nm. The background signal was determined using PBS. The encapsulation efficiency (equation below) was calculated according to Joshi et al.[200]

$$Encapsulation\ Efficieny = \frac{(Total\ Mass\ of\ Nanoparticles\ \times Peptide\ Loading)}{Initial\ Mass\ of\ Peptide\ Used} \times 100$$

To measure CaMKIIN release, 29.4 mg of NPs were suspended in 0.5 mL PBS and agitated at 300 rpm and 37°C. At time points from 30 minutes to 48 hours, the sample was centrifuged at 15,000 x g to pellet NPs. The supernatant was collected and NPs resuspended in 0.5 mL PBS. Samples were stored at -20°C until the time of analysis. The amount of CaMKIIN released at each time point was determined using a SpectraMax Plus 384 microplate reader (Molecular Devices) with 500 nm excitation and 530 nm emission as described for analysis of CaMKIIN loading.

5.3.6. In Vitro Cellular Uptake

Human airway epithelial cells (HAECs) were cultured in keratinocyte serum-free medium supplemented with 1% penicillin/streptomycin (Gibco) on collagen (rat tail, type 1, Sigma-Aldrich) at 37 °C and 5% CO_2.[201] Next, HAECs were plated in a 6-well plate at a density of 2×10^5 cells per well and incubated at 37 °C and 5% CO_2 for 24 hours. After changing the medium, chitosan-coated and uncoated CaMKIIN-loaded PLGA NPs (300 µg) were added to the wells and incubated for 24 hours. The cells were collected from the wells by trypsinization and centrifuged at 230 x g for 5 minutes. The supernatant was removed and replaced with 0.5 mL fresh medium and cells were stored on ice until analysis. The amount of fluorescently-labeled CaMKIIN associated with the cells was assessed by flow cytometry (FACScan, Becton Dickinson Immunocytometry Systems). The excitation wavelength was 488 nm and the emission was collected at 530 nm using a 30 nm bandpass filter. The mean fluorescence intensity for 10,000 cells was determined for each sample.

5.3.7. Animals

Six to ten week old C57Bl/6J female and male mice (equal proportions) were obtained from Charles Rivers Laboratories International, Inc. All animal studies complied with NIH guidelines and were approved by the University of Iowa Institutional Animal Care and Use Committee.

5.3.8. OVA Sensitization, Challenge and NP Delivery

Mice were sensitized by intraperitoneal injection (IP) of 10 µg OVA (Sigma) mixed with 1 mg alum (or saline alone for control) on days 0 and 7. Mice were subsequently challenged with by nebulization of OVA (1% solution in 0.9% saline, 40 minutes. challenge) or saline on days 14-17. Prior to OVA challenge by inspiration of soluble OVA, on days 14 and 16, oropharyngeal (OP) delivery of chitosan-coated NPs was performed as described previously with some modifications.[202-203] Briefly, mice were anesthetized with 2% isoflurane vapor in oxygen and then suspended by cranial incisors on a thin rubber band from a ring stand. To visualize the base of the tongue and the pharynx, the nares were pinched with curved forceps and the tongue gently extracted from the mouth using blunt forceps. NPs (25, 50 or 100 µL corresponding to 25, 50 or 100 µg NP) were placed in the posterior pharynx with a micropipettor. Respiration was monitored to ensure the suspension was fully delivered before the tongue and nares were released. Airway reactivity to methacholine was determined 24 hours after the last OVA challenge (Day 18). In control experiments, 25 ng CaMKIIN peptide alone was administered. Based on a loading of 0.6 (± 0.02) µg CaMKIIN per mg of NPs, this dose corresponds to the delivery of 50 µg CaMKIIN-loaded NPs.

5.3.9. Biodistribution

Near infrared dye-loaded nanoparticles were administered to mice via OP delivery. Particles were chitosan coated as described above or uncoated and instilled by OP delivery. For controls, mice were instilled with PBS alone. At one, 24 and 48 hr time points the fluorescence intensity of the organs was measured using a Xenogen In Vivo Imaging System (IVIS-200).

5.3.10. Assessment of Airway Hyperreactivity (AHR)

AHR in response to methacholine was measured on a flexiVent small-animal ventilator (Scireq) using a single compartment model, which determines the dynamic resistance of the respiratory system (R), as described previously.[190]

5.3.11. Bronchoalveolar Lavage

After the assessment of AHR, mice were euthanized, the trachea was cannulated, and two PBS washings were collected for analysis of total and differential counts in the bronchoalveolar lavage fluid (BALF). BALF cellular differential was determined on 250 μL cytospins stained with Diff-Quik (Dade Behring).

5.3.12. Liver Toxicity

Commercially available kits were used to evaluate bilirubin concentration (Sigma) and AST activity (Sigma) in the blood serum of mice. For bilirubin analysis, all experimental groups were normalized to saline control. The weight of individual mice was recorded before they were given any treatments and at the end of the treatment regimen (i.e., immediately before assessment of AHR) to determine percent weight change.

5.3.13. Lung Histology

Lungs were fixed with 4% paraformaldehyde and then processed by paraffin embedding. Tissue sections (5 μm) were cut and stained using hematoxylin and eosin (H&E) or Alcian Blue/periodic acid–Schiff (PAS) to determine mucin distribution. Images were acquired using a Leica light microscope. Eosinophilia from H&E sections was determined using the 40× objective; 4-5 random digital images per group were taken within areas of overt peri-bronchiolar inflammation. Total eosinophil cell counts were determined using NIH ImageJ software (ImageJ64, version 1.48, National Institutes of Health), and expressed as number of cells per 10 μm^2. Severity of perivascular inflammation was quantified by a 4-point scoring system where 0 = absence of cell cuffs, 1 = rare to few scattered perivascular

inflammatory cell cuffs, 2 = multifocal to moderate numbers of perivascular inflammatory cell cuffs, 3 = large number of diffuse perivascular inflammatory cell cuffs.[204] 13 For mucin measurements, PAS-stained slides were imaged (20× objective) and then ImageJ software was used to determine the percentage of positively stained area per total area.

5.3.14. IL-5 Cytokine Determination

IL-5 was analyzed in lung homogenates by cytokine-specific ELISA Duo Set kit (R&D Systems) and normalized to total protein content (DC Assay, Bio-Rad) according to the manufacturer's instructions.

5.3.15. Quantitative Real-Time Polymerase Chain Reaction

Total RNA was isolated using the Qiagen RNeasy column-based kits. Complementary DNA was prepared using the SuperScript III reverse transcription system (Invitrogen) with random nanomer primers. Expression of mRNA was quantified with the iQ LightCycler (Bio-Rad) and SYBR Green dye system and normalized to acidic ribosomal phosphoprotein 1 (Arp) mRNA. Primer sequences (mouse): Arp forward – TCA TCC AGC TGT TTG ACA A, Arp reverse – ATT GCG GAC ACC CTG TAG GAA G. Muc5ac forward-GTG GTG GAA ACT GAC ATT GG, Muc5ac reverse - CAT CAA AGT TCC CAC ACA GG. Eotaxin forward - CAC TTC CTT CAC CTC CCA GGT GC, Eotaxin reverse - CCC ACT TCT TCT TGG GGT CAG CA.

5.3.16. Statistical Analysis

Data are shown as means ± standard error of the mean. Analysis of experiments was performed using two-way ANOVA or one-way ANOVA and post hoc comparisons tested using Tukey correction. The GraphPad Prism statistical software program was used for the analyses. $P < 0.05$ was regarded as statistically significant. Results of experiments are compared between OVA-challenged mice or OVA-challenge in the presence of empty NPs.

5.4. Results and Discussion

5.4.1. NP Characterization

CaMKII is activated by ROS (oxidized-CaMKII or ox-CaMKII).[205] Ox-CaMKII is increased in airway epithelium from asthmatic patients after allergen exposure and correlates with asthma severity.[190] Inhibition of CaMKII in the lungs of mice protected against allergen-induced phenotypes. Inhibitory peptides such as CaMKIIN are notable for lacking activity against other calmodulin kinases or protein kinase C and provide a potential approach for highly specific CaMKII inhibition.[206] Herein we examined CaMKIIN-loaded PLGA NPs as an inhalable therapeutic tool for allergic airway disease. PLGA NPs were loaded with the 21-amino acid peptide CaMKIIN which was conjugated with a HiLyte™ Fluor moiety for ease of detection. Afterwards, NPs were coated with chitosan and imaged using scanning electron microscopy (SEM). We established that the NPs were smooth in morphology and spherical in shape (Figure 5-1a). The loading of CaMKIIN in the PLGA NPs was 0.5 (± 0.02) µg CaMKIIN per mg of NPs. Because of the high water solubility of the peptide, the encapsulation efficiency was around 3%. An in vitro release study demonstrated that ~50% of CaMKIIN was released within the first 30 minutes, with an additional 15% released by 48 hours (Figure 5-1b).

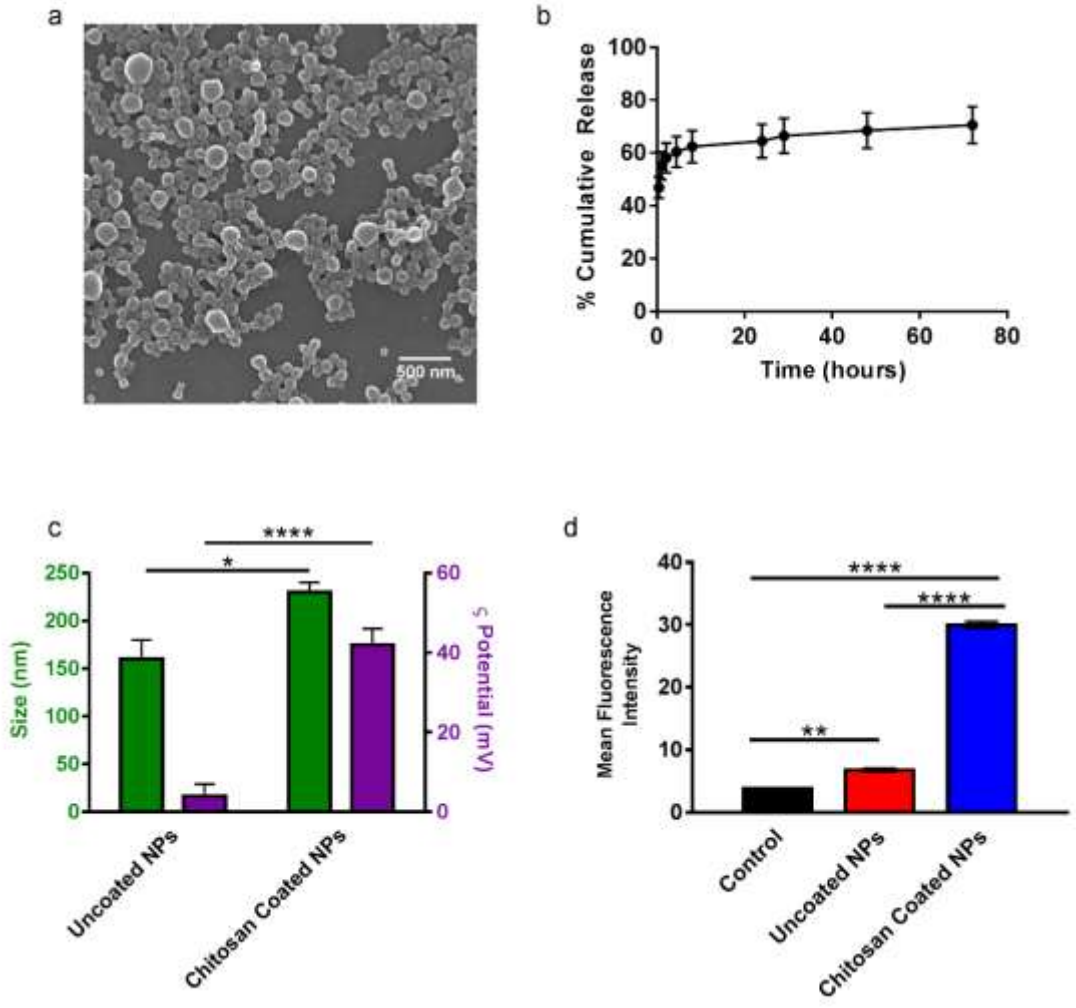

Figure 5-1. Chitosan coating of PLGA NPs increases size, zeta potential and cellular uptake by human airway epithelial cells. a, Representative SEM image of chitosan-coated PLGA NPs. b, Cumulative CaMKIIN release from PLGA NPs incubated at 37°C and agitated at 300 rpm (n=3). c, Size and zeta potential of PLGA NPs with and without chitosan-coating determined by DLS. d, Cellular uptake of CaMKIIN loaded PLGA NPs with and without chitosan in HAECs as measured by flow cytometry. Control: cells incubated with culture medium alone. (*P ≤ 0.05, **P < 0.01, ****P < 0.0001)

Chitosan is a natural, cationic polymer with known mucoadhesive properties and has been shown to promote adsorption, uptake and retention of therapeutic compounds into lung epithelial cells[207-208] in a mechanism that may include glycoprotein-mediated endocytosis.[209] To optimize the formulation of CaMKIIN delivery to the lungs, a chitosan layer was self-assembled onto the surface of the PLGA NPs via electrostatic interactions. To confirm the adsorption of chitosan on the surface of the NPs, DLS was

used to measure size and zeta potential. In the absence of chitosan, the average hydrodynamic diameter of the PLGA NPs was 160 nm and the average zeta potential was 4 mV (Figure 5-1c). After coating of the NPs with the chitosan layer, the average hydrodynamic diameter increased to 230 nm and the zeta potential to approximately 40 mV (Figure 5-1c). This confirmed that the surface of the NPs was modified by chitosan.[210] Furthermore, the polydispersity index (PDI) of uncoated and chitosan-coated NPs were 0.2 (± 0.1) and 0.22 (±0.09) respectively, indicating that there was no aggregation after coating the NPs with chitosan.

5.4.2. In Vitro Cell Uptake

To determine the functional properties of chitosan-coated CaMKIIN-loaded PLGA NPs, we assessed cellular uptake in primary human airway epithelial cells (HAECs) by flow cytometry. There was a significant increase in uptake of chitosan-coated NPs in HAECs compared to uncoated NPs and the control (Figure 5-1d).

5.4.3. Biodistribution and Toxicity of NPs in Mice

To assess specific delivery of NPs to the lungs, we performed a biodistribution study in male and female C57Bl/6J mice using chitosan-coated and uncoated PLGA NPs loaded with a near-infrared dye (thought to be retained within the PLGA matrix) administered by oropharyngeal instillation (OP) which would directly deliver NPs to the lung.[211] After 1 hour, both coated and uncoated NPs were robustly detected in the lungs. Other organs had no appreciable increase in signal over PBS controls (Figure 5-2a, b). Compared to mice treated with uncoated NPs, the signal for near IP-dye was significantly lower at 1 hour post instilliation (Figure 5-2b). However, there was a higher consistency between detection of IR-dye signal within the chitosan-coated group compared to non-coated NPs in which there was higher variability in signal detection (1 hour, Figure 5-2b). In addition, at 24 and 48 hours after nanoparticle instillation, the near-IR dye signal was significantly reduced in mice treated with

uncoated NP compared to 1 hour. In contrast, mice exposed to chitosan-coated NPs had steady-state retention between 1, 24 and 48 hours (Figure 5-2a, b).

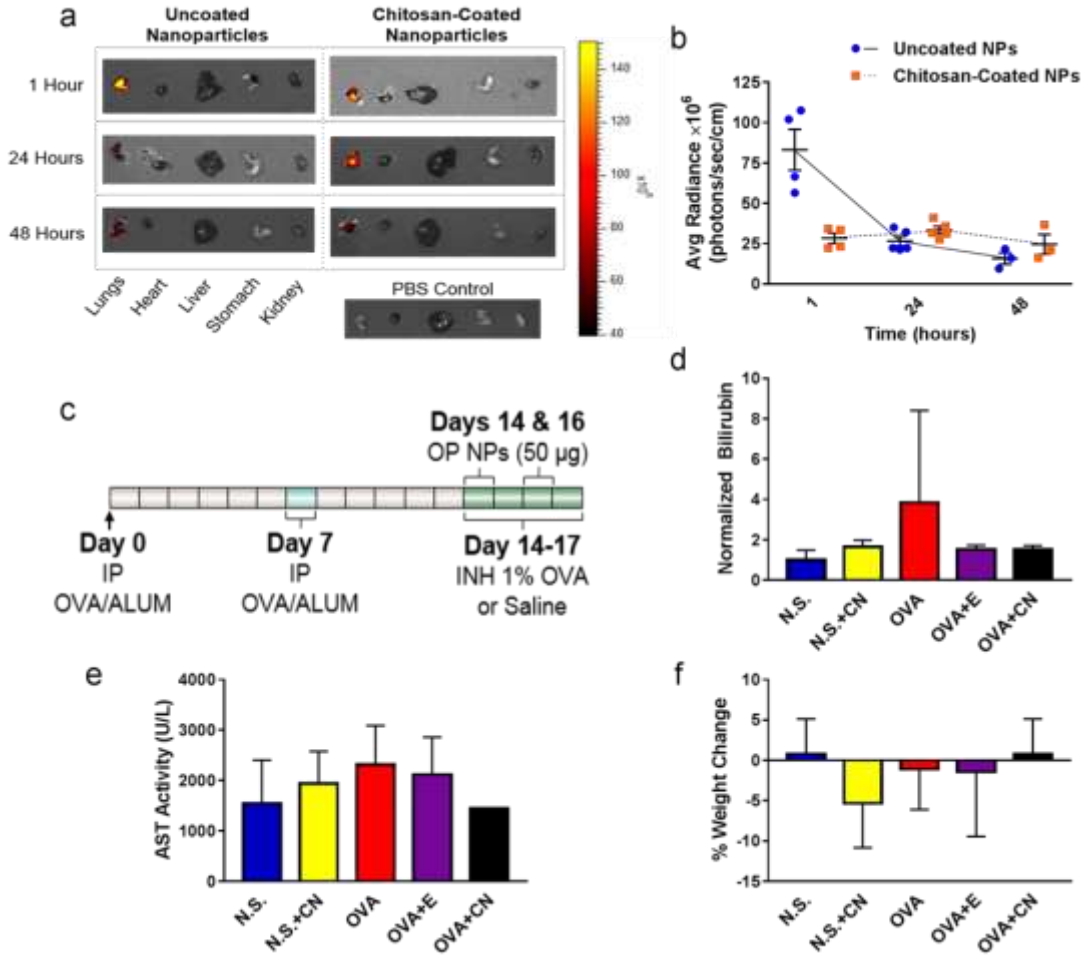

Figure 5-2. Chitosan-coated NPs localize in the lungs of mice and cause no significant toxicity in vivo. a, Representative images of control (PBS), uncoated and coated NPs (50µg NPs) loaded with fluorescent dye in various organ systems 1, 24 and 48 hours after oropharyngeal administration. b, Graphical analysis of NPs measured in lungs of mice at 1, 24 and 48 hours (n = 3-5 mice/group). c, Timeline of OVA sensitization (IP) and challenge and NP treatment (oropharyngeal (OP), inhalation (INH) of ovalbumin and alum (OVA/ALUM)). d,e Normalized (to saline control group) bilirubin content (d) and AST activity (e) in serum of OVA sensitized mice after treatment with normal saline (N.S.), saline + CaMKIIN-loaded NPs (N.S.+CN), OVA alone (OVA), OVA + empty NPs (OVA+E), and OVA + CaMKIIN NPs (OVA+CN). f, Percent weight change during sensitization and NP treatment protocol. Data were calculated relative to body weight on day 0. For toxicity studies, all NPs were coated with chitosan.

It is known that after delivery to the lung, NPs can be detected in other organs such as the liver, heart, spleen, gastrointestinal tract and brain.[212-215] We next examined toxicity using serum biomarkers including

bilirubin and aspartate transaminase (AST).[216] Administration of chitosan-coated CaMKIIN-loaded PLGA nanoparticles, as diagrammed in Figure 5-2d, had no significant effect on total bilirubin (Figure 5-2e), serum AST activity (Figure 5-2f), or animal weight (Figure 5-2g).

5.4.4. Assessment of CaMKIIN-Loaded NPs to Reduce AHR

To assess if CaMKIIN-loaded, chitosan-coated PLGA NPs are potential therapeutic agents for asthma, we used an established murine model of allergic asthma by sensitization to ovalbumin (OVA, Figure 5-2c).[190] We first tested whether CaMKIIN alone without encapsulation in a nanoparticle would have any effect on OVA-mediated airway hyperreactivity (AHR). After challenge with methacholine, mice exposed to OVA or OVA with peptide had significantly higher AHR compared to saline (Figure 5-3a). To test the hypothesis that encapsulation of CaMKIIN peptide in PLGA-NPs would be a better therapeutic tool, we first evaluated the effect of three doses (25, 50 or 100 μg) of empty NPs on OVA-mediated, methacholine induced AHR. Mice exposed to empty NPs combined with OVA had a similar effect as OVA alone, however, there was no dose-dependent effect (Figure 5-3b). To determine the therapeutic effect of NPs instilled with a set concentration of CaMKIIN peptide (0.5 μg/mg, see materials and methods) to alter OVA-mediated methacholine-induced AHR, we treated mice to the same doses of NPs as above. The low dose of CaMKIIN-loaded NPs (25 μg) did not alleviate OVA-mediated AHR, while the high dose (100 μg) caused a significant increase in OVA-induced AHR compared to OVA alone (Figure 5-3c) possibly due to the high amount of NPs delivered to the lungs. This suggested there was a no observable effect level (NOEL) at the low dose and an adverse effect at the highest dose. However, the intermediate dose (50 μg) was effective at reducing OVA-induced AHR (Figure 5-3c). These data also emphasize that NP-based approaches can be adapted to deliver to other peptide-based therapies in asthma and other lung diseases.

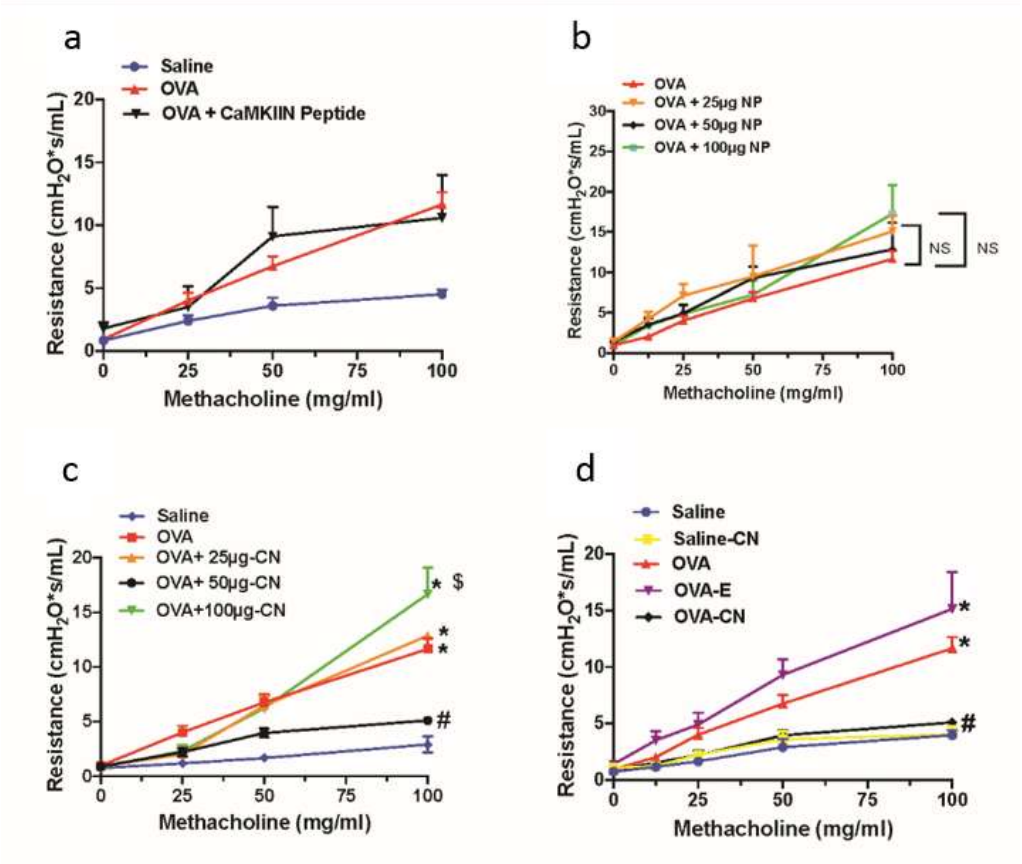

Figure 5-3. Cationic CaMKIIN-loaded nanoparticles (NPs) reduce airway hyperreactivity (AHR). Mice were sensitized to OVA alone or in the presence of 25 ng of soluble CaMKIIN peptide. The dose of soluble CaMKIIN peptide was calculated based on the total amount of CaMKIIN peptide present in 50 µg of NPs (50 µg of NPs loaded with 0.5 µg CaMKIIN/mg NP =25 ng total CaMKIIN). Control mice were sensitized to saline. b, AHR of OVA alone or OVA in the presence of empty chitosan-coated NPs (25 ng of soluble CaMKIIN, 25, 50 and 100 µg CaMKIIN-NPs). c, AHR of saline, OVA alone or instilled with chitosan-coated NPs (25, 50 and 100 µg) loaded with CaMKIIN. d, AHR in OVA-sensitized mice exposed to 50 µg of chitosan-coated empty NPs (OVA-E) or 50 µg of chitosan-coated NPs loaded with 0.5 µg/mg CaMKIIN (OVA-CN). Additional controls were not sensitized to OVA and given chitosan-coated NPs loaded with CaMKIIN (N.S.-CN). Data are means ± SEM; *P < 0.05 vs. saline; $P < 0.05 100 µg-CN vs. OVA; # P < 0.05 versus OVA+NP or OVA alone (n = 5-9 mice).

Exposure of mice to CaMKIIN-loaded NPs (OVA+CN) significantly reduced resistance, whereas empty NPs (OVA+E) did not protect against OVA-mediated AHR (Figure 5-3d). Administration of CaMKIIN-loaded NP to non-asthmatic control mice did not alter airway resistance (Figure 5-3d). As the 50 µg dose was effective at preventing increased airway resistance in OVA challenged mice after methacholine exposure and did not induce notable toxicity (Figure 5-2g), this dose was utilized for subsequent experiments.

5.4.5. Airway Inflammation, Cytokine Expression and Mucus Production in Mice Treated with CaMKIIN-Loaded NPs

Asthma is characterized by excessive airway inflammation and accumulation of eosinophils.[217] We determined whether chitosan-coated NPs loaded with CaMKIIN could attenuate lung eosinophilic inflammation induced by allergen challenge. Sensitization to OVA significantly increased total cell counts (Figure 5-4a) and eosinophils in bronchoalveolar lavage (BAL) fluid (Figure 5-4b). Although empty-NPs alone (OVA+E) significantly reduced OVA-mediated eosinophilic inflammation in the BAL, OVA-challenged mice exposed to CaMKIIN-loaded NPs had a further reduction in cell count and BAL-eosinophils (Figure 5-4a, b). Similarly, histologic analysis of lung sections demonstrated that, following allergen challenge, eosinophil infiltration into the airway was significantly abrogated by CaMKIIN-loaded NPs compared to OVA-alone or OVA-exposure with empty NPs (Figure 5-4c, d). Further assessment of allergen-mediated inflammation was determined by quantification of perivascular cuffs present in lung tissue sections. There was a reduction in perivascular cuffing in the lungs of mice exposed to CaMKIIN-loaded NPs compared to OVA-alone or mice challenged with OVA and exposed to empty NPs (Figure 5-4e).

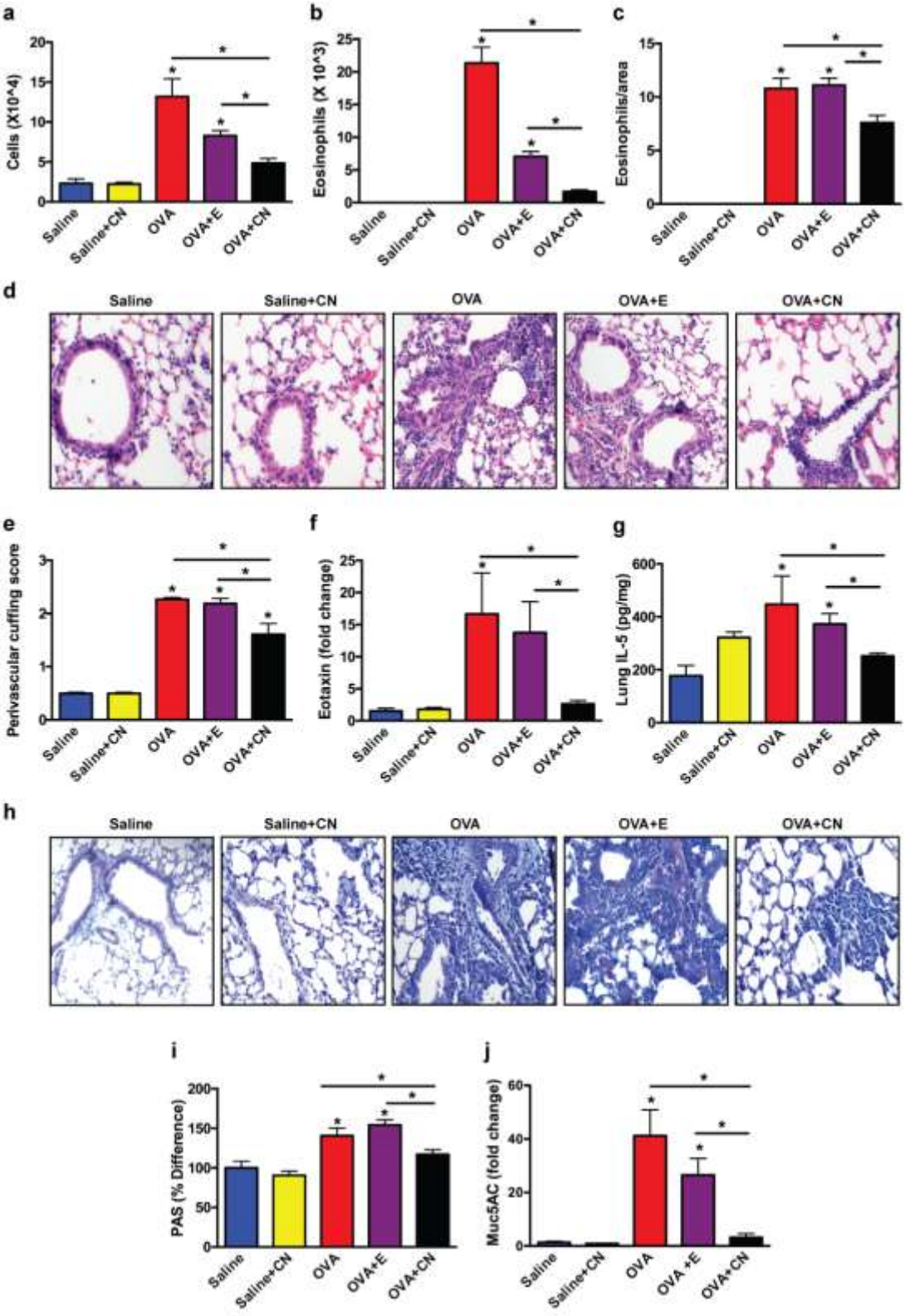

Figure 5-4. Airway inflammation, cytokine expression and mucus production are decreased by cationic CaMKIIN-loaded NPs. a, Total cell counts in bronchoalveolar lavage fluid (BALF) and b, Eosinophil counts in BALF (n=7-12 mice). c, Quantification of eosinophils/10 μm2 area (40× magnification). d,

H&E staining of lung sections. e, Perivascular cuffing score (10× magnification). f, qRT-PCR for eotaxin in lung homogenates. g, IL-5 protein levels in lung homogenates by ELISA. h, i, Representative images of PAS staining (h, 20× magnification) and (i) quantification (3-5 sections per mouse). j, qRT-PCR for MUC5AC in lungs of allergen challenged mice. Data shown are mean ± SEM (n = 3 for saline groups and n= 6-8 for all OVA-challenged groups). * $P < 0.05$ OVA alone vs. saline or as indicated by brackets. For g, $p < 0.09$ N.S.

Eotaxin, an eosinophil chemoattractant, is induced in different allergy models.[217-218] CaMKIIN-loaded NPs eliminated eotaxin mRNA expression following OVA challenge, in contrast to control or empty NP-treated mice where eotaxin mRNA was significantly increased (Figure 5-4f). Eotaxin cooperates with other interleukins, including IL-5, to promote tissue eosinophilia.[202] Compared to saline-treated mice, animals exposed to saline in conjunction with CaMKIIN-loaded NPs (N.S. +CN) showed a trend towards an increase in lung-derived IL-5 protein, however OVA alone or in the presence of empty NPs had significantly increased cytokine levels while CaMKIIN-loaded NPs reduced IL-5 protein (Figure 5-4g). These results provide compelling evidence that delivery of chitosan-coated CaMKIIN-loaded PLGA NPs reduce key features of allergic asthma, including AHR, eosinophilic airway inflammation and production of inflammatory cytokines.

Another key feature of allergic asthma is increased mucus production in the lungs[203], and previous work from our group implicated CaMKII in this process.[190] Consistently, mucin expression and MUC5AC mRNA gene expression were significantly reduced in CaMKIIN NP-exposed mice compared to empty NPs following OVA challenge or OVA challenge alone (Figure 5-4h,i,j). Although mice instilled with empty NPs also had a significant reduction in MUC5AC mRNA, CaMKIIN-loaded NPs had a significantly greater effect compared to OVA alone (Figure 5-4j). These data support the finding that CaMKII is a key mediator of the asthma disease phenotypes and suggest that inhibition of CaMKII activity in asthmatic patients may be a viable treatment option.

5.5. Conclusions

In summary, we have demonstrated that cationic NPs are effective vehicles for drug delivery to the lung. Surface modification of PLGA NPs with chitosan enhanced the uptake of the encapsulated therapeutic agent in primary airway epithelial cells compared to uncoated NPs, with a favorable in vivo safety profile. In addition, we provide evidence for a novel peptide-based formulation for CaMKII inhibition in the lungs. The translational potential of our findings are high given that CaMKII inhibitors and the use of nanotechnology to improve retention of therapeutic agents are currently under development.[204, 219] As such, utilization of NPs for drug delivery to the lungs could offer a novel, more efficacious and safer treatment option for asthmatic patients. In future studies, we plan to optimize the peptide loading in the PLGA NPs by varying the formulation used during fabrication and to test the NPs in a therapeutic setting.

This chapter was adapted from A.S. Morris, S.C. Sebag, J.D. Paschke, A. Wongrakpanich, K. Ebeid, M.E. Anderson, I.M. Grumbach and A.K. Salem. Cationic CaMKII inhibiting nanoparticles prevent allergic asthma. Molecular Pharmaceutics. 2017.

6. MITOCHONDRIA TARGETED PLGA NANOPARTICLES

6.1. Abstract

An excess of calcium (Ca^{2+}) influx into mitochondria during mitochondrial re-energization is one of the causes of myocardial cell death during ischemic/reperfusion injury. This overload of Ca^{2+} triggers the mitochondrial permeability transition pore (mPTP) opening which leads to programmed cell death. During the ischemic/reperfusion stage, the activated Ca^{2+}/calmodulin-dependent protein kinase II (CaMKII) enzyme is responsible for Ca^{2+} influx. To reduce CaMKII-related cell death, sub-micron particles composed of poly(lactic-co-glycolic acid) (PLGA), loaded with a CaMKII inhibitor peptide were fabricated. The CaMKII inhibitor peptide-loaded (CIP) particles were coated with a mitochondria targeting moiety, triphenylphosphonium cation (TPP), which allowed the particles to accumulate and release the peptide inside mitochondria to inhibit CaMKII activity. The fluorescently labeled TPP-CIP were taken up by mitochondria and successfully reduced ROS caused by Isoprenaline (ISO) in a differentiated rat cardiomyocyte-like cell line. When cells were treated with TPP-CIP prior to ISO exposure, they maintained mitochondrial membrane potential. The TPP-CIP protected cells from ISO-induced ROS production and decreased mitochondrial membrane potential. Thus, TPP-CIP have the potential to be used in protection against ischemia/reperfusion injury.

6.2. Introduction

Myocardial infarction (MI) or heart attack, is a commonly observed symptom of coronary heart disease which is a leading cause of death and disability worldwide.[220] According to the American Heart Association, one American will have a MI approximately every 42 seconds.[221] Typically, reducing acute myocardial ischemic injury and limiting the infarct size using thrombolytic therapy to gain myocardial reperfusion is an effective therapeutic intervention.[222] However, the injury caused during ischemia/reperfusion remains. One of the causes of myocardial cell death during ischemia/reperfusion injury in MI patients is an excess of calcium (Ca^{2+}) influx into mitochondria during mitochondrial membrane potential ($\Delta\Psi$) restoration.[223] This overload of Ca^{2+} leads to mitochondria permeability

transition pore (mPTP) opening and increased levels of reactive oxygen species (ROS), which eventually leads to myocardial cell death. The multifunctional calcium/calmodulin dependent protein kinase II (CaMKII) enzyme is rapidly activated during the ischemia/reperfusion stage and is responsible for mitochondrial Ca^{2+} influx.[224-225] Inhibiting CaMKII in the mitochondria reduces cell death from ischemia/reperfusion injury in vivo.[224] A potent CaMKII inhibitor (CaMKIIN) protein is thought to reduce Ca^{2+} flux into mitochondria, thereby preventing mPTP opening.[226] Chang et al. have identified a 21-amino acid sequence (CaMKIIN peptide, Figure 6-1A) derived from CaMKIIN protein at the amino acid sequence 43 – 63, has exhibited potent CaMKII inhibitory activity.[206, 227]

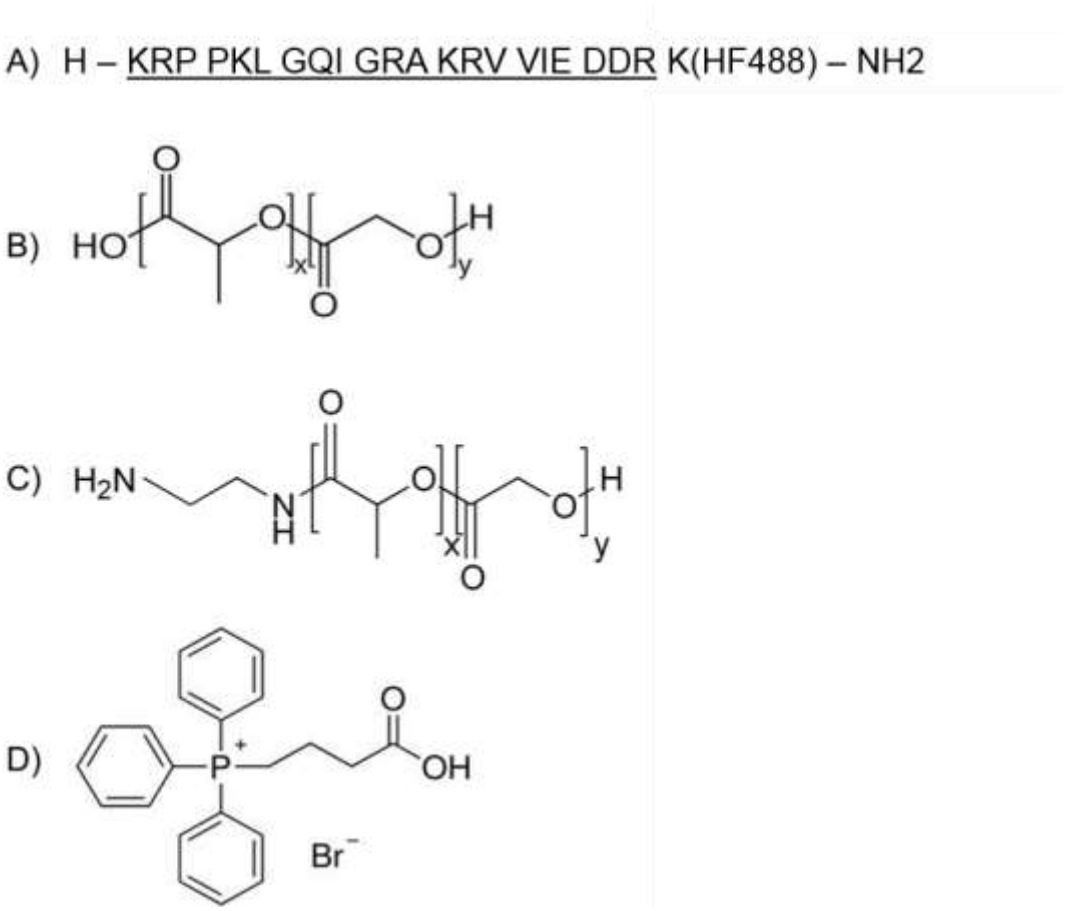

Figure 6-1. Chemical structures of (A) CaMKIIN peptide (21-amino acid sequence that binds to CaMKII is underlined, HiLyte™ Fluor 488 (HF488) was added for fluorescence detection); (B) poly (lactic-co-glycolic acid) ester endcap (PLGA); (C) poly(lactic-co-glycolic acid) amine endcap (diamine) (PLGA-NH_2); and (D) triphenylphosphonium (TPP).

To achieve a therapeutic effect, CaMKIIN peptide needs to be able to enter the cells and reach mitochondria. All studies performed so far have focused on modifying the protein/peptide itself to increase cellular uptake or target the mitochondria. Examples include mtCaMKIIN (which contains a mitochondrial localization sequence)[224], palmitoyl-CaMKIIN (which contains a membrane localization motif) and TatCN21 (a membrane permeable CaMKIIN peptide).[228] Besides delivery of the peptide to cardiomyocyte mitochondria, avoiding physiological degradation of the peptide must be considered. Submicron sized particles made from poly(lactic-co-glycolic acid) (PLGA, Figure 6-1B), an FDA-approved biodegradable polymer, can be loaded with various molecules such as peptides/proteins and protect them from degradation by proteases.[229-230] The PLGA polymer can be conjugated with various targeting moieties[231-232] and therefore could be used to increase cellular uptake and deliver the CaMKIIN peptide to mitochondria. The targeting moiety chosen for this current study was the triphenylphosphonium cation (TPP, Figure 6-1D). In 1984, TPP was reported to have an uptake and binding ability to the matrix face and cytosolic face of the mitochondria inner membrane.[233] Since then, TPP has been a popular choice for mitochondria targeting strategies. Moreover, TPP has been reported to promote the rate and amount of cellular internalization of conjugated nanomaterials.[234] There are various TPP-conjugated drug molecules and bioactive compounds such as, vitamin E (MitoVit E)[235], a ubiquinone derivative (MitoQ)[236] and doxorubicin.[237] There are also liposomes formulated with TPP in the lipid layers to target mitochondria.[238] TPP can be conjugated to PLGA-block-poly(ethylene glycol) (PEG) polymer and blended with either non-targeted PLGA-block-PEG-OH or PLGA-COOH to prepare solid PLGA particles using a nanoprecipitation method.[239] These particles can be loaded with lipophilic drugs such as curcumin and 2, 4-dinitrophenol, and were reported to be taken up into the mitochondria of human cervical cancer (HeLa) cells.[239]

The well characterized cell line, H9c2, derived from rat cardiac tissue[240], was used in this study. This cell line has been used extensively as a model for ischemia/reperfusion injury[240-244] due to its high sensitivity to ischemia/reperfusion injury in terms of cell viability and mitochondrial respiration.[242]

Moreover, H9c2 cells have been used in several studies involving CaMKII.[245-248] In these studies, the chronic exposure to all-trans retinoic acid was used to induce H9c2 cells to differentiate from cardiomyoblast-like to cardiomyocyte-like cells as has been previously described.[249]

Instead of modifying the peptide structure to achieve an increase in both cellular uptake and mitochondrial targeting, in this report, we describe a new drug delivery system for transporting CaMKIIN peptide to mitochondria using functionalized PLGA particles. To the best of our knowledge, this is the first time that a CaMKII inhibitor peptide has been incorporated into a drug delivery system, specifically, into surface-modified PLGA particles. These submicron sized PLGA particles loaded with CaMKIIN peptide were prepared using a modified double emulsion solvent diffusion/evaporation method. The particle surface was conjugated with TPP, using carbodiimide crosslinker chemistry. The ability of the particles to inhibit CaMKII activity was tested using differentiated H9c2 cells that were treated with isoprenaline.

6.3. Materials and methods

6.3.1. Fabrication of PLGA Particles

CaMKIIN peptide-loaded particles (CIP) were made using two types of polymer: PLGA (PLGA 50:50 lactic acid: glycolic acid, ester endcap, MW: 24,000 – 38,000 Da; Resomer® RG503, Boehringer Ingelheim Pharma Gmbh & Co., Figure 6-1B) and PLGA-NH_2 (50:50 lactic acid: glycolic acid, diamine endcap, MW: 10,000 – 20,000 Da; PolySciTech Division, Akina, Inc., Figure 6-1C). The fluorescently-labeled CaMKIIN peptide (H-KRP PKL GQI GRA KRV VIE DDR K(HF488)-NH_2) was custom produced (Anaspec, Inc. (EGT group)) with a purity ≥ 90% according to HPLC analysis by the company. CaMKIIN peptide-loaded particles (CIP) were prepared using a double emulsion solvent diffusion/evaporation method with some modifications.[250-252] Briefly, 138 µL containing 625 µg of CaMKIIN peptide in 1% polyvinyl alcohol (PVA, Mowiol® 8-88, Mw 67,000, Sigma-Aldrich) was sonicated into a solution of 50 mg of PLGA and 50 mg of PLGA-NH_2 dissolved in 150 µL of dimethyl sulfoxide (DMSO) and 2.5 mL of ethyl acetate. Sonication using a Sonic Dismembrator Ultrasonic

processor (Fisher Scientific) was conducted at 40% amplitude for 45 seconds to create the primary emulsion. To create the secondary emulsion, the primary emulsion was sonicated in 9 mL of 2.5% PVA in 1x PBS containing 1 mL of ethyl acetate at 40% amplitude for 60 seconds. The emulsion was then poured into 2.5% PVA in 1x PBS (51 mL), and stirred in a fume hood for 30 minutes for the particles to solidify. Separation/pelleting of unwanted particles (> 300 nm) was performed by differential centrifugation at 4,500 x g for 5 minutes (Eppendorf centrifuge 5804 R, Eppendorf). The desired particles in the supernatant were then collected by centrifugation at 10,000 x g for 30 minutes and were washed twice with sterile water, and then frozen and lyophilized using a FreeZone 4.5-L Benchtop Freeze Dry System (Labconco Corporation). This particle preparation method is illustrated in Figure 6-2A.

Particle surfaces were functionalized with (4-carboxybutyl) triphenylphosphonium bromide (TPP, Sigma-Aldrich) using carbodiimide crosslinker chemistry (ThermoFisher Scientific) during the fabrication process. In this reaction, a TPP-derivative containing a carboxylic acid (-COOH) functional group was used along with a mixture of ester end capped PLGA and amine end capped PLGA (PLGA-NH_2) in particle fabrication. Thus, the carbodiimide compound was used to activate carboxylic acids for subsequent primary amine conjugation through the formation of amide bonds. While the particles were stirred in the fume hood, 4 mL of (triphenyl phosphate) - (1-ethyl-3-3(3-dimethylaminopropyl) carbodiimide HCl) - (N-hydroxysucciniide) (TPP-EDC-NHS solution) in 0.1 M 2-(N-morpholino) ethanesulfonic acid (MES) buffer solution was added dropwise. Particles were reacted with this solution for 2 hours before being collected, washed and lyophilized. Excess molar ratios of TPP, EDC and NHS were used. For 1 mg PLGA and PLGA-NH_2 polymer, 1 mg, 4 mg and 6 mg, of TPP, EDC and NHS were used, respectively.

6.3.2. Quantification of CaMKIIN peptide loading in CIP

The loading capacity was quantified using a method described by Joshi et al.[200] Since the CaMKIIN peptide was fluorescently labeled, the peptide loading in lyophilized particles could be quantified using a SpectraMax® plus 384 Microplate Spectrophotometer (Molecular Devices) (excitation/emission: 500

nm/530 nm). A known amount of lyophilized CIP was degraded using 0.3 N NaOH. After all particles were degraded, the solution was neutralized with 1 N HCl to approximately pH 7 then the fluorescence intensity was measured and compared to the intensity of standard CaMKIIN peptide solutions in 1x PBS. The linear range for the CaMKIIN peptide is between 0.05 – 6.25 μg/mL.

6.3.3. Morphology, size and zeta potential of particles

The surface morphology of particles was assessed using Scanning Electron Microscopy (SEM: Hitachi S-4800, Hitachi High-Technologies). The lyophilized particles prepared using the method mentioned above were resuspended in deionized water. A drop of this particle suspension (approximately 10 μL) was placed onto a silicon wafer mounted on a SEM stub using double stick carbon tape and air dried. The silicon wafer was then coated with gold-palladium using a sputter coater (K550 sputter coater, Emitech Ltd.). The images were collected at 1.5 kV accelerating voltage. The size and zeta potential from each batch of particles were measured using a Zetasizer Nano ZS (Malvern).

6.3.4. Confirmation of TPP conjugation on the particle surface using fluorescamine

Fluorescamine interacts with primary amines to yield highly fluorescent derivatives.[253] In this study, fluorescamine was used to quantify the availability of primary amines on the surface of particles prepared using the mixture of PLGA and PLGA-NH_2 (as an indirect measurement of TPP conjugation). Three types of particles were tested, blank (without CaMKIIN peptide) particles made from PLGA and PLGA-NH_2 (PLGA:PLGA-NH_2, 50:50), TPP conjugated-blank particles made from PLGA and PLGA-NH_2 (TPP-PLGA:PLGA-NH_2, 50:50) and blank particles made purely from ester-end capped PLGA (PLGA:PLGA-NH_2, 100:0).

Lyophilized particles were resuspended in 1 mL PBS. Then, 50 μL of fluorescamine dissolved in acetone (9 mg/mL) was added to the particles. The reaction was allowed to continue for 5 minutes. The particles were then washed three times with PBS. The fluorescence intensity of the particle surface was determined using flow cytometry (LSR II flow cytometer).

6.3.5. Cell lines and cell culture

Rat cardiomyoblast-derived cells (H9c2, ATCC® CRL-1446TM) were maintained in DMEM medium (Gibco®, Life technologies). All of the media were supplemented with 10% fetal bovine serum (FBS, Atlanta Biologicals), 2 mM Glutamax (Gibco®) and 1% penicillin/streptomycin (Gibco®). Cells were incubated at 37°C and 5% CO_2. Sub-culturing was performed before cells reached 80% confluency to prevent the loss of differentiation potential.[254]

According to Comelli et al., H9c2 cells can differentiate into cardiomyocyte-like cells using a low percentage (1%) of FBS in combination with retinoic acid.[249] H9c2 cells were seeded at a concentration of 4×10^5 cells/well in 150-mm dishes using DMEM supplemented with 1% FBS, 10 nM all-trans retinoic acid, 2 mM Glutamax (Gibco®) and 1% penicillin/streptomycin (Gibco®). Media was replenished every two days. Differentiated H9c2 cells were used after 7 days of differentiation. Cells were maintained in the differentiation media throughout all experiments.

6.3.6. Flow cytometry analysis of Mitotracker® Red stained cells

Seven days after the differentiation process, H9c2 cells were gently rinsed with pre-warmed PBS, trypsinized with 0.25% trypsin-EDTA and collected using centrifugation at 230 x g for 5 minutes. Cells were then incubated with 200 nM Mitotracker® Red (CMSRos, Molecular Probes, Life technologies) for 15 mins in an incubator (37 °C, 5% CO_2) to stain the mitochondria. Cells were collected by centrifugation and resuspended in pre-warmed PBS without any fixatives. The fluorescent signal from Mitotracker® Red was quantified immediately using flow cytometry (FACScan: Becton Dickinson Immunocytometry Systems). Undifferentiated H9c2 cells incubated in DMEM media supplemented with 10% FBS were used as a control group.

6.3.7. Measurement of intracellular reactive oxygen species (ROS) production by dihydroethidium (DHE) staining

After H9c2 cells were differentiated, the CaMKIIN peptide in either solution or particulate form was added into each 150-mm dish at a concentration of 100 nM, 4 hours prior to adding 125 μM of isoprenaline (ISO). Cells were incubated with particles and ISO for 28 and 24 hours, respectively. The treatment groups (CISol (CaMKIIN peptide in soluble form), CIP (CaMKIIN peptide loaded particles), TPP-CIP (TPP functionalized CaMKIIN peptide loaded particles) and ISO were maintained in the media until the end of the experiment. After the exposure, media was removed. Cells were gently rinsed with pre-warmed PBS to remove excess particles (see treatment timeline: Figure 6-2B). Cells were trypsinized with 0.25% trypsin-EDTA and collected by centrifugation at 230 x g for 5 minutes. The cells were washed with pre-warmed PBS containing 5 mM sodium pyruvate and incubated at 37 °C with dihydroethidium (DHE, 10 μM in DMSO) in PBS containing 5 mM sodium pyruvate. After 40 minutes of incubation, the cells were analyzed using flow cytometry (FACScan). The relative mean fluorescence intensity (MFI) of 20,000 cells was recorded. All groups were normalized to the untreated control group. Antimycin A or AntA (an electron transport chain blocker, 10 μM in DMSO) was used as a positive control and subsequently increased the DHE oxidation levels by 2.6-fold higher than the control group (data not shown).

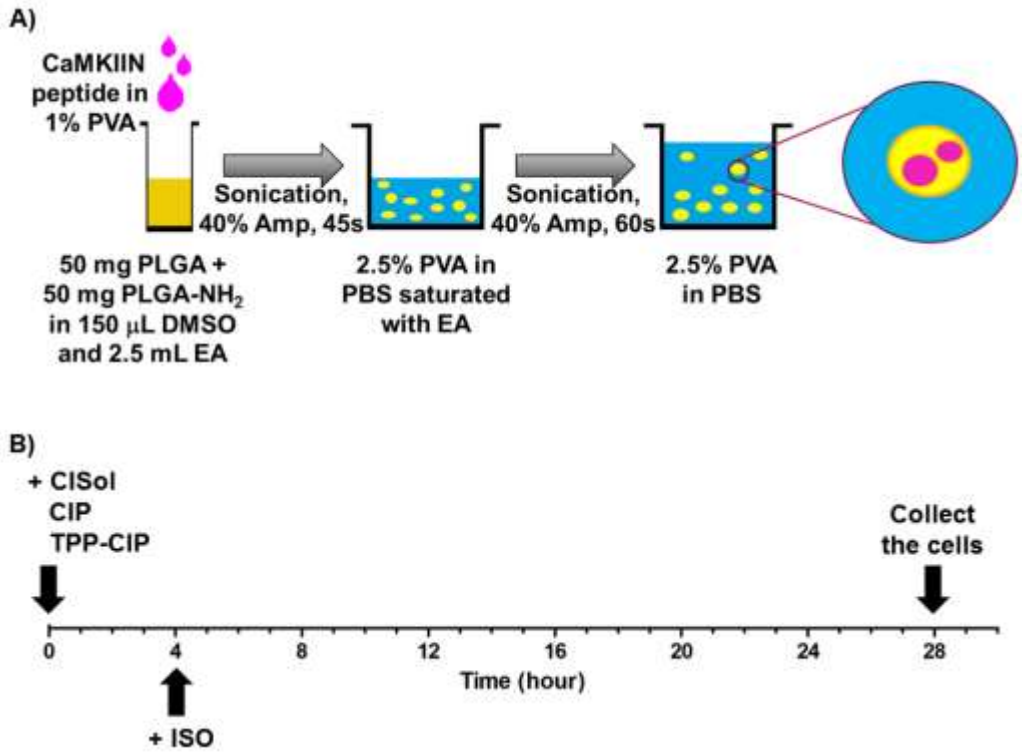

Figure 6-2. (A) Fabrication of CaMKIIN-loaded particles (CIP): schematic of the protocol for loading CaMKIIN peptides into PLGA particles (see method for further details). PLGA, poly(lactic-co-glycolic-acid); PLGA-NH_2, amine endcapped poly(lactic-co-glycolic-acid); PVA, polyvinyl alcohol; EA, ethyl acetate; Amp, amplitude.

(B) Timeline of in vitro experiments with differentiated H9c2 cells: cells were treated with different formulations of CaMKIIN peptide at t = 0, incubated with ISO at t = 4 and collected at t = 28. CaMKIIN peptide solution (CISol); CaMKIIN loaded particles (CIP); TPP conjugated CaMKIIN loaded particles (TPP-CIP); Isoprenaline (ISO).

6.3.8. Quantification of particle uptake in differentiated H9c2 cells

The excitation and emission wavelengths of oxidized product from DHE are 535 and 610 nm, respectively.[255] The CaMKIIN peptide was tagged with a fluorophore (HF488, HiLyte Flour Dye, Anaspec. Inc,) possessing excitation and emission wavelengths of 500 nm and 530 nm, respectively. ROS production in H9c2 cells and the fluorescent signal from the CaMKIIN peptide were measured simultaneously using flow cytometry. The relative mean fluorescence intensities (MFI) of 20,000 cells were recorded. All groups were normalized to the untreated control group.

6.3.9. Measurement of mitochondrial membrane potential by Tetramethylrhodamine, methyl ester, Perchlorate (TMRM) staining

Differentiated H9c2 cells were seeded at $1x10^5$ cells per dish one day prior to the experiment. Cells were treated in the same manner as described in section 6.3.7. After the exposure, the medium was removed. Cells were trypsinized and resuspended in 250 µL of media which contained 25 µM tetramethylrhodamine, methyl ester, perchlorate (TMRM) in Hanks' balanced salt solution (HBSS). Cells were exposed to TMRM containing media in the dark for 30 mins at 37 °C. After the incubation was completed, the old media was replaced with DMEM media containing 1% FBS, retinoic acid and sodium pyruvate. Cell images were obtained using an epi-fluorescence, inverted Olympus IX-81.

The fluorescent intensity from H9c2 mitochondria in each group was obtained using the raw intensity data (F1) / background intensity data (F0) which is the area in the image with no cells.

6.3.10. Statistical Analysis

Data are expressed as mean ± SEM. Statistical significance was determined using an unpaired T-test or One-Way ANOVA with Bonferroni's multiple comparison tests. All statistical tests were performed using GraphPad Prism. A p-value less than 0.05 was considered significant.

6.4. Results and Discussion

6.4.1. Particle characterization

CIP were fabricated using a water in oil in water double emulsion solvent diffusion/evaporation method as previously described with some modifications. [250-251] Ethyl acetate was used as the organic phase with PVA as a stabilizer. This method was developed to load water soluble drugs into nanometer-sized particles. The hydrodynamic diameters for CIP (PLGA/PLGA-NH_2) and TPP-CIP (TPP-PLGA/PLGA-NH_2) were approximately 210 ± 4 nm (n=5) and 280 ± 42 nm (n=3), respectively with a narrow size distribution. All particles had a negative overall surface charge. The drug loading of CIP (PLGA/PLGA/NH_2) and TPP-CIP (TPP-PLGA/PLGA-NH_2) were approximately 0.47 ± 0.04 µg/mg

lyophilized particles (n=3) and 0.38 ± 0.06 μg/mg lyophilized particles (n=3), respectively. Entrapment efficiency of CIP was approximately 10.15%. Production yield of NPs (% yield) was approximately 57 ± 9 (n=5). The surface morphology of the particles was studied using SEM and they were shown to have smooth surfaces, were spherical in shape and were uniform in size (Figure 6-3). A release study was performed to determine the drug release profile from CIP (Figure 6-4). The results indicated that more than 50% of CaMKIIN peptide was released from the particles within the first hour and more than 90% after 13 days.

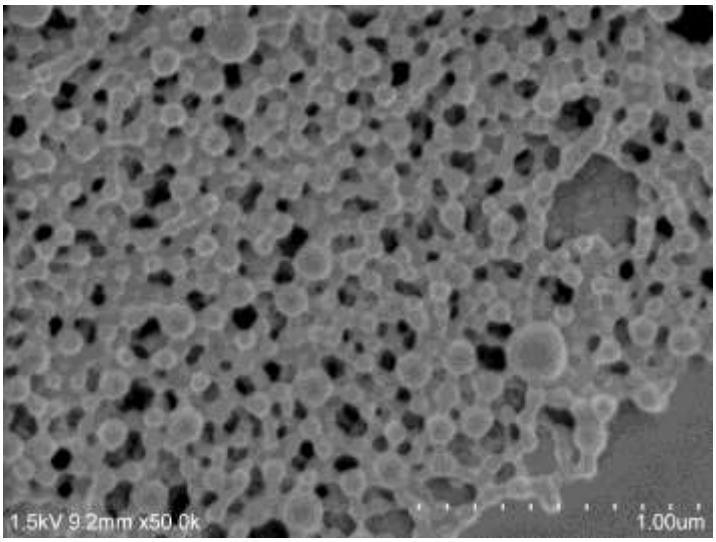

Figure 6-3. Representative scanning electron micrograph of particles made from PLGA and PLGA-NH_2 with TPP functionalization on the particle surface. Scale bar represents 1.00 μm.

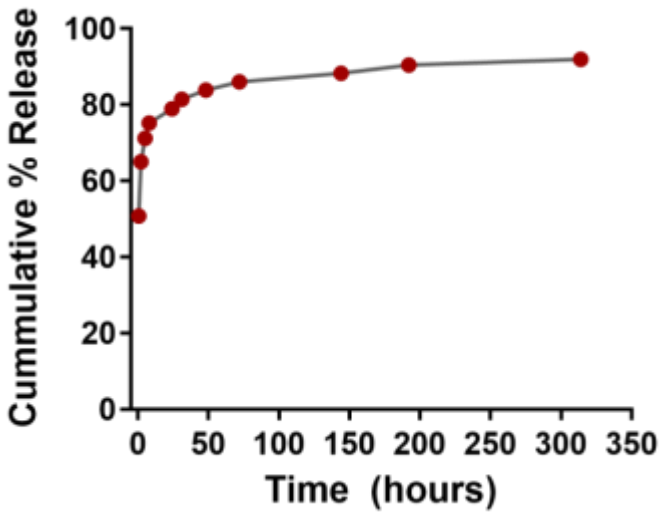

Figure 6-4. Cumulative release profile of CaMKIIN peptide from CIP.

6.4.2. TPP was successfully conjugated onto the particle surface

To create mitochondria-targeting particles, TPP was conjugated onto the particle surface using carbodiimide crosslinker chemistry as described in the methods section. Two assays were performed to confirm TPP-particle conjugation: 1) zeta potential measurements and 2) detection of residual primary amines with fluorescamine. Since TPP is a lipophilic cation its successful conjugation onto the particle surface results in an increase in zeta potential.[256] As shown in Figure 6-5, TPP-PLGA:PLGA-NH_2, 50:50 particles demonstrated significantly higher zeta potential when compared to unmodified particles (PLGA:PLGA-NH_2, 50:50). These results suggest that the TPP group was present on the particle surface of the TPP-PLGA:PLGA-NH_2, 50:50 particles.

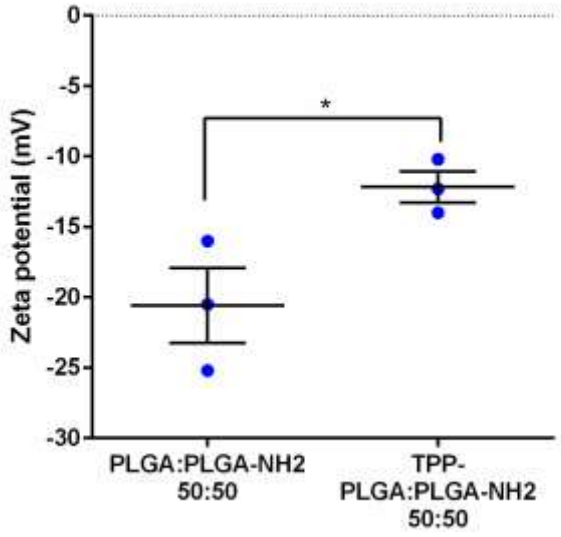

Figure 6-5. Zeta potential of particles before and after TPP conjugation: PLGA: PLGA-NH_2, 50:50 represents particles prepared using a mixture of PLGA and PLGA-NH_2 at the ratio of 50:50. TPP- PLGA: PLGA-NH_2, 50:50 represents particles made from mixture of PLGA and PLGA-NH_2 at the ratio of 50:50 with TPP conjugation. Data are expressed as scatter plots (n = 3). Unpaired two-tailed t-test was conducted to determine significant differences between PLGA: PLGA-NH_2, 50:50 and TPP-PLGA: PLGA-NH_2, 50:50. *$p < 0.05$.

The second method that was used to confirm TPP conjugation involved treating the particles with the amine-reactive dye, fluorescamine. In theory, if the particle surface contains free primary amines, it will react with fluorescamine to yield a highly fluorescent product. However, if the particles surface was occupied with TPP group, there would be lower number of free amines to react with fluorescamine. Thus, TPP-conjugated particles should yield a lower fluorescence intensity compared to unconjugated particles. Schematic images representing the different types of particles made in this experiment are shown in Figure 6-6A. In Figure 6-6B, TPP-PLGA:PLGA-NH_2, 50:50 particles that were incubated with fluorescamine showed significantly lower fluorescence intensity (p-value < 0.05) compared to PLGA:PLGA-NH_2, 50:50 particles that were incubated with fluorescamine. The control group (PLGA particles without primary amines, PLGA:PLGA-NH_2, 100:0) showed no significant fluorescence intensity. The results obtained from this experiment were consistent with zeta potential measurements (Figure 6-5) and suggested that TPP was successfully conjugated onto the surface of the particles.

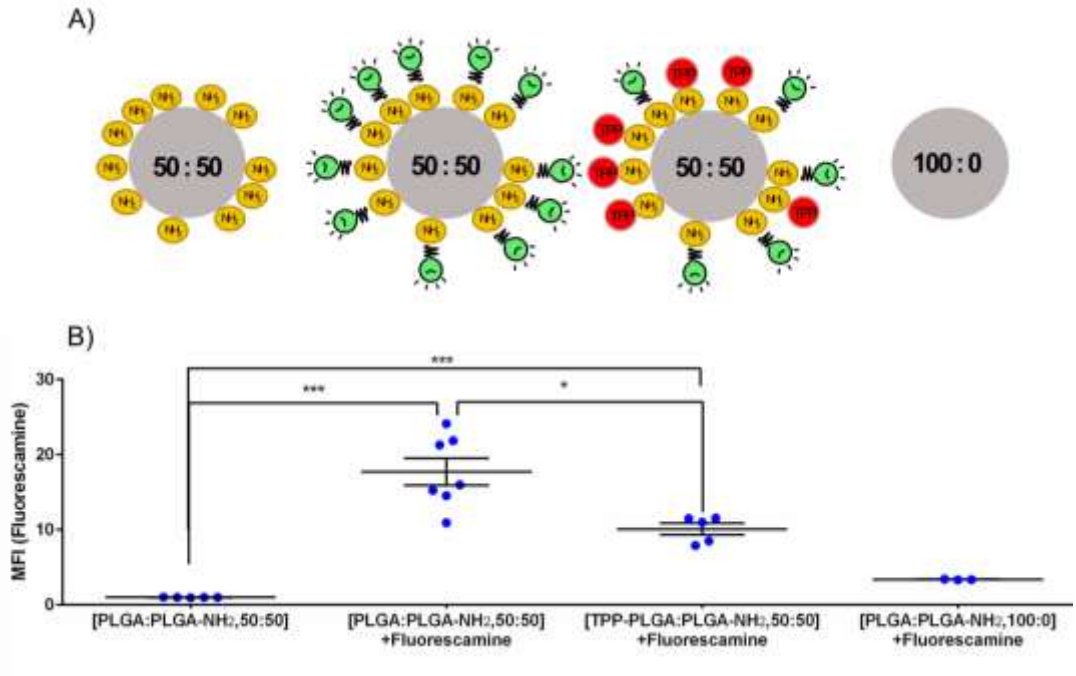

Figure 6-6. TPP conjugation to PLGA:PLGA-NH_2 particles. (A) Schematic of particles with and without TPP conjugation (PLGA:PLGA-NH_2 and TPP-PLGA:PLGA-NH_2) and incubated with fluorescamine. (B) Mean fluorescence intensity (MFI) obtained from particles treated with/without fluorescamine as indicated. PLGA:PLGA-NH_2, 50:50 = particles made from a mixture of PLGA and PLGA-NH_2 at the ratio of 50:50; TPP-PLGA:PLGA-NH_2, 50:50 = TPP-conjugated particles made from a mixture of PLGA and PLGA-NH_2 at the ratio of 50:50; PLGA:PLGA-NH_2, 100:0 = particles made purely from PLGA with no amine functionalization. Green light bulbs represent fluorescamine. Data are expressed as scatter plots (n = 3 - 7). One-way analysis of variance with Bonferroni's multiple comparisons test was performed. ***p < 0.001, *p < 0.05.

6.4.3. Differentiated H9c2 cells have mitochondrial content higher than undifferentiated H9c2 cells

Undifferentiated H9c2 cells are used as an alternative to primary cardiomyocytes as they are recognized as being representative of the cardiomyoblast lineage.[240, 257] These cells have the ability to differentiate into cardiomyocyte-like cells when they are exposed to all-trans retinoic acid in reduced-serum media. After differentiation, H9c2 cells express a more cardiac-like phenotype such as having a greater mitochondrial mass[249], as well as having an increased expression of proteins involved in Ca^{2+} handling and mitochondrial metabolism.[258] Such characteristics are of importance in these studies since the particles being tested were designed to target the mitochondria of cardiomyocytes. Moreover, there

have been reports suggesting that differentiated H9c2 cells were more susceptible to cytotoxic substances such as isoprenaline[258] and doxorubicin[254] than undifferentiated cells. Since this study is focused on the protective ability of the particles against isoprenaline-induced toxicity, differentiated cells which are more sensitive to toxic substances, would generate more distinct results than undifferentiated cells. Flow cytometric analysis of Mitotracker® Red fluorescence was used as a semi-quantitative indicator of mitochondrial mass. After 7 days of differentiation in the presence of all-trans retinoic acid and 1% FBS, H9c2 cells had a relative mean fluorescence intensity (MFI) 2.2-fold higher than untreated cells (Figure 6-7).

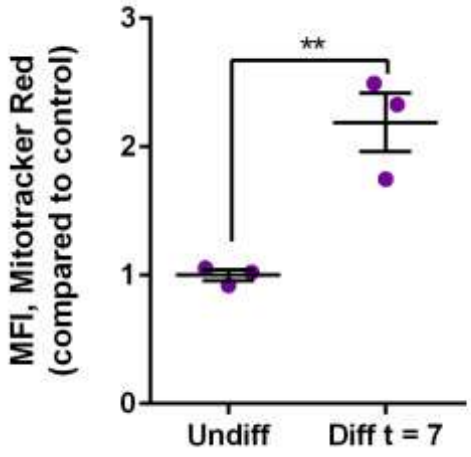

Figure 6-7. Relative mitochondrial mass as determined using Mitotracker® Red: Relative mean fluorescence intensity (MFI) due to Mitotracker® Red comparing two groups of cells: H9c2 cells that were exposed to the differentiation agent, all-trans-retinoic acid, for 7 days (Diff t = 7) and H9c2 cells not treated with all-trans retinoic acid (Undiff). Data are expressed as scatter plots (n = 3). Unpaired two-tailed t-test was performed. **$p < 0.01$.

It has been previously established that treating H9c2 cells with all-trans retinoic acid for 7 days results in an increase in mitochondrial content which is considered one of the markers for the differentiation-associated changes in mitochondrial biogenesis.[249] The aforementioned flow cytometry data was verified using confocal microscopy which showed an increase in mitochondrial mass after

Mitotracker® Red staining (Figure 6-8). Taken together, these results confirmed that significant differentiation of H9c2 cells had been achieved.

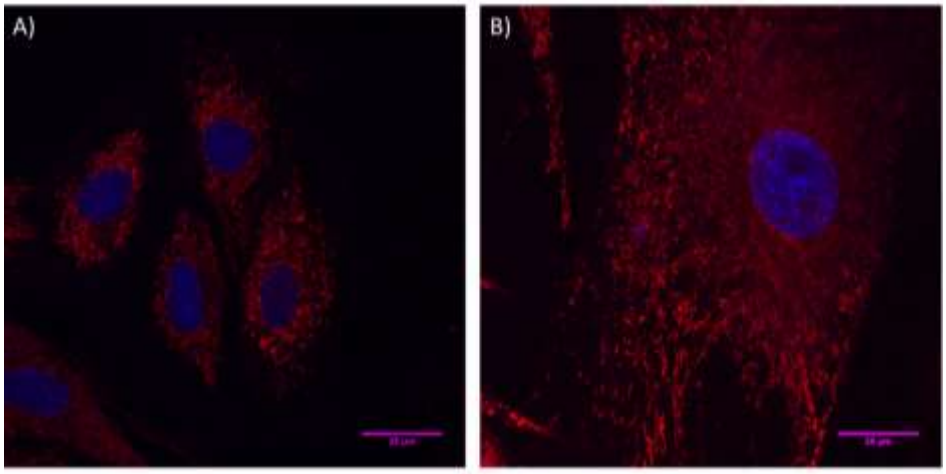

Figure 6-8. Representative confocal microscopy images of H9c2 cells (A) before treatment with all-trans-retinoic acid (undifferentiated) and (B) H9c2 cells after exposure to all-trans-retinoic acid (differentiated). Mitochondria were stained in red using Mitotracker® Red and nuclei were stained in blue using DAPI. Images were taken via Zeiss LSM 510 confocal microscope at 63x oil. Scale bar represents 25 μm.

6.4.4. TPP-CIP were most efficiently taken up by differentiated H9c2 cells compared to other particle formulations

After differentiated H9c2 cells were incubated with various CaMKIIN peptide formulations and ISO, cells were collected and analyzed for particle uptake using flow cytometry, exploiting the fluorescent signal from the CaMKIIN peptide itself. Cells that were treated with TPP-CIP had the highest fluorescent signal amongst all groups tested which was 14.7-fold higher than the untreated cells (control group, Figure 6-9A). Cells that were incubated with CIP and CISol had similar levels of fluorescence with 4.1- and 3.5-fold higher than untreated cells, respectively. Thus, using TPP conjugation to the surface of PLGA particles significantly increased cellular uptake by differentiated H9c2 cells.

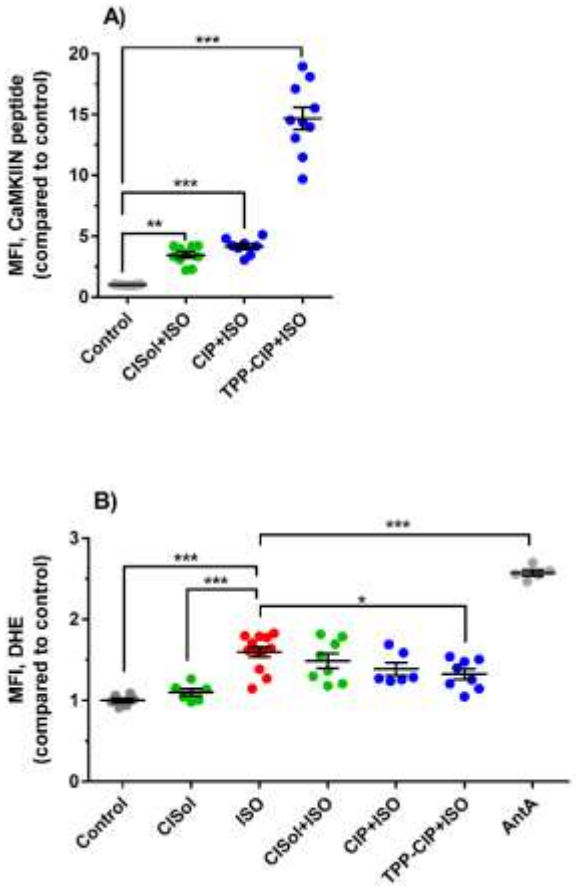

Figure 6-9. Enhanced uptake of, and reduced pro-oxidants levels due to, TPP-CIP in H9c2 cells: (A) Mean fluorescence intensity (MFI) from fluorescently-tagged CaMKIIN peptide obtained from cells that were incubated with CaMKIIN solution (CISol), CaMKIIN loaded particles (CIP) and TPP-conjugated CaMKIIN loaded particles (TPP-CIP) and treated with isoprenaline (ISO). Data are expressed scatter plots, (n = 8 - 12). One-way analysis of variance with Bonferroni's multiple comparisons test compared to the control was performed. ***$p < 0.001$, **$p < 0.01$. (B) Mean fluorescence intensity (MFI) due to the presence of intracellular pro-oxidants as detected by dihydroethidium oxidation (DHE) obtained from cells that were incubated with CaMKIIN solution (CISol), CaMKIIN loaded particles (CIP) and TPP-conjugated CaMKIIN loaded particles (TPP-CIP) and treated with isoprenaline (ISO). Antimycin A (AntA) was used as a positive control. AntA increased the MFI by 2.6-fold when compared to the control group. Data are expressed as scatter plots, (n = 5 - 12). One-way analysis of variance with Bonferroni's multiple comparisons test compared to the ISO was performed. ***$p < 0.001$, **$p < 0.01$, *$p < 0.05$.

6.4.5. TPP-CIP reduced intracellular ROS induced by ISO

In the same set of experiments, differentiated H9c2 cells were also analyzed for intracellular ROS (pro-oxidants such as superoxide) induced by ISO (Figure 6-9B). Without the CaMKIIN peptide, cells that were treated with 125 µM ISO for 24 hours had 1.6-fold higher fluorescent signal, generated by the oxidized DHE product, than the control group. When cells were pre-treated with CaMKIIN peptide in

either soluble form (CISol) or particulate forms (CIP, TPP-CIP) 4 hours prior to treatment with ISO, the intracellular ROS decreased. Among the different CaMKIIN peptide formulations, TPP-CIP had the lowest fluorescent signal (1.3-fold higher than the control group) and was therefore the most effective at mitigating ROS levels (p-value < 0.05 when compared to ISO-treated cells).

6.4.6. TPP-CIP maintained mitochondrial membrane potential in differentiated H9c2 cells after ISO treatment

Differentiated H9c2 cells were treated with ISO with and without CIP or TPP-CIP pre-treatment. Mitochondrial membrane potential was measured using TMRM. Cells treated with ISO alone or cells pretreated with CIP then ISO showed a decrease in membrane potential compared to that of cells pre-treated with TPP-CIP (Figure 6-10). This suggests that cells pretreated with TPP-CIP had more polarized mitochondria compared to other groups.

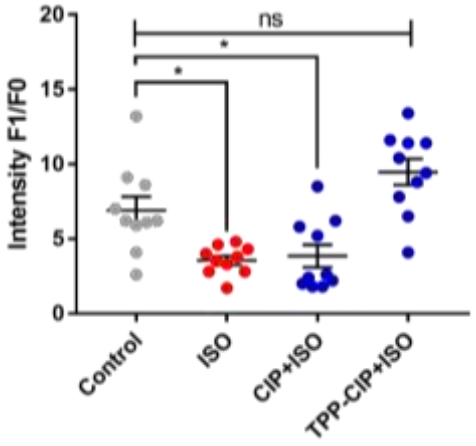

Figure 6-10. Effect of pretreatment with CIP at maintaining the mitochondria membrane potential in ISO-treated H9c2 cells: TMRM intensity (F1/F0) obtained from epi-fluorescence images of H9c2 cells that were stained with TMRM dye after incubation with either CAMKIIN loaded particles (CIP) or TPP-conjugated CaMKIIN loaded particles (TPP-CIP) then treated with isoprenaline (ISO). F1 represents the raw intensity data. F0 represents the background intensity data which were obtained from the areas of the images that contained no cells. Control group is untreated cells. Data are expressed as scatter plots, (n = 10). One-way analysis of variance with Bonferroni's multiple comparisons test compared to the control group was performed. *p < 0.05. ns, not statistically significant.

In the studies presented here, a CaMKIIN peptide was successfully entrapped inside PLGA particles. These PLGA particles comprised a mixture of PLGA (ester endcapped) with PLGA-NH_2 (amine endcapped) and, to impart mitochondrial targeting capabilities to these particles, a test group was conjugated to TPP by linking the carboxylate group on TPP to the amine group on PLGA-NH_2. TPP was conjugated onto the surface of PLGA particles using carbodiimide crosslinker chemistry. Confirmation of successful TPP conjugation to the surface of the particles was achieved through zeta potential measurements of the particles and assessing amine availability on the particle surface.

Using submicron-sized particles is necessary for the purposes of targeting mitochondria. Mitochondria targeting polymeric particles with diameters equal to or smaller than approximately 200 nm have been found in the mitochondria of HeLa cells.[239] Here, the mean hydrodynamic diameter of the particles was approximately 200 nm. The mechanism of how polymeric particles can locate to mitochondria remains unclear. However, it is likely that the TPP group on the particle surface plays an important role in a unique endosomal escape pathway after cellular uptake[259] and facilitates particle transport to the inside of mitochondria with its binding ability to the matrix of the negatively charged mitochondrial inner membrane.[236]

Whilst TPP is a desirable agent to include into particulate formulations designed to target mitochondria, excessive TPP accumulation in mitochondria is arguably toxic to cells.[260-261] Examples of toxic effects include the inhibition of the mitochondrial electron transport chain and inducing mitochondrial proton leakage.[260] In order to minimize possible cytotoxicity of TPP cations, short linker chains of the TPP cation, (4-carboxybutyl) triphenylphosphonium bromide, were used in the studies presented here. Furthermore, the amount of TPP used was minimized by conjugating the TPP group onto the surface of PLGA particles as opposed to every single polymer chain. This was done by adding TPP-EDC-NHS in 0.1 M MES buffer solution into the formulation after the CIP were formed. Since the conjugation was conducted before the particles were washed and lyophilized, the loss in drug loading

(CaMKIIN peptide) during formulation was minimized; which is an outstanding feature of this novel method.

TPP-CIP were more readily taken up by cardiomyocyte-like H9c2 cells than non-targeting CIP as indicated in Figure 6A. This result is consistent with previously published data.[234, 256, 261] Bielski et al. found that conjugating TPP onto poly(amidoamine) (PAMAM) dendrimer nanocarriers increased both cellular internalization and mitochondrial targeting in the human lung adenocarcinoma cell line, A549.[234] Guzman-Villaneuva et al. (2015) reported that TPP-liposomes had higher cellular uptake than liposomes without surface-conjugated TPP.[261]

CaMKII is a multifunctional signaling enzyme expressed in heart cells which can be activated by stimulating the beta-adrenergic receptor.[262] To study the effect of CaMKII inhibition by TPP-CIP, CaMKII induction is necessary. This can be done by adding a beta-adrenergic receptor agonist called isoprenaline (ISO) to differentiated H9c2 cells.[263-264] It is known that CaMKII activity promotes mitochondrial-triggered cell death due to Ca^{2+} overload and excess ROS.[225] Since ISO treatment increases mitochondrial ROS production, the reduction in intracellular ROS production in cells pretreated with TPP-CIP indicates the ability of these particles to inhibit CaMKII. Cells pretreated with TPP-CIP was the only group which had intracellular ROS (pro-oxidants) levels significantly lower than cells treated with ISO alone, suggesting that TPP-CIP helped to protect cells against ISO induced intracellular ROS generation (Figure 6B).

In addition to intracellular ROS, mitochondrial membrane potential (ψ) of differentiated H9c2 cells was also measured. $\Delta\psi$ is the total transmembrane electrical potential or voltage gradient which is an indicator of the health of cells.[265-266] TMRM is a fluorescent lipophilic cationic dye which can accumulate within mitochondria at levels that depend on the $\Delta\psi$ value. Since the inner membrane of polarized mitochondria have a higher negative charge than depolarized mitochondria, TMRM can accumulate more in polarized mitochondria.[267] During cellular stress, as when ISO is added, $\Delta\psi$ can be altered by the

intracellular ionic charges such as Ca^{2+} [268] which result in $\Delta\psi$ collapse and mitochondria depolarization.[267] From the results shown here, TPP-CIP can protect cardiomyocyte-like cells from ISO-induced mitochondrial damage as seen from the reduction in intracellular ROS (pro-oxidants) (Figure 6-9B) and the high $\Delta\Psi$ (Figure 6-10).

6.5. Conclusions

This study reports on the development of a new submicron sized particulate drug delivery system carrying a CaMKIIN peptide designed to protect cells against mitochondrial injury. The cellular uptake and mitochondrial targeting ability were achieved through the surface conjugation of PLGA-based carriers with a mitochondrial targeting molecule, TPP. The conjugation with TPP was confirmed using zeta potential measurements and an assay measuring fluorescamine reactivity. TPP-CIP protected cardiomyocyte-like cells from ISO-induced ROS production and decreased mitochondrial membrane potential. TPP-CIP have the potential to be used in protection against ischemia/reperfusion injury in susceptible patients such as patients undergoing heart surgery.

*This chapter was adapted from Wongrakpanich, A.; Morris, A. S.; Geary, S. M.; Joiner, M. A.; Salem, A. K., Surface-modified particles loaded with CaMKII inhibitor protect cardiac cells against mitochondrial injury. Int J Pharm **2017**, 520 (1-2), 275-283.*

7. CONCLUSIONS AND FUTURE DIRECTIONS

Currently, there are over 120,000 research articles published in the scientific literature (according to a search using Thompson Reuters Web of Science™) that aim to develop nanomaterials for drug delivery and other biomedical applications. As nanotechnology advances, the need for carefully engineered and functional nanomaterials is necessary for optimizing their use in biomedical applications. By incorporating coating materials onto the nanoparticle surface, it is possible to specifically tune the nanoparticle properties to enhance the desired biological interactions. Many reports demonstrate improved biocompatibility of surface modified nanoparticles compared to uncoated nanoparticles of the same composition as well as increased cell uptake and the ability to target nanoparticles to cells or tissues. This thesis concerning the surface properties of engineered nanoparticles emphasizes the need for carefully designed nanoparticle systems to develop safer and more efficient materials.

In this work, it was demonstrated that inorganic NPs cause adverse side effects in biological systems. When it comes to surface degradable nanoparticles such as CuO, it is important to understand the dissolution properties of the material and whether this plays a role in toxicity outcomes. It was shown that dissolved Cu^{2+} ions from CuO NPs may be involved in cytotoxicity to A549 and BEAS-2B cells, however, this was not the main cause of cell death. Furthermore, the surface chemistry of nonporous silica NPs was directly related to lung inflammation in vivo which was not detected by in vitro screening. Specifically, amine-modified nonporous silica NPs caused less lung injury in mice compared to bare silica NPs and may be a safer material to use in silica NP-related applications.

The surface chemistry of polymeric NPs is also very important for biological interactions as described in chapters 5 and 6. PLGA NPs coated with chitosan were developed for the delivery of a therapeutic peptide to treat allergic asthma. Chitosan-coated NPs were taken up by human lung cells 4-times more efficiently compared to uncoated PLGA NPs. Additionally, chitosan-coated PLGA NPs when loaded with a CaMKIIN peptide and delivered to the lungs were able to prevent the onset of allergic asthma in mice.

Another drug delivery application using PLGA NPs demonstrated that when TPP moieties were added to the surface of the NPs, they could be targeted specifically to the mitochondria of cells. These TPP-NPs were loaded with CaMKIIN peptide and were used to protect heart cells from ischemia/reperfusion injury.

The research encompassed in this thesis can be widely expanded upon to advance the field of nanotechnology. The role of surface chemistry on specific cell-NP interactions needs to be studied more in depth. For example, the mechanism of cell uptake could be elucidated by using agents to block endocytosis pathways followed by evaluation of NP uptake using methods described herein. Furthermore, the PLGA NP formulations mentioned previously need to be investigated more thoroughly for their therapeutic potential. There are two examples reported in this work where CaMKIIN-loaded PLGA NPs were effective at preventing or reducing disease-related cellular phenotypes. Additional formulations of CaMKIIN-loaded PLGA NPs are worth developing as is analyzing them in other disease models in order to gain a more complete therapeutic profile. These future studies could be of great importance for designing safer nanomaterials or optimizing their properties for drug delivery applications.

REFERENCES

1. Faraday, M., AuNP117-The Bakerian Lecture: Experimental Relations of Gold (and Other Metals) to Light. *Philosophical Transactions of the Royal Society of London* **1857,** *147*, 145–81.

2. Feynman, R. P., There's Plenty of Room at the Bottom: An Invitation to Enter a New Field of Physics *Engineering and Science* **1960,** *23*, 22–35.

3. Vert, M.; Doi, Y.; Hellwich, K. H.; Hess, M.; Hodge, P.; Kubisa, P.; Rinaudo, M.; Schue, F., Terminology for biorelated polymers and applications (IUPAC Recommendations 2012). *Pure Appl Chem* **2012,** *84* (2), 377-408.

4. Benn, T. M.; Westerhoff, P., Nanoparticle silver released into water from commercially available sock fabrics. *Environ Sci Technol* **2008,** *42* (11), 4133-4139.

5. Keller, A. A.; Vosti, W.; Wang, H. T.; Lazareva, A., Release of engineered nanomaterials from personal care products throughout their life cycle. *J Nanopart Res* **2014,** *16* (7).

6. Shukla, R. K.; Sharma, V.; Pandey, A. K.; Singh, S.; Sultana, S.; Dhawan, A., ROS-mediated genotoxicity induced by titanium dioxide nanoparticles in human epidermal cells. *Toxicol in Vitro* **2011,** *25* (1), 231-241.

7. Auffan, M.; Pedeutour, M.; Rose, J.; Masion, A.; Ziarelli, F.; Borschneck, D.; Chaneac, C.; Botta, C.; Chaurand, P.; Labille, J.; Bottero, J. Y., Structural Degradation at the Surface of a TiO2-Based Nanomaterial Used in Cosmetics. *Environ Sci Technol* **2010,** *44* (7), 2689-2694.

8. Jin, C. Y.; Zhu, B. S.; Wang, X. F.; Lu, Q. H., Cytotoxicity of titanium dioxide nanoparticles in mouse fibroblast cells. *Chem Res Toxicol* **2008,** *21* (9), 1871-1877.

9. Weir, A.; Westerhoff, P.; Fabricius, L.; Hristovski, K.; von Goetz, N., Titanium Dioxide Nanoparticles in Food and Personal Care Products. *Environ Sci Technol* **2012,** *46* (4), 2242-2250.

10. Benn, T.; Cavanagh, B.; Hristovski, K.; Posner, J. D.; Westerhoff, P., The release of nanosilver from consumer products used in the home. *J Environ Qual* **2010,** *39* (6), 1875-82.

11. Wagner, V.; Dullaart, A.; Bock, A. K.; Zweck, A., The emerging nanomedicine landscape. *Nat Biotechnol* **2006,** *24* (10), 1211-1217.

12. Etheridge, M. L.; Campbell, S. A.; Erdman, A. G.; Haynes, C. L.; Wolf, S. M.; McCullough, J., The big picture on nanomedicine: the state of investigational and approved nanomedicine products. *Nanomed-Nanotechnol* **2013,** *9* (1), 1-14.

13. Li, M. Q.; Tang, Z. H.; Lv, S. X.; Song, W. T.; Hong, H.; Jing, X. B.; Zhang, Y. Y.; Chen, X. S., Cisplatin crosslinked pH-sensitive nanoparticles for efficient delivery. of doxorubicin. *Biomaterials* **2014,** *35* (12), 3851-3864.

14. Jin, Y. H.; Hu, H. Y.; Qiao, M. X.; Zhu, J.; Qi, J. W.; Hu, C. J.; Zhang, Q.; Chen, D. W., pH-sensitive chitosan-derived nanoparticles as doxorubicin carriers for effective anti-tumor activity: preparation and in vitro evaluation. *Colloid Surface B* **2012,** *94*, 184-191.

15. Nogueira, D. R.; Tavano, L.; Mitjans, M.; Perez, L.; Infante, M. R.; Vinardell, M. P., In vitro antitumor activity of methotrexate via pH-sensitive chitosan nanoparticles. *Biomaterials* **2013,** *34* (11), 2758-2772.

16. Liu, J.; Huang, Y. R.; Kumar, A.; Tan, A.; Jin, S. B.; Mozhi, A.; Liang, X. J., pH-Sensitive nano-systems for drug delivery in cancer therapy. *Biotechnol Adv* **2014,** *32* (4), 693-710.

17. Ding, H. M.; Ma, Y. Q., Controlling Cellular Uptake of Nanoparticles with pH-Sensitive Polymers. *Sci Rep-Uk* **2013,** *3*.

18. Parveen, S.; Misra, R.; Sahoo, S. K., Nanoparticles: a boon to drug delivery, therapeutics, diagnostics and imaging. *Nanomed-Nanotechnol* **2012,** *8* (2), 147-166.

19. Mackowiak, S. A.; Schmidt, A.; Weiss, V.; Argyo, C.; von Schirnding, C.; Bein, T.; Brauchle, C., Targeted Drug Delivery in Cancer Cells with Red-Light Photoactivated Mesoporous Silica Nanoparticles. *Nano Lett* **2013,** *13* (6), 2576-2583.

20. Pan, L. M.; He, Q. J.; Liu, J. N.; Chen, Y.; Ma, M.; Zhang, L. L.; Shi, J. L., Nuclear-Targeted Drug Delivery of TAT Peptide-Conjugated Monodisperse Mesoporous Silica Nanoparticles. *J Am Chem Soc* **2012,** *134* (13), 5722-5725.

21. Xiao, D.; Jia, H. Z.; Zhang, J.; Liu, C. W.; Zhuo, R. X.; Zhang, X. Z., A Dual-Responsive Mesoporous Silica Nanoparticle for Tumor-Triggered Targeting Drug Delivery. *Small* **2014,** *10* (3), 591-598.

22. Wang, Y. S., A.; Evdokiou A.; Losic D., An overview of nanotoxicity and nanomedicine research: principles, progress and implications for cancer therapy. *J. Mater. Chem. B* **2015,** *3*, 7153-7172.

23. Lee, J. H.; Huh, Y. M.; Jun, Y. W.; Seo, J. W.; Jang, J. T.; Song, H. T.; Kim, S.; Cho, E. J.; Yoon, H. G.; Suh, J. S.; Cheon, J., Artificially engineered magnetic nanoparticles for ultra-sensitive molecular imaging. *Nat Med* **2007,** *13* (1), 95-9.

24. Lee, S. H.; Kim, B. H.; Na, H. B.; Hyeon, T., Paramagnetic inorganic nanoparticles as T1 MRI contrast agents. *Wiley Interdiscip Rev Nanomed Nanobiotechnol* **2014,** *6* (2), 196-209.

25. Xiu, Z. M.; Zhang, Q. B.; Puppala, H. L.; Colvin, V. L.; Alvarez, P. J., Negligible particle-specific antibacterial activity of silver nanoparticles. *Nano Lett* **2012,** *12* (8), 4271-5.

26. Tran, Q. H.; Nguyen, V. Q.; Le, A. T., Silver nanoparticles: synthesis, properties, toxicology, applications and perspectives. *Adv Nat Sci-Nanosci* **2013,** *4* (3).

27. Conde, J.; Doria, G.; Baptista, P., Noble metal nanoparticles applications in cancer. *J Drug Deliv* **2012,** *2012*, 751075.

28. Karlsson, H. L.; Cronholm, P.; Gustafsson, J.; Moller, L., Copper oxide nanoparticles are highly toxic: a comparison between metal oxide nanoparticles and carbon nanotubes. *Chem Res Toxicol* **2008,** *21* (9), 1726-32.

29. Soenen, S. J.; Manshian, B.; Montenegro, J. M.; Amin, F.; Meermann, B.; Thiron, T.; Cornelissen, M.; Vanhaecke, F.; Doak, S.; Parak, W. J.; De Smedt, S.; Braeckmans, K., Cytotoxic effects of gold nanoparticles: a multiparametric study. *Acs Nano* **2012,** *6* (7), 5767-83.

30. Anderson, J. M.; Rodriguez, A.; Chang, D. T., Foreign body reaction to biomaterials. *Semin Immunol* **2008,** *20* (2), 86-100.

31. Kohane, D. S.; Langer, R., Biocompatibility and drug delivery systems. *Chem Sci* **2010,** *1* (4), 441-446.

32. Wongrakpanich, A.; Mudunkotuwa, I. A.; Geary, S. M.; Morris, A. S.; Mapuskar, K. A.; Spitz, D. R.; Grassian, V. H.; Salem, A. K., Size-dependent cytotoxicity of copper oxide nanoparticles in lung epithelial cells. *Environmental Science-Nano* **2016,** *3* (2), 365-374.

33. Carlson, C.; Hussain, S. M.; Schrand, A. M.; Braydich-Stolle, L. K.; Hess, K. L.; Jones, R. L.; Schlager, J. J., Unique Cellular Interaction of Silver Nanoparticles: Size-Dependent Generation of Reactive Oxygen Species. *J Phys Chem B* **2008,** *112* (43), 13608-13619.

34. Passagne, I.; Morille, M.; Rousset, M.; Pujalte, I.; L'Azou, B., Implication of oxidative stress in size-dependent toxicity of silica nanoparticles in kidney cells. *Toxicology* **2012,** *299* (2-3), 112-24.

35. Gatoo, M. A.; Naseem, S.; Arfat, M. Y.; Dar, A. M.; Qasim, K.; Zubair, S., Physicochemical Properties of Nanomaterials: Implication in Associated Toxic Manifestations. *Biomed Research International* **2014**.

36. Alkilany, A. M.; Nagaria, P. K.; Wyatt, M. D.; Murphy, C. J., Cation Exchange on the Surface of Gold Nanorods with a Polymerizable Surfactant: Polymerization, Stability, and Toxicity Evaluation. *Langmuir* **2010,** *26* (12), 9328-9333.

37. Chithrani, B. D.; Ghazani, A. A.; Chan, W. C., Determining the size and shape dependence of gold nanoparticle uptake into mammalian cells. *Nano Lett* **2006,** *6* (4), 662-8.

38. Coradeghini, R.; Gioria, S.; Garcia, C. P.; Nativo, P.; Franchini, F.; Gilliland, D.; Ponti, J.; Rossi, F., Size-dependent toxicity and cell interaction mechanisms of gold nanoparticles on mouse fibroblasts. *Toxicol Lett* **2013,** *217* (3), 205-16.

39. Zhang, X. D.; Wu, D.; Shen, X.; Liu, P. X.; Yang, N.; Zhao, B.; Zhang, H.; Sun, Y. M.; Zhang, L. A.; Fan, F. Y., Size-dependent in vivo toxicity of PEG-coated gold nanoparticles. *Int J Nanomedicine* **2011,** *6*, 2071-81.

40. Napierska, D.; Thomassen, L. C.; Rabolli, V.; Lison, D.; Gonzalez, L.; Kirsch-Volders, M.; Martens, J. A.; Hoet, P. H., Size-dependent cytotoxicity of monodisperse silica nanoparticles in human endothelial cells. *Small* **2009,** *5* (7), 846-53.

41. Huang, X.; Teng, X.; Chen, D.; Tang, F.; He, J., The effect of the shape of mesoporous silica nanoparticles on cellular uptake and cell function. *Biomaterials* **2010,** *31* (3), 438-48.

42. Studer, A. M.; Limbach, L. K.; Van Duc, L.; Krumeich, F.; Athanassiou, E. K.; Gerber, L. C.; Moch, H.; Stark, W. J., Nanoparticle cytotoxicity depends on intracellular solubility: Comparison of stabilized copper metal and degradable copper oxide nanoparticles. *Toxicol Lett* **2010,** *197* (3), 169-174.

43. Midander, K.; Cronholm, P.; Karlsson, H. L.; Elihn, K.; Moller, L.; Leygraf, C.; Wallinder, I. O., Surface characteristics, copper release, and toxicity of nano- and micrometer-sized copper and copper(II) oxide particles: a cross-disciplinary study. *Small* **2009,** *5* (3), 389-99.

44. Lehman, S. E. M., A. S.; Mueller, P. S.; Salem, A. K.; Grassian, V. H.; Larsen, S. C., Silica nanoparticle-generated ROS as a predictor of cellular toxicity: mechanistic insights and safety by design. *Environmental Science: Nano* **2015,** *3*, 56-66.

45. Morris, A. S.; Adamcakova-Dodd, A.; Lehman, S. E.; Wongrakpanich, A.; Thorne, P. S.; Larsen, S. C.; Salem, A. K., Amine modification of nonporous silica nanoparticles reduces inflammatory response following intratracheal instillation in murine lungs. *Toxicol Lett* **2016,** *241*, 207-215.

46. Wang, X.; Ji, Z. X.; Chang, C. H.; Zhang, H. Y.; Wang, M. Y.; Liao, Y. P.; Lin, S. J.; Meng, H.; Li, R. B.; Sun, B. B.; Winkle, L. V.; Pinkerton, K. E.; Zink, J. I.; Xia, T.; Nel, A. E., Use of Coated Silver Nanoparticles to Understand the Relationship of Particle Dissolution and Bioavailability to Cell and Lung Toxicological Potential. *Small* **2014,** *10* (2), 385-398.

47. Yu, M.; Huang, S. H.; Yu, K. J.; Clyne, A. M., Dextran and Polymer Polyethylene Glycol (PEG) Coating Reduce Both 5 and 30 nm Iron Oxide Nanoparticle Cytotoxicity in 2D and 3D Cell Culture. *Int J Mol Sci* **2012,** *13* (5), 5554-5570.

48. Manke, A.; Wang, L.; Rojanasakul, Y., Mechanisms of nanoparticle-induced oxidative stress and toxicity. *Biomed Res Int* **2013,** *2013*, 942916.

49. Fu, P. P.; Xia, Q.; Hwang, H. M.; Ray, P. C.; Yu, H., Mechanisms of nanotoxicity: generation of reactive oxygen species. *J Food Drug Anal* **2014,** *22* (1), 64-75.

50. Park, E. J.; Park, K., Oxidative stress and pro-inflammatory responses induced by silica nanoparticles in vivo and in vitro. *Toxicol Lett* **2009,** *184* (1), 18-25.

51. Barillet, S.; Simon-Deckers, A.; Herlin-Boime, N.; Mayne-L'Hermite, M.; Reynaud, C.; Cassio, D.; Gouget, B.; Carriere, M., Toxicological consequences of TiO2, SiC nanoparticles and multi-walled carbon nanotubes exposure in several mammalian cell types: an in vitro study. *J Nanopart Res* **2010,** *12* (1), 61-73.

52. Nel, A.; Xia, T.; Madler, L.; Li, N., Toxic potential of materials at the nanolevel. *Science* **2006,** *311* (5761), 622-7.

53. Nishanth, R. P.; Jyotsna, R. G.; Schlager, J. J.; Hussain, S. M.; Reddanna, P., Inflammatory responses of RAW 264.7 macrophages upon exposure to nanoparticles: Role of ROS-NF kappa B signaling pathway. *Nanotoxicology* **2011,** *5* (4), 502-516.

54. Mendoza, A.; Torres-Hernandez, J. A.; Ault, J. G.; Pedersen-Lane, J. H.; Gao, D. H.; Lawrence, D. A., Silica nanoparticles induce oxidative stress and inflammation of human peripheral blood mononuclear cells. *Cell Stress Chaperon* **2014,** *19* (6), 777-790.

55. Singh, N.; Manshian, B.; Jenkins, G. J. S.; Griffiths, S. M.; Williams, P. M.; Maffeis, T. G. G.; Wright, C. J.; Doak, S. H., NanoGenotoxicology: The DNA damaging potential of engineered nanomaterials. *Biomaterials* **2009,** *30* (23-24), 3891-3914.

56. AshaRani, P. V.; Mun, G. L. K.; Hande, M. P.; Valiyaveettil, S., Cytotoxicity and Genotoxicity of Silver Nanoparticles in Human Cells. *Acs Nano* **2009,** *3* (2), 279-290.

57. Ghosh, M.; Manivannan, J.; Sinha, S.; Chakraborty, A.; Mallick, S. K.; Bandyopadhyay, M.; Mukherjee, A., In vitro and in vivo genotoxicity of silver nanoparticles. *Mutat Res-Gen Tox En* **2012,** *749* (1-2), 60-69.

58. Ahamed, M.; Siddiqui, M. A.; Akhtar, M. J.; Ahmad, I.; Pant, A. B.; Alhadlaq, H. A., Genotoxic potential of copper oxide nanoparticles in human lung epithelial cells. *Biochem Bioph Res Co* **2010,** *396* (2), 578-583.

59. Colognato, R.; Bonelli, A.; Ponti, J.; Farina, M.; Bergamaschi, E.; Sabbioni, E.; Migliore, L., Comparative genotoxicity of cobalt nanoparticles and ions on human peripheral leukocytes in vitro. *Mutagenesis* **2008,** *23* (5), 377-382.

60. Xu, A.; Chai, Y. F.; Nohmi, T.; Hei, T. K., Genotoxic responses to titanium dioxide nanoparticles and fullerene in gpt delta transgenic MEF cells. *Part Fibre Toxicol* **2009,** *6*.

61. Dufour, E. K.; Kumaravel, T.; Nohynek, G. J.; Kirkland, D.; Toutain, H., Clastogenicity, photo-clastogenicity or pseudo-photo-clastogenicity: Genotoxic effects of zinc oxide in the dark, in pre-irradiated or simultaneously irradiated Chinese Hamster Ovary cells. *Toxicol Lett* **2006,** *164*, S290-S291.

62. Singh, N.; Jenkins, G. J.; Asadi, R.; Doak, S. H., Potential toxicity of superparamagnetic iron oxide nanoparticles (SPION). *Nano Rev* **2010,** *1*.

63. Li, N.; Sioutas, C.; Cho, A.; Schmitz, D.; Misra, C.; Sempf, J.; Wang, M. Y.; Oberley, T.; Froines, J.; Nel, A., Ultrafine particulate pollutants induce oxidative stress and mitochondrial damage. *Environ Health Persp* **2003,** *111* (4), 455-460.

64. Yu, K. N.; Yoon, T. J.; Minai-Tehrani, A.; Kim, J. E.; Park, S. J.; Jeong, M. S.; Ha, S. W.; Lee, J. K.; Kim, J. S.; Cho, M. H., Zinc oxide nanoparticle induced autophagic cell death and mitochondrial damage via reactive oxygen species generation. *Toxicol in Vitro* **2013,** *27* (4), 1187-1195.

65. Sun, L.; Li, Y.; Liu, X. M.; Jin, M. H.; Zhang, L.; Du, Z. J.; Guo, C. X.; Huang, P. L.; Sun, Z. W., Cytotoxicity and mitochondrial damage caused by silica nanoparticles. *Toxicol in Vitro* **2011,** *25* (8), 1619-1629.

66. Teodoro, J. S.; Simoes, A. M.; Duarte, F. V.; Rolo, A. P.; Murdoch, R. C.; Hussain, S. M.; Palmeira, C. M., Assessment of the toxicity of silver nanoparticles in vitro: A mitochondrial perspective. *Toxicol in Vitro* **2011,** *25* (3), 664-670.

67. Huerta-Garcia, E.; Perez-Arizti, J. A.; Marquez-Ramirez, S. G.; Delgado-Buenrostro, N. L.; Chirino, Y. I.; Iglesias, G. G.; Lopez-Marure, R., Titanium dioxide nanoparticles induce strong oxidative stress and mitochondrial damage in glial cells. *Free Radical Bio Med* **2014,** *73*, 84-94.

68. Padmanabhan, J.; Kyriakides, T. R., Nanomaterials, Inflammation, and Tissue Engineering. *Wires Nanomed Nanobi* **2015,** *7* (3), 355-370.

69. Shvedova, A. A.; Kisin, E. R.; Mercer, R.; Murray, A. R.; Johnson, V. J.; Potapovich, A. I.; Tyurina, Y. Y.; Gorelik, O.; Arepalli, S.; Schwegler-Berry, D.; Hubbs, A. F.; Antonini, J.; Evans, D. E.; Ku, B. K.; Ramsey, D.; Maynard, A.; Kagan, V. E.; Castranova, V.; Baron, P., Unusual inflammatory and fibrogenic pulmonary responses to single-walled carbon nanotubes in mice. *Am J Physiol-Lung C* **2005,** *289* (5), L698-L708.

70. Kroll, A.; Pillukat, M. H.; Hahn, D.; Schnekenburger, J., Current in vitro methods in nanoparticle risk assessment: limitations and challenges. *Eur J Pharm Biopharm* **2009,** *72* (2), 370-7.

71. LeBel, C. P.; Ischiropoulos, H.; Bondy, S. C., Evaluation of the probe 2',7'-dichlorofluorescin as an indicator of reactive oxygen species formation and oxidative stress. *Chem Res Toxicol* **1992,** *5* (2), 227-31.

72. Zielonka, J.; Kalyanaraman, B., "ROS-generating mitochondrial DNA mutations can regulate tumor cell metastasis"-a critical commentary. *Free Radical Bio Med* **2008,** *45* (9), 1217-1219.

73. Kalyanaraman, B.; Darley-Usmar, V.; Davies, K. J.; Dennery, P. A.; Forman, H. J.; Grisham, M. B.; Mann, G. E.; Moore, K.; Roberts, L. J., 2nd; Ischiropoulos, H., Measuring reactive oxygen and nitrogen species with fluorescent probes: challenges and limitations. *Free Radic Biol Med* **2012,** *52* (1), 1-6.

74. Worthington, K. L.; Adamcakova-Dodd, A.; Wongrakpanich, A.; Mudunkotuwa, I. A.; Mapuskar, K. A.; Joshi, V. B.; Allan Guymon, C.; Spitz, D. R.; Grassian, V. H.; Thorne, P. S.; Salem, A. K., Chitosan coating of copper nanoparticles reduces in vitro toxicity and increases inflammation in the lung. *Nanotechnology* **2013,** *24* (39), 395101.

75. Sa, L. T. M.; Albernaz, M. D.; Patricio, B. F. D.; Falcao, M. V.; Coelho, B. F.; Bordim, A.; Almeida, J. C.; Santos-Oliveira, R., Biodistribution of nanoparticles: Initial considerations. *J Pharmaceut Biomed* **2012,** *70*, 602-604.

76. Sedlak, T. W.; Saleh, M.; Higginson, D. S.; Paul, B. D.; Juluri, K. R.; Snyder, S. H., Bilirubin and glutathione have complementary antioxidant and cytoprotective roles. *P Natl Acad Sci USA* **2009,** *106* (13), 5171-5176.

77. Liu, J.; Erogbogbo, F.; Yong, K. T.; Ye, L.; Liu, J.; Hu, R.; Chen, H.; Hu, Y.; Yang, Y.; Yang, J.; Roy, I.; Karker, N. A.; Swihart, M. T.; Prasad, P. N., Assessing clinical prospects of silicon quantum dots: studies in mice and monkeys. *Acs Nano* **2013,** *7* (8), 7303-10.

78. Rutkowsk.Rb; Debaare, L., An Ultramicro Colorimetric Method for Determination of Total and Direct Serum Bilirubin. *Clin Chem* **1966,** *12* (7), 432-&.

79. Walters, M. I.; Gerarde, H. W., An Ultramicromethod for Determination of Conjugated and Total Bilirubin in Serum or Plasma. *Microchem J* **1970,** *15* (2), 231-&.

80. Hafkenscheid, J. C. M.; Dijt, C. C. M., Determination of Serum Aminotransferases - Activation by Pyridoxal-5'-Phosphate in Relation to Substrate Concentration. *Clin Chem* **1979,** *25* (1), 55-59.

81. Huang, X. J.; Choi, Y. K.; Im, H. S.; Yarimaga, O.; Yoon, E.; Kim, H. S., Aspartate aminotransferase (AST/GOT) and alanine aminotransferase (ALT/GPT) detection techniques. *Sensors-Basel* **2006,** *6* (7), 756-782.

82. Naya, M.; Kobayashi, N.; Ema, M.; Kasamoto, S.; Fukumuro, M.; Takami, S.; Nakajima, M.; Hayashi, M.; Nakanishi, J., In vivo genotoxicity study of titanium dioxide nanoparticles using comet assay following intratracheal instillation in rats. *Regul Toxicol Pharm* **2012,** *62* (1), 1-6.

83. Cho, W. S.; Cho, M. J.; Jeong, J.; Choi, M.; Cho, H. Y.; Han, B. S.; Kim, S. H.; Kim, H. O.; Lim, Y. T.; Chung, B. H.; Jeong, J., Acute toxicity and pharmacokinetics of 13 nm-sized PEG-coated gold nanoparticles. *Toxicol Appl Pharm* **2009,** *236* (1), 16-24.

84. Mody, V. V.; Siwale, R.; Singh, A.; Mody, H. R., Introduction to metallic nanoparticles. *J Pharm Bioallied Sci* **2010,** *2* (4), 282-9.

85. Nowack, B.; Bucheli, T. D., Occurrence, behavior and effects of nanoparticles in the environment. *Environmental Pollution* **2007,** *150* (1), 5-22.

86. Ju-Nam, Y.; Lead, J. R., Manufactured nanoparticles: An overview of their chemistry, interactions and potential environmental implications. *Science of The Total Environment* **2008,** *400* (1–3), 396-414.

87. Buzea, C.; Pacheco, II; Robbie, K., Nanomaterials and nanoparticles: sources and toxicity. *Biointerphases* **2007,** *2* (4), MR17-71.

88. Chang, Y.-N.; Zhang, M.; Xia, L.; Zhang, J.; Xing, G., The Toxic Effects and Mechanisms of CuO and ZnO Nanoparticles. *Materials* **2012,** *5* (12), 2850-2871.

89. Grillo, R.; Rosa, A. H.; Fraceto, L. F., Engineered nanoparticles and organic matter: A review of the state-of-the-art. *Chemosphere* **2015,** *119* (0), 608-619.

90. Elsaesser, A.; Howard, C. V., Toxicology of nanoparticles. *Advanced Drug Delivery Reviews* **2012,** *64* (2), 129-137.

91. Schrand, A. M.; Rahman, M. F.; Hussain, S. M.; Schlager, J. J.; Smith, D. A.; Syed, A. F., Metal-based nanoparticles and their toxicity assessment. *Wiley Interdiscip Rev Nanomed Nanobiotechnol* **2010,** *2* (5), 544-68.

92. Oberdorster, G.; Oberdorster, E.; Oberdorster, J., Nanotoxicology: an emerging discipline evolving from studies of ultrafine particles. *Environ Health Perspect* **2005,** *113* (7), 823-39.

93. Pettibone, J. M.; Adamcakova-Dodd, A.; Thorne, P. S.; O'Shaughnessy, P. T.; Weydert, J. A.; Grassian, V. H., Inflammatory response of mice following inhalation exposure to iron and copper nanoparticles. *Nanotoxicology* **2008,** *2* (4), 189-204.

94. Klinbumrung, A.; Thongtem, T.; Thongtem, S., Characterization and gas sensing properties of CuO synthesized by DC directly applying voltage. *Applied Surface Science* **2014,** *313* (0), 640-646.

95. El-Trass, A.; ElShamy, H.; El-Mehasseb, I.; El-Kemary, M., CuO nanoparticles: Synthesis, characterization, optical properties and interaction with amino acids. *Applied Surface Science* **2012,** *258* (7), 2997-3001.

96. Karthick Kumar, S.; Suresh, S.; Murugesan, S.; Raj, S. P., CuO thin films made of nanofibers for solar selective absorber applications. *Solar Energy* **2013,** *94* (0), 299-304.

97. Laha, D.; Pramanik, A.; Laskar, A.; Jana, M.; Pramanik, P.; Karmakar, P., Shape-dependent bactericidal activity of copper oxide nanoparticle mediated by DNA and membrane damage. *Materials Research Bulletin* **2014,** *59* (0), 185-191.

98. Abboud, Y.; Saffaj, T.; Chagraoui, A.; El Bouari, A.; Brouzi, K.; Tanane, O.; Ihssane, B., Biosynthesis, characterization and antimicrobial activity of copper oxide nanoparticles (CONPs) produced using brown alga extract (Bifurcaria bifurcata). *Applied Nanoscience* **2014,** *4* (5), 571-576.

99. Thekkae Padil, V. V.; Cernik, M., Green synthesis of copper oxide nanoparticles using gum karaya as a biotemplate and their antibacterial application. *Int J Nanomedicine* **2013,** *8*, 889-98.

100. Pelgrift, R. Y.; Friedman, A. J., Nanotechnology as a therapeutic tool to combat microbial resistance. *Advanced Drug Delivery Reviews* **2013,** *65* (13–14), 1803-1815.

101. Yoosefi Booshehri, A.; Wang, R.; Xu, R., Simple method of deposition of CuO nanoparticles on a cellulose paper and its antibacterial activity. *Chemical Engineering Journal* **2015,** *262*, 999-1008.

102. Agarwala, M.; Choudhury, B.; Yadav, R. N., Comparative study of antibiofilm activity of copper oxide and iron oxide nanoparticles against multidrug resistant biofilm forming uropathogens. *Indian J Microbiol* **2014,** *54* (3), 365-8.

103. Murthy, P. S.; Venugopalan, V. P.; Das, D. A.; Dhara, S.; Pandiyan, R.; Tyagi, A. K. In *Antibiofilm activity of nano sized CuO*, Nanoscience, Engineering and Technology (ICONSET), 2011 International Conference on, 28-30 Nov. 2011; 2011; pp 580-583.

104. Perlman, O.; Weitz, I. S.; Azhari, H., Copper oxide nanoparticles as contrast agents for MRI and ultrasound dual-modality imaging. *Physics in Medicine and Biology* **2015,** *60* (15), 5767-5783.

105. Elzey, S.; Grassian, V. H., Nanoparticle dissolution from the particle perspective: insights from particle sizing measurements. *Langmuir* **2010,** *26* (15), 12505-8.

106. Jin, Y.; Zhao, X., Cytotoxicity of Photoactive Nanoparticles. In *Safety of Nanoparticles*, Webster, T. J., Ed. Springer New York: 2009; pp 19-31.

107. Mudunkotuwa, I. A.; Pettibone, J. M.; Grassian, V. H., Environmental implications of nanoparticle aging in the processing and fate of copper-based nanomaterials. *Environ Sci Technol* **2012,** *46* (13), 7001-10.

108. Sahu, S. C.; Casciano, D. A., *Nanotoxicity: From In Vivo and In Vitro Models to Health Risks*. Wiley: 2009.

109. Shi, X.; Castranova, V.; Vallyathan, V.; Perry, W. G., *Molecular Mechanisms of Metal Toxicity and Carcinogenesis*. Springer US: 2012.

110. Wang, Z.; Li, N.; Zhao, J.; White, J. C.; Qu, P.; Xing, B., CuO nanoparticle interaction with human epithelial cells: cellular uptake, location, export, and genotoxicity. *Chem Res Toxicol* **2012,** *25* (7), 1512-21.

111. Melegari, S. P.; Perreault, F.; Costa, R. H.; Popovic, R.; Matias, W. G., Evaluation of toxicity and oxidative stress induced by copper oxide nanoparticles in the green alga Chlamydomonas reinhardtii. *Aquat Toxicol* **2013,** *143*, 431-40.

112. Rossetto, A. L.; Melegari, S. P.; Ouriques, L. C.; Matias, W. G., Comparative evaluation of acute and chronic toxicities of CuO nanoparticles and bulk using Daphnia magna and Vibrio fischeri. *Sci Total Environ* **2014,** *490*, 807-14.

113. Mancuso, L.; Cao, G., Acute toxicity test of CuO nanoparticles using human mesenchymal stem cells. *Toxicol Mech Methods* **2014,** *24* (7), 449-54.

114. Isani, G.; Falcioni, M. L.; Barucca, G.; Sekar, D.; Andreani, G.; Carpenè, E.; Falcioni, G., Comparative toxicity of CuO nanoparticles and CuSO4 in rainbow trout. *Ecotoxicology and Environmental Safety* **2013,** *97*, 40-46.

115. Dai, L.; Banta, G. T.; Selck, H.; Forbes, V. E., Influence of copper oxide nanoparticle form and shape on toxicity and bioaccumulation in the deposit feeder, Capitella teleta. *Mar Environ Res* **2015**.

116. Ivask, A.; Titma, T.; Visnapuu, M.; Vija, H.; Kakinen, A.; Sihtmae, M.; Pokhrel, S.; Madler, L.; Heinlaan, M.; Kisand, V.; Shimmo, R.; Kahru, A., Toxicity of 11 Metal Oxide Nanoparticles to Three Mammalian Cell Types In Vitro. *Curr Top Med Chem* **2015,** *15* (18), 1914-29.

117. Semisch, A.; Ohle, J.; Witt, B.; Hartwig, A., Cytotoxicity and genotoxicity of nano - and microparticulate copper oxide: role of solubility and intracellular bioavailability. *Part Fibre Toxicol* **2014,** *11*, 10.

118. Karlsson, H. L.; Gustafsson, J.; Cronholm, P.; Moller, L., Size-dependent toxicity of metal oxide particles--a comparison between nano- and micrometer size. *Toxicol Lett* **2009,** *188* (2), 112-8.

119. Gao, H.; Shi, W.; Freund, L. B., Mechanics of receptor-mediated endocytosis. *Proc Natl Acad Sci U S A* **2005,** *102* (27), 9469-74.

120. Park, E. J.; Choi, J.; Park, Y. K.; Park, K., Oxidative stress induced by cerium oxide nanoparticles in cultured BEAS-2B cells. *Toxicology* **2008,** *245* (1-2), 90-100.

121. Eom, H. J.; Choi, J., Oxidative stress of silica nanoparticles in human bronchial epithelial cell, Beas-2B. *Toxicol in Vitro* **2009,** *23* (7), 1326-32.

122. Nymark, P.; Catalan, J.; Suhonen, S.; Jarventaus, H.; Birkedal, R.; Clausen, P. A.; Jensen, K. A.; Vippola, M.; Savolainen, K.; Norppa, H., Genotoxicity of polyvinylpyrrolidone-coated silver nanoparticles in BEAS 2B cells. *Toxicology* **2013,** *313* (1), 38-48.

123. Lechner, J. F. L., M. A., A serum-free method for culturing normal human bronchial epithelial cells at clonal density. *J Tissue Culture Methods* **1985,** *9*, 43-48.

124. Lechner, J. F.; Haugen, A.; Mcclendon, I. A.; Pettis, E. W., Clonal Growth of Normal Adult Human Bronchial Epithelial-Cells in a Serum-Free Medium. *In Vitro Cell Dev B* **1982,** *18* (7), 633-642.

125. Lechner, J. F.; Haugen, A.; Mcclendon, I. A.; Shamsuddin, A. M., Induction of Squamous Differentiation of Normal Human Bronchial Epithelial-Cells by Small Amounts of Serum. *Differentiation* **1984,** *25* (3), 229-237.

126. Lechner, J. F.; Tokiwa, T.; Curren, R. D.; Yeager, H.; Harris, C. C., Effects of Asbestos on Cultured Human-Lung Epithelial and Mesothelial Cells. *P Am Assoc Canc Res* **1983,** *24* (Mar), 58-58.

127. Yang, J. A.; Lohse, S. E.; Murphy, C. J., Tuning cellular response to nanoparticles via surface chemistry and aggregation. *Small* **2014,** *10* (8), 1642-51.

128. Wiogo, H. T.; Lim, M.; Bulmus, V.; Yun, J.; Amal, R., Stabilization of magnetic iron oxide nanoparticles in biological media by fetal bovine serum (FBS). *Langmuir* **2011,** *27* (2), 843-50.

129. Lesniak, A.; Fenaroli, F.; Monopoli, M. R.; Aberg, C.; Dawson, K. A.; Salvati, A., Effects of the Presence or Absence of a Protein Corona on Silica Nanoparticle Uptake and Impact on Cells. *Acs Nano* **2012,** *6* (7), 5845-5857.

130. Izak-Nau, E.; Voetz, M.; Eiden, S.; Duschl, A.; Puntes, V. F., Altered characteristics of silica nanoparticles in bovine and human serum: the importance of nanomaterial characterization prior to its toxicological evaluation. *Part Fibre Toxicol* **2013,** *10*.

131. Zhao, F.; Klimecki, W. T., Culture conditions profoundly impact phenotype in BEAS-2B, a human pulmonary epithelial model. *J Appl Toxicol* **2015,** *35* (8), 945-951.

132. Stober, W.; Fink, A.; Bohn, E., Controlled Growth of Monodisperse Silica Spheres in Micron Size Range. *Journal of Colloid and Interface Science* **1968,** *26* (1), 62-&.

133. He, X.; Nie, H.; Wang, K.; Tan, W.; Wu, X.; Zhang, P., In vivo study of biodistribution and urinary excretion of surface-modified silica nanoparticles. *Anal Chem* **2008,** *80* (24), 9597-603.

134. Bharali, D. J.; Klejbor, I.; Stachowiak, E. K.; Dutta, P.; Roy, I.; Kaur, N.; Bergey, E. J.; Prasad, P. N.; Stachowiak, M. K., Organically modified silica nanoparticles: a nonviral vector for in vivo gene delivery and expression in the brain. *Proc Natl Acad Sci U S A* **2005,** *102* (32), 11539-44.

135. Cao, A.; Ye, Z.; Cai, Z.; Dong, E.; Yang, X.; Liu, G.; Deng, X.; Wang, Y.; Yang, S. T.; Wang, H.; Wu, M.; Liu, Y., A facile method to encapsulate proteins in silica nanoparticles: encapsulated green fluorescent protein as a robust fluorescence probe. *Angew Chem Int Ed Engl* **2010,** *49* (17), 3022-5.

136. Stevens, E. V.; Carpenter, A. W.; Shin, J. H.; Liu, J.; Der, C. J.; Schoenfisch, M. H., Nitric oxide-releasing silica nanoparticle inhibition of ovarian cancer cell growth. *Mol Pharm* **2010,** *7* (3), 775-85.

137. Tang, L.; Fan, T. M.; Borst, L. B.; Cheng, J., Synthesis and biological response of size-specific, monodisperse drug-silica nanoconjugates. *Acs Nano* **2012,** *6* (5), 3954-66.

138. Benezra, M.; Penate-Medina, O.; Zanzonico, P. B.; Schaer, D.; Ow, H.; Burns, A.; DeStanchina, E.; Longo, V.; Herz, E.; Iyer, S.; Wolchok, J.; Larson, S. M.; Wiesner, U.; Bradbury, M. S., Multimodal silica nanoparticles are effective cancer-targeted probes in a model of human melanoma. *J Clin Invest* **2011,** *121* (7), 2768-80.

139. Bradbury, M. S.; Phillips, E.; Montero, P. H.; Cheal, S. M.; Stambuk, H.; Durack, J. C.; Sofocleous, C. T.; Meester, R. J.; Wiesner, U.; Patel, S., Clinically-translated silica nanoparticles as dual-modality cancer-targeted probes for image-guided surgery and interventions. *Integr Biol (Camb)* **2013,** *5* (1), 74-86.

140. Lin, W.; Huang, Y. W.; Zhou, X. D.; Ma, Y., In vitro toxicity of silica nanoparticles in human lung cancer cells. *Toxicol Appl Pharmacol* **2006,** *217* (3), 252-9.

141. Rimal, B.; Greenberg, A. K.; Rom, W. N., Basic pathogenetic mechanisms in silicosis: current understanding. *Curr Opin Pulm Med* **2005,** *11* (2), 169-73.

142. Hnizdo, E.; Sullivan, P. A.; Bang, K. M.; Wagner, G., Association between chronic obstructive pulmonary disease and employment by industry and occupation in the US population: a study of data from the Third National Health and Nutrition Examination Survey. *Am J Epidemiol* **2002,** *156* (8), 738-46.

143. Hnizdo, E.; Vallyathan, V., Chronic obstructive pulmonary disease due to occupational exposure to silica dust: a review of epidemiological and pathological evidence. *Occup Environ Med* **2003,** *60* (4), 237-43.

144. Ross, M. H.; Murray, J., Occupational respiratory disease in mining. *Occup Med (Lond)* **2004,** *54* (5), 304-10.

145. Hamilton, R. F.; Thakur, S. A.; Holian, A., Silica binding and toxicity in alveolar macrophages. *Free Radical Bio Med* **2008,** *44* (7), 1246-1258.

146. Reiser, K. M.; Last, J. A., Silicosis and fibrogenesis: fact and artifact. *Toxicology* **1979,** *13* (1), 51-72.

147. Saffiotti, U., Lung cancer induction by crystalline silica. *Prog Clin Biol Res* **1992,** *374*, 51-69.

148. Jiang, W.; Kim, B. Y.; Rutka, J. T.; Chan, W. C., Nanoparticle-mediated cellular response is size-dependent. *Nat Nanotechnol* **2008,** *3* (3), 145-50.

149. Verma, A.; Uzun, O.; Hu, Y.; Hu, Y.; Han, H. S.; Watson, N.; Chen, S.; Irvine, D. J.; Stellacci, F., Surface-structure-regulated cell-membrane penetration by monolayer-protected nanoparticles. *Nat Mater* **2008,** *7* (7), 588-95.

150. Oberdorster, G., Pulmonary effects of inhaled ultrafine particles. *Int Arch Occup Environ Health* **2001,** *74* (1), 1-8.

151. Sager, T. M.; Kommineni, C.; Castranova, V., Pulmonary response to intratracheal instillation of ultrafine versus fine titanium dioxide: role of particle surface area. *Part Fibre Toxicol* **2008,** *5*, 17.

152. Nel, A. E.; Madler, L.; Velegol, D.; Xia, T.; Hoek, E. M.; Somasundaran, P.; Klaessig, F.; Castranova, V.; Thompson, M., Understanding biophysicochemical interactions at the nano-bio interface. *Nat Mater* **2009,** *8* (7), 543-57.

153. Kairdolf, B. A.; Mancini, M. C.; Smith, A. M.; Nie, S., Minimizing nonspecific cellular binding of quantum dots with hydroxyl-derivatized surface coatings. *Anal Chem* **2008,** *80* (8), 3029-34.

154. Seipenbusch, M.; Binder, A.; Kasper, G., Temporal evolution of nanoparticle aerosols in workplace exposure. *Ann Occup Hyg* **2008,** *52* (8), 707-16.

155. Shen, M.; Cai, H.; Wang, X.; Cao, X.; Li, K.; Wang, S. H.; Guo, R.; Zheng, L.; Zhang, G.; Shi, X., Facile one-pot preparation, surface functionalization, and toxicity assay of APTS-coated iron oxide nanoparticles. *Nanotechnology* **2012,** *23* (10), 105601.

156. van Schooneveld, M. M.; Vucic, E.; Koole, R.; Zhou, Y.; Stocks, J.; Cormode, D. P.; Tang, C. Y.; Gordon, R. E.; Nicolay, K.; Meijerink, A.; Fayad, Z. A.; Mulder, W. J., Improved biocompatibility and pharmacokinetics of silica nanoparticles by means of a lipid coating: a multimodality investigation. *Nano Lett* **2008,** *8* (8), 2517-25.

157. Nowak, J. S.; Mehn, D.; Nativo, P.; Garcia, C. P.; Gioria, S.; Ojea-Jimenez, I.; Gilliland, D.; Rossi, F., Silica nanoparticle uptake induces survival mechanism in A549 cells by the activation of autophagy but not apoptosis. *Toxicol Lett* **2014,** *224* (1), 84-92.

158. Yang, X.; Liu, J.; He, H.; Zhou, L.; Gong, C.; Wang, X.; Yang, L.; Yuan, J.; Huang, H.; He, L.; Zhang, B.; Zhuang, Z., SiO2 nanoparticles induce cytotoxicity and protein expression alteration in HaCaT cells. *Part Fibre Toxicol* **2010,** *7*, 1.

159. Ye, Y.; Liu, J.; Chen, M.; Sun, L.; Lan, M., In vitro toxicity of silica nanoparticles in myocardial cells. *Environ Toxicol Pharmacol* **2010,** *29* (2), 131-7.

160. Kim, Y. H.; Boykin, E.; Stevens, T.; Lavrich, K.; Gilmour, M. I., Comparative lung toxicity of engineered nanomaterials utilizing in vitro, ex vivo and in vivo approaches. *J Nanobiotechnology* **2014,** *12* (1), 47.

161. Frohlich, E.; Salar-Behzadi, S., Toxicological assessment of inhaled nanoparticles: role of in vivo, ex vivo, in vitro, and in silico studies. *Int J Mol Sci* **2014,** *15* (3), 4795-822.

162. Yildirimer, L.; Thanh, N. T.; Loizidou, M.; Seifalian, A. M., Toxicology and clinical potential of nanoparticles. *Nano Today* **2011,** *6* (6), 585-607.

163. Csogor, Z.; Nacken, M.; Sameti, M.; Lehr, C. M.; Schmidt, H., Modified silica particles for gene delivery. *Materials Science & Engineering C-Biomimetic and Supramolecular Systems* **2003,** *23* (1-2), 93-97.

164. Kneuer, C.; Sameti, M.; Haltner, E. G.; Schiestel, T.; Schirra, H.; Schmidt, H.; Lehr, C. M., Silica nanoparticles modified with aminosilanes as carriers for plasmid DNA. *International Journal of Pharmaceutics* **2000,** *196* (2), 257-261.

165. Kumar, R.; Roy, I.; Hulchanskyy, T. Y.; Goswami, L. N.; Bonoiu, A. C.; Bergey, E. J.; Tramposch, K. M.; Maitra, A.; Prasad, P. N., Covalently dye-linked, surface-controlled, and bioconjugated organically modified silica nanoparticles as targeted probes for optical imaging. *Acs Nano* **2008,** *2* (3), 449-456.

166. IARC Working Group on the Evaluation of Carcinogenic Risks to Humans: Silica, Some Silicates, Coal Dust and Para-Aramid Fibrils. Lyon, 15-22 October 1996. *IARC Monogr Eval Carcinog Risks Hum* **1997,** *68*, 1-475.

167. Donaldson, K.; Borm, P. J., The quartz hazard: a variable entity. *Ann Occup Hyg* **1998,** *42* (5), 287-94.

168. Lehman, S. E.; Tataurova, Y.; Larsen, S. C., NMR studies of functionalized mesoporous silica nanomaterials in aqueous solution. *Abstracts of Papers of the American Chemical Society* **2014,** *248*.

169. Wongrakpanich, A.; Adamcakova-Dodd, A.; Xie, W.; Joshi, V. B.; Mapuskar, K. A.; Geary, S. M.; Spitz, D. R.; Thorne, P. S.; Salem, A. K., The absence of CpG in plasmid DNA-chitosan polyplexes enhances transfection efficiencies and reduces inflammatory responses in murine lungs. *Mol Pharm* **2014,** *11* (3), 1022-31.

170. Chithrani, B. D.; Chan, W. C., Elucidating the mechanism of cellular uptake and removal of protein-coated gold nanoparticles of different sizes and shapes. *Nano Lett* **2007,** *7* (6), 1542-50.

171. Lu, F.; Wu, S. H.; Hung, Y.; Mou, C. Y., Size effect on cell uptake in well-suspended, uniform mesoporous silica nanoparticles. *Small* **2009,** *5* (12), 1408-13.

172. Verstraelen, S.; Remy, S.; Casals, E.; De Boever, P.; Witters, H.; Gatti, A.; Puntes, V.; Nelissen, I., Gene expression profiles reveal distinct immunological responses of cobalt and cerium dioxide nanoparticles in two in vitro lung epithelial cell models. *Toxicol Lett* **2014,** *228* (3), 157-169.

173. DeLoid, G.; Cohen, J. M.; Darrah, T.; Derk, R.; Rojanasakul, L.; Pyrgiotakis, G.; Wohlleben, W.; Demokritou, P., Estimating the effective density of engineered nanomaterials for in vitro dosimetry. *Nature Communications* **2014,** *5*.

174. Bowman, C. R.; Bailey, F. C.; Elrod-Erickson, M.; Neigh, A. M.; Otter, R. R., Effects of silver nanoparticles on zebrafish (Danio rerio) and Escherichia coli (ATCC 25922): a comparison of toxicity based on total surface area versus mass concentration of particles in a model eukaryotic and prokaryotic system. *Environ Toxicol Chem* **2012,** *31* (8), 1793-800.

175. Sauer, U. G.; Vogel, S.; Hess, A.; Kolle, S. N.; Ma-Hock, L.; van Ravenzwaay, B.; Landsiedel, R., In vivo-in vitro comparison of acute respiratory tract toxicity using human 3D airway epithelial models and human A549 and murine 3T3 monolayer cell systems. *Toxicol in Vitro* **2013,** *27* (1), 174-90.

176. Panas, A.; Comouth, A.; Saathoff, H.; Leisner, T.; Al-Rawi, M.; Simon, M.; Seemann, G.; Dossel, O.; Mulhopt, S.; Paur, H. R.; Fritsch-Decker, S.; Weiss, C.; Diabate, S., Silica nanoparticles are less toxic to human lung cells when deposited at the air-liquid interface compared to conventional submerged exposure. *Beilstein J Nanotechnol* **2014,** *5*, 1590-602.

177. Kasper, J. Y.; Feiden, L.; Hermanns, M. I.; Bantz, C.; Maskos, M.; Unger, R. E.; Kirkpatrick, C. J., Pulmonary surfactant augments cytotoxicity of silica nanoparticles: Studies on an in vitro air-blood barrier model. *Beilstein J Nanotechnol* **2015,** *6*, 517-28.

178. Cho, W. S.; Choi, M.; Han, B. S.; Cho, M.; Oh, J.; Park, K.; Kim, S. J.; Kim, S. H.; Jeong, J., Inflammatory mediators induced by intratracheal instillation of ultrafine amorphous silica particles. *Toxicol Lett* **2007,** *175* (1-3), 24-33.

179. Brown, D. M.; Kanase, N.; Gaiser, B.; Johnston, H.; Stone, V., Inflammation and gene expression in the rat lung after instillation of silica nanoparticles: effect of size, dispersion medium and particle surface charge. *Toxicol Lett* **2014,** *224* (1), 147-56.

180. Hemenway, D.; Absher, A.; Fubini, B.; Trombley, L.; Vacek, P.; Volante, M.; Cavenago, A., Surface Functionalities Are Related to Biological Response and Transport of Crystalline Silica. *Inhaled Particles Vii* **1994**, 447-454.

181. Slowing, I. I.; Wu, C. W.; Vivero-Escoto, J. L.; Lin, V. S. Y., Mesoporous Silica Nanoparticles for Reducing Hemolytic Activity Towards Mammalian Red Blood Cells. *Small* **2009,** *5* (1), 57-62.

182. Yu, T.; Malugin, A.; Ghandehari, H., Impact of Silica Nanoparticle Design on Cellular Toxicity and Hemolytic Activity. *Acs Nano* **2011,** *5* (7), 5717-5728.

183. Pavan, C.; Tomatis, M.; Ghiazza, M.; Rabolli, V.; Bolis, V.; Lison, D.; Fubini, B., In Search of the Chemical Basis of the Hemolytic Potential of Silicas. *Chem Res Toxicol* **2013,** *26* (8), 1188-1198.

184. Shalaby, K. H.; Allard-Coutu, A.; O'Sullivan, M. J.; Nakada, E.; Qureshi, S. T.; Day, B. J.; Martin, J. G., Inhaled birch pollen extract induces airway hyperresponsiveness via oxidative stress but independently of pollen-intrinsic NADPH oxidase activity, or the TLR4-TRIF pathway. *J Immunol* **2013,** *191* (2), 922-33.

185. Chan, T. K.; Loh, X. Y.; Peh, H. Y.; Tan, W. N.; Tan, W. S.; Li, N.; Tay, I. J.; Wong, W. S.; Engelward, B. P., House dust mite-induced asthma causes oxidative damage and DNA double-strand breaks in the lungs. *J Allergy Clin Immunol* **2016,** *138* (1), 84-96 e1.

186. Luo, M.; Joiner, M. L. A., Stress Response Signaling Pathways May Lead to Mitochondrial Biogenesis. *Diabetes* **2014,** *63* (6), 1831-1832.

187. Scott, J. A.; Klutho, P. J.; El Accaoui, R.; Nguyen, E.; Venema, A. N.; Xie, L. T.; Jiang, S. X.; Dibbern, M.; Scroggins, S.; Prasad, A. M.; Luczak, E. D.; Davis, M. K.; Li, W. W.; Guan, X. Q.; Backs, J.; Schlueter, A. J.; Weiss, R. M.; Miller, F. J.; Anderson, M. E.; Grumbach, I. M., The Multifunctional Ca2+/Calmodulin-Dependent Kinase II delta (CaMKII delta) Regulates Arteriogenesis in a Mouse Model of Flow-Mediated Remodeling. *Plos One* **2013,** *8* (8).

188. Zhu, L. J.; Klutho, P. J.; Scott, J. A.; Xie, L. T.; Luczak, E. D.; Dibbern, M. E.; Prasad, A. M.; Jaffer, O. A.; Venema, A. N.; Nguyen, E. K.; Guan, X. Q.; Anderson, M. E.; Grumbach, I. M., Oxidative activation of the Ca2+/calmodulin-dependent protein kinase II (CaMKII) regulates vascular smooth muscle migration and apoptosis. *Vasc Pharmacol* **2014,** *60* (2), 75-83.

189. Anderson, M. E., Oxidant stress promotes disease by activating CaMKII. *J Mol Cell Cardiol* **2015,** *89* (Pt B), 160-7.

190. Sanders, P. N.; Koval, O. M.; Jaffer, O. A.; Prasad, A. M.; Businga, T. R.; Scott, J. A.; Hayden, P. J.; Luczak, E. D.; Dickey, D. D.; Allamargot, C.; Olivier, A. K.; Meyerholz, D. K.; Robison, A. J.; Winder, D. G.; Blackwell, T. S.; Dworski, R.; Sammut, D.; Wagner, B. A.; Buettner, G. R.; Pope, R. M.; Miller, F. J., Jr.; Dibbern, M. E.; Haitchi, H. M.; Mohler, P. J.; Howarth, P. H.; Zabner, J.; Kline, J. N.; Grumbach, I. M.; Anderson, M. E., CaMKII is essential for the proasthmatic effects of oxidation. *Sci Transl Med* **2013,** *5* (195), 195ra97.

191. Chung, K. F.; Wenzel, S. E.; Brozek, J. L.; Bush, A.; Castro, M.; Sterk, P. J.; Adcock, I. M.; Bateman, E. D.; Bel, E. H.; Bleecker, E. R.; Boulet, L. P.; Brightling, C.; Chanez, P.; Dahlen, S. E.; Djukanovic, R.; Frey, U.; Gaga, M.; Gibson, P.; Hamid, Q.; Jajour, N. N.; Mauad, T.; Sorkness, R. L.; Teague, W. G., International ERS/ATS guidelines on definition, evaluation and treatment of severe asthma. *Eur Respir J* **2014,** *43* (2), 343-373.

192. Barnes, P. J., New therapies for asthma: is there any progress? *Trends Pharmacol Sci* **2010,** *31* (7), 335-43.

193. Olin, J. T.; Wechsler, M. E., Asthma: pathogenesis and novel drugs for treatment. *BMJ* **2014,** *349*, g5517.

194. Hoda, M.; Pajaniradje, S.; Shakya, G.; Mohankumar, K.; Rajagopalan, R., Anti-proliferative and apoptosis-triggering potential of Disulfiram and Disulfiram-loaded polysorbate 80-stabilized PLGA nanoparticles on hepatocellular carcinoma Hep3B cell line. *Nanomedicine* **2016**.

195. Panyam, J.; Zhou, W. Z.; Prabha, S.; Sahoo, S. K.; Labhasetwar, V., Rapid endo-lysosomal escape of poly(DL-lactide-co-glycolide) nanoparticles: implications for drug and gene delivery. *FASEB J* **2002,** *16* (10), 1217-26.

196. Yang, X. Z.; Dou, S.; Sun, T. M.; Mao, C. Q.; Wang, H. X.; Wang, J., Systemic delivery of siRNA with cationic lipid assisted PEG-PLA nanoparticles for cancer therapy. *J Control Release* **2011,** *156* (2), 203-211.

197. Mahapatro, A.; Singh, D. K., Biodegradable nanoparticles are excellent vehicle for site directed in-vivo delivery of drugs and vaccines. *J Nanobiotechnology* **2011,** *9*, 55.

198. Oh, Y. J.; Lee, J.; Seo, J. Y.; Rhim, T.; Kim, S. H.; Yoon, H. J.; Lee, K. Y., Preparation of budesonide-loaded porous PLGA microparticles and their therapeutic efficacy in a murine asthma model. *J Control Release* **2011,** *150* (1), 56-62.

199. Lakatos, H. F.; Burgess, H. A.; Thatcher, T. H.; Redonnet, M. R.; Hernady, E.; Williams, J. P.; Sime, P. J., Oropharyngeal aspiration of a silica suspension produces a superior model of silicosis in the mouse when compared to intratracheal instillation. *Exp Lung Res* **2006,** *32* (5), 181-99.

200. Joshi, V. B.; Geary, S. M.; Salem, A. K., Biodegradable Particles as Vaccine Delivery Systems: Size Matters. *Aaps J* **2013,** *15* (1), 85-94.

201. Karp, P. H.; Moninger, T. O.; Weber, S. P.; Nesselhauf, T. S.; Launspach, J. L.; Zabner, J.; Welsh, M. J., An in vitro model of differentiated human airway epithelia. Methods for establishing primary cultures. *Methods Mol Biol* **2002,** *188*, 115-37.

202. Pope, S. M.; Fulkerson, P. C.; Blanchard, C.; Akei, H. S.; Nikolaidis, N. M.; Zimmermann, N.; Molkentin, J. D.; Rothenberg, M. E., Identification of a cooperative mechanism involving interleukin-13 and eotaxin-2 in experimental allergic lung inflammation. *J Biol Chem* **2005,** *280* (14), 13952-61.

203. Evans, C. M.; Kim, K.; Tuvim, M. J.; Dickey, B. F., Mucus hypersecretion in asthma: causes and effects. *Curr Opin Pulm Med* **2009,** *15* (1), 4-11.

204. Park, K., Nanotechnology: What it can do for drug delivery. *J Control Release* **2007,** *120* (1-2), 1-3.

205. Erickson, J. R.; Joiner, M. L.; Guan, X.; Kutschke, W.; Yang, J.; Oddis, C. V.; Bartlett, R. K.; Lowe, J. S.; O'Donnell, S. E.; Aykin-Burns, N.; Zimmerman, M. C.; Zimmerman, K.; Ham, A. J.; Weiss, R. M.; Spitz, D. R.; Shea, M. A.; Colbran, R. J.; Mohler, P. J.; Anderson, M. E., A dynamic pathway for calcium-independent activation of CaMKII by methionine oxidation. *Cell* **2008,** *133* (3), 462-74.

206. Chang, B. H.; Mukherji, S.; Soderling, T. R., Characterization of a calmodulin kinase II inhibitor protein in brain. *Proc Natl Acad Sci U S A* **1998,** *95* (18), 10890-5.

207. Arca, H. C.; Gunbeyaz, M.; Senel, S., Chitosan-based systems for the delivery of vaccine antigens. *Expert Rev Vaccines* **2009,** *8* (7), 937-53.

208. Lee, C.; Choi, J. S.; Kim, I.; Oh, K. T.; Lee, E. S.; Park, E. S.; Lee, K. C.; Youn, Y. S., Long-acting inhalable chitosan-coated poly(lactic-co-glycolic acid) nanoparticles containing hydrophobically modified exendin-4 for treating type 2 diabetes. *Int J Nanomedicine* **2013,** *8*, 2975-83.

209. Artursson, P.; Lindmark, T.; Davis, S. S.; Illum, L., Effect of chitosan on the permeability of monolayers of intestinal epithelial cells (Caco-2). *Pharm Res* **1994,** *11* (9), 1358-61.

210. Guo, C.; Gemeinhart, R. A., Understanding the adsorption mechanism of chitosan onto poly(lactide-co-glycolide) particles. *Eur J Pharm Biopharm* **2008,** *70* (2), 597-604.

211. Lakatos, H. F.; Burgess, H. A.; Thatcher, T. H.; Redonnet, M. R.; Hernady, E.; Williams, J. P.; Sime, P. J., Oropharyngeal aspiration of a silica suspension produces a superior model of silicosis in the mouse when compared to intratracheal instillation. *Exp Lung Res* **2006,** *32* (5), 181-199.

212. Hagens, W. I.; Oomen, A. G.; de Jong, W. H.; Cassee, F. R.; Sips, A. J. A. M., What do we (need to) know about the kinetic properties of nanoparticles in the body? *Regul Toxicol Pharm* **2007,** *49* (3), 217-229.

213. Nemmar, A.; Hoet, P. H. M.; Vanquickenborne, B.; Dinsdale, D.; Thomeer, M.; Hoylaerts, M. F.; Vanbilloen, H.; Mortelmans, L.; Nemery, B., Passage of inhaled particles into the blood circulation in humans. *Circulation* **2002,** *105* (4), 411-414.

214. Takenaka, S.; Karg, E.; Roth, C.; Schulz, H.; Ziesenis, A.; Heinzmann, U.; Schramel, P.; Heyder, J., Pulmonary and systemic distribution of inhaled ultrafine silver particles in rats. *Environ Health Persp* **2001,** *109*, 547-551.

215. Bahadar, H.; Maqbool, F.; Niaz, K.; Abdollahi, M., Toxicity of Nanoparticles and an Overview of Current Experimental Models. *Iran Biomed J* **2016,** *20* (1), 1-11.

216. Stevens, J. L.; Baker, T. K., The future of drug safety testing: expanding the view and narrowing the focus. *Drug Discov Today* **2009,** *14* (3-4), 162-7.

217. Conroy, D. M.; Williams, T. J., Eotaxin and the attraction of eosinophils to the asthmatic lung. *Respir Res* **2001,** *2* (3), 150-6.

218. Pease, J. E.; Williams, T. J., Eotaxin and asthma. *Curr Opin Pharmacol* **2001,** *1* (3), 248-53.

219. Luczak, E. D.; Anderson, M. E., CaMKII oxidative activation and the pathogenesis of cardiac disease. *J Mol Cell Cardiol* **2014,** *73*, 112-6.

220. Mendis, S.; Puska, P.; Norrving, B.; Organization, W. H.; Federation, W. H.; Organization, W. S., *Global Atlas on Cardiovascular Disease Prevention and Control*. World Health Organization in collaboration with the World Heart Federation and the World Stroke Organization: 2011.

221. Mozaffarian, D.; Benjamin, E. J.; Go, A. S.; Arnett, D. K.; Blaha, M. J.; Cushman, M.; Das, S. R.; de Ferranti, S.; Despres, J. P.; Fullerton, H. J.; Howard, V. J.; Huffman, M. D.; Isasi, C. R.; Jimenez, M. C.; Judd, S. E.; Kissela, B. M.; Lichtman, J. H.; Lisabeth, L. D.; Liu, S.; Mackey, R. H.; Magid, D. J.; McGuire, D. K.; Mohler, E. R., 3rd; Moy, C. S.; Muntner, P.; Mussolino, M. E.; Nasir, K.; Neumar, R. W.; Nichol, G.; Palaniappan, L.; Pandey, D. K.; Reeves, M. J.; Rodriguez, C. J.; Rosamond, W.; Sorlie, P. D.; Stein, J.; Towfighi, A.; Turan, T. N.; Virani, S. S.; Woo, D.; Yeh, R. W.; Turner, M. B., Heart Disease and Stroke Statistics-2016 Update: A Report From the American Heart Association. *Circulation* **2016,** *133* (4), e38-e360.

222. Maxwell, S., Emergency management of acute myocardial infarction. *British Journal of Clinical Pharmacology* **1999,** *48* (3), 284-298.

223. Hausenloy, D. J.; Yellon, D. M., Myocardial ischemia-reperfusion injury: a neglected therapeutic target. *The Journal of Clinical Investigation 123* (1), 92-100.

224. Joiner, M. L.; Koval, O. M.; Li, J.; He, B. J.; Allamargot, C.; Gao, Z.; Luczak, E. D.; Hall, D. D.; Fink, B. D.; Chen, B.; Yang, J.; Moore, S. A.; Scholz, T. D.; Strack, S.; Mohler, P. J.; Sivitz, W. I.; Song, L. S.; Anderson, M. E., CaMKII determines mitochondrial stress responses in heart. *Nature* **2012,** *491* (7423), 269-73.

225. Joiner, M. L.; Koval, O. M., CaMKII and stress mix it up in mitochondria. *Frontiers in pharmacology* **2014,** *5*, 67.

226. Correll, R. N.; Molkentin, J. D., CaMKII does it again: even the mitochondria cannot escape its influence. *Circulation research* **2013,** *112* (9), 1208-11.

227. Chang, B. H.; Mukherji, S.; Soderling, T. R., Calcium/calmodulin-dependent protein kinase II inhibitor protein: localization of isoforms in rat brain. *Neuroscience* **2001,** *102* (4), 767-77.

228. Tao-Cheng, J. H.; Yang, Y.; Bayer, K. U.; Reese, T. S.; Dosemeci, A., Effects of CaMKII inhibitor tatCN21 on activity-dependent redistribution of CaMKII in hippocampal neurons. *Neuroscience* **2013,** *244*, 188-96.

229. Danhier, F.; Ansorena, E.; Silva, J. M.; Coco, R.; Le Breton, A.; Preat, V., PLGA-based nanoparticles: an overview of biomedical applications. *J Control Release* **2012,** *161* (2), 505-22.

230. Mundargi, R. C.; Babu, V. R.; Rangaswamy, V.; Patel, P.; Aminabhavi, T. M., Nano/micro technologies for delivering macromolecular therapeutics using poly(D,L-lactide-co-glycolide) and its derivatives. *J Control Release* **2008,** *125* (3), 193-209.

231. Sah, H.; Thoma, L. A.; Desu, H. R.; Sah, E.; Wood, G. C., Concepts and practices used to develop functional PLGA-based nanoparticulate systems. *International Journal of Nanomedicine* **2013,** *8*, 747-765.

232. Prabhu, R. H.; Patravale, V. B.; Joshi, M. D., Polymeric nanoparticles for targeted treatment in oncology: current insights. *Int J Nanomedicine* **2015,** *10*, 1001-18.

233. Rottenberg, H., Membrane potential and surface potential in mitochondria: uptake and binding of lipophilic cations. *The Journal of membrane biology* **1984,** *81* (2), 127-38.

234. Bielski, E. R.; Zhong, Q.; Brown, M.; da Rocha, S. R., Effect of the Conjugation Density of Triphenylphosphonium Cation on the Mitochondrial Targeting of Poly(amidoamine) Dendrimers. *Molecular pharmaceutics* **2015,** *12* (8), 3043-53.

235. Smith, R. A.; Porteous, C. M.; Coulter, C. V.; Murphy, M. P., Selective targeting of an antioxidant to mitochondria. *European journal of biochemistry / FEBS* **1999,** *263* (3), 709-16.

236. Murphy, M. P., Targeting lipophilic cations to mitochondria. *Biochimica et Biophysica Acta (BBA) - Bioenergetics* **2008,** *1777* (7–8), 1028-1031.

237. Han, M.; Vakili, M. R.; Soleymani Abyaneh, H.; Molavi, O.; Lai, R.; Lavasanifar, A., Mitochondrial delivery of doxorubicin via triphenylphosphine modification for overcoming drug resistance in MDA-MB-435/DOX cells. *Molecular pharmaceutics* **2014,** *11* (8), 2640-9.

238. Wongrakpanich, A.; Geary, S. M.; Joiner, M.-l. A.; Anderson, M. E.; Salem, A. K., Mitochondria-targeting particles. *Nanomedicine (London, England)* **2014,** *9* (16), 2531-2543.

239. Marrache, S.; Dhar, S., Engineering of blended nanoparticle platform for delivery of mitochondria-acting therapeutics. *Proc Natl Acad Sci U S A* **2012,** *109* (40), 16288-93.

240. Hescheler, J.; Meyer, R.; Plant, S.; Krautwurst, D.; Rosenthal, W.; Schultz, G., Morphological, biochemical, and electrophysiological characterization of a clonal cell (H9c2) line from rat heart. *Circulation research* **1991,** *69* (6), 1476-86.

241. Bonavita, F.; Stefanelli, C.; Giordano, E.; Columbaro, M.; Facchini, A.; Bonafè, F.; Caldarera, C. M.; Guarnieri, C., H9c2 cardiac myoblasts undergo apoptosis in a model of ischemia consisting of serum deprivation and hypoxia: inhibition by PMA. *FEBS Letters* **2003,** *536* (1–3), 85-91.

242. Kuznetsov, A. V.; Javadov, S.; Sickinger, S.; Frotschnig, S.; Grimm, M., H9c2 and HL-1 cells demonstrate distinct features of energy metabolism, mitochondrial function and sensitivity to hypoxia-reoxygenation. *Biochimica et biophysica acta* **2015,** *1853* (2), 276-284.

243. Chen, Y.-W.; Chou, H.-C.; Lin, S.-T.; Chen, Y.-H.; Chang, Y.-J.; Chen, L.; Chan, H.-L., Cardioprotective Effects of Quercetin in Cardiomyocyte under Ischemia/Reperfusion Injury. *Evidence-Based Complementary and Alternative Medicine* **2013,** *2013*, 16.

244. Peng, Y.-W.; Buller, C. L.; Charpie, J. R., Impact of N-Acetylcysteine on Neonatal Cardiomyocyte Ischemia-Reperfusion Injury. *Pediatr Res* **2011,** *70* (1), 61-66.

245. Ronkainen, J. J.; Hänninen, S. L.; Korhonen, T.; Koivumäki, J. T.; Skoumal, R.; Rautio, S.; Ronkainen, V.-P.; Tavi, P., Ca2+–calmodulin-dependent protein kinase II represses cardiac transcription of the L-type calcium channel α1C-subunit gene (Cacna1c) by DREAM translocation. *The Journal of Physiology* **2011,** *589* (11), 2669-2686.

246. Zhao, L.; Cheng, G.; Jin, R.; Chen, L.; Chen, X.; Davani, A.; Samanta, A.; Girgis, M.; Choksi, K.; Yang, Y.; Vincent, R.; Dawn, B., CAMKII IS CRITICAL FOR THE UPREGULATION OF STAT3 SIGNALING IN PATHOGENESIS OF CARDIOMYOCYTE HYPERTROPHY. *Journal of the American College of Cardiology* **2015,** *65* (10_S).

247. Hoch, B.; Haase, H.; Schulze, W.; Hagemann, D.; Morano, I.; Krause, E. G.; Karczewski, P., Differentiation-dependent expression of cardiac delta-CaMKII isoforms. *Journal of cellular biochemistry* **1998,** *68* (2), 259-68.

248. Cipolletta, E.; Rusciano, M. R.; Maione, A. S.; Santulli, G.; Sorriento, D.; Del Giudice, C.; Ciccarelli, M.; Franco, A.; Crola, C.; Campiglia, P.; Sala, M.; Gomez-Monterrey, I.; De Luca, N.; Trimarco, B.; Iaccarino, G.; Illario, M., Targeting the CaMKII/ERK Interaction in the Heart Prevents Cardiac Hypertrophy. *PLoS ONE* **2015,** *10* (6), e0130477.

249. Comelli, M.; Domenis, R.; Bisetto, E.; Contin, M.; Marchini, M.; Ortolani, F.; Tomasetig, L.; Mavelli, I., Cardiac differentiation promotes mitochondria development and ameliorates oxidative capacity in H9c2 cardiomyoblasts. *Mitochondrion* **2011,** *11* (2), 315-26.

250. Song, K. C.; Lee, H. S.; Choung, I. Y.; Cho, K. I.; Ahn, Y.; Choi, E. J., The effect of type of organic phase solvents on the particle size of poly(d,l-lactide-co-glycolide) nanoparticles. *Colloids and Surfaces A: Physicochemical and Engineering Aspects* **2006,** *276* (1–3), 162-167.

251. Gross, B.; Wongrakpanich, A.; Francis, M.; Salem, A.; Norian, L., A Therapeutic Microparticle-Based Tumor Lysate Vaccine Reduces Spontaneous Metastases in Murine Breast Cancer. *The AAPS Journal* **2014,** *16* (6), 1194-1203.

252. Meng, F. T.; Ma, G. H.; Qiu, W.; Su, Z. G., W/O/W double emulsion technique using ethyl acetate as organic solvent: effects of its diffusion rate on the characteristics of microparticles. *J Control Release* **2003,** *91* (3), 407-16.

253. Udenfriend, S.; Stein, S.; Bohlen, P.; Dairman, W.; Leimgruber, W.; Weigele, M., Fluorescamine: a reagent for assay of amino acids, peptides, proteins, and primary amines in the picomole range. *Science (New York, N.Y.)* **1972,** *178* (4063), 871-2.

254. Branco, A. F.; Sampaio, S. F.; Moreira, A. C.; Holy, J.; Wallace, K. B.; Baldeiras, I.; Oliveira, P. J.; Sardao, V. A., Differentiation-dependent doxorubicin toxicity on H9c2 cardiomyoblasts. *Cardiovascular toxicology* **2012,** *12* (4), 326-40.

255. Arunachalam, G.; Samuel, S. M.; Marei, I.; Ding, H.; Triggle, C. R., Metformin modulates hyperglycaemia-induced endothelial senescence and apoptosis through SIRT1. *British Journal of Pharmacology* **2014,** *171* (2), 523-35.

256. Chakraborty, A.; Jana, N. R., Design and Synthesis of Triphenylphosphonium Functionalized Nanoparticle Probe for Mitochondria Targeting and Imaging. *The Journal of Physical Chemistry C* **2015,** *119* (5), 2888-2895.

257. Kimes, B. W.; Brandt, B. L., Properties of a clonal muscle cell line from rat heart. *Experimental cell research* **1976,** *98* (2), 367-81.

258. Branco, A. F.; Pereira, S. P.; Gonzalez, S.; Gusev, O.; Rizvanov, A. A.; Oliveira, P. J., Gene Expression Profiling of H9c2 Myoblast Differentiation towards a Cardiac-Like Phenotype. *PLoS ONE* **2015,** *10* (6), e0129303.

259. Pathak, R. K.; Kolishetti, N.; Dhar, S., Targeted Nanoparticles in Mitochondrial Medicine. *Wiley interdisciplinary reviews. Nanomedicine and nanobiotechnology* **2015,** *7* (3), 315-329.

260. Trnka, J.; Elkalaf, M.; Andel, M., Lipophilic triphenylphosphonium cations inhibit mitochondrial electron transport chain and induce mitochondrial proton leak. *PLoS One* **2015,** *10* (4), e0121837.

261. Guzman-Villanueva, D.; Mendiola, M. R.; Nguyen, H. X.; Weissig, V., Influence of Triphenylphosphonium (TPP) Cation Hydrophobization with Phospholipids on Cellular Toxicity and Mitochondrial Selectivity. *SOJ Pharm Pharm Sci* **2015,** *2* (1), 1-9.

262. Grimm, M.; Brown, J. H., Beta-adrenergic receptor signaling in the heart: role of CaMKII. *J Mol Cell Cardiol* **2010,** *48* (2), 322-30.

263. Curran, J.; Tang, L.; Roof, S. R.; Velmurugan, S.; Millard, A.; Shonts, S.; Wang, H.; Santiago, D.; Ahmad, U.; Perryman, M.; Bers, D. M.; Mohler, P. J.; Ziolo, M. T.; Shannon, T. R., Nitric oxide-dependent activation of CaMKII increases diastolic sarcoplasmic reticulum calcium release in cardiac myocytes in response to adrenergic stimulation. *PLoS One* **2014,** *9* (2), e87495.

264. Popolo, A.; Pecoraro, M.; Pinto, A., Effect of Adenosine on Isoproerenol-induced Hypertrophy In Vitro. A Preliminary Study. *Pharmacologyonline* **2014,** *1*, 121-126.

265. Solaini, G.; Sgarbi, G.; Lenaz, G.; Baracca, A., Evaluating mitochondrial membrane potential in cells. *Bioscience reports* **2007,** *27* (1-3), 11-21.

266. Perelman, A.; Wachtel, C.; Cohen, M.; Haupt, S.; Shapiro, H.; Tzur, A., JC-1: alternative excitation wavelengths facilitate mitochondrial membrane potential cytometry. *Cell Death Dis* **2012,** *3*, e430.

267. Perry, S. W.; Norman, J. P.; Barbieri, J.; Brown, E. B.; Gelbard, H. A., Mitochondrial membrane potential probes and the proton gradient: a practical usage guide. *BioTechniques* **2011,** *50* (2), 98-115.

268. Szabadkai, G.; Duchen, M. R., Mitochondria: the hub of cellular Ca2+ signaling. *Physiology (Bethesda, Md.)* **2008,** *23*, 84-94.